1991

Prediction of diesel engine particulate emission during transient cycles

Qiqing Jiang
Iowa State University

Prediction of diesel engine particulate emission during transient cycles

by

Qiqing Jiang

A Dissertation Submitted to the
Graduate Faculty in Partial Fulfillment of the
Requirements for the Degree of
DOCTOR OF PHILOSOPHY

Major: Mechanical Engineering

Iowa State University
Ames, Iowa
1991

TABLE OF CONTENTS

ACKNOWLEDGEMENTS xii

1. INTRODUCTION 1

1.1 The Need for this Investigation 1

1.2 Research Goals 4

1.3 Dissertation Organization 4

2. LITERATURE REVIEW 6

2.1 Combustion and Emissions in Diesel Engines 6

2.1.1 Combustion 6

2.1.2 Diesel emissions 7

2.1.3 Particulate matter 8

2.2 Particulate Emission Measurements 13

2.2.1 In-cylinder measurements of particulate 14

2.2.2 Measurement of particulate matter 15

2.3 Modeling Particulate Emission 20

2.3.1 Modeling steady particulate emission 20

2.3.2 Modeling transient particulate emission 22

2.3.3 Modeling engine performance 24

3. DEVELOPMENT OF THE ENGINE MODEL 26
3.1 Introduction 26
3.1.1 Overview of the engine model 26
3.1.2 Strategies of the engine model 29
3.2 Models for the Engine Processes 32
3.2.1 Model for thermodynamic processes in the cylinder 33
3.2.2 Model for the intake and exhaust flows 40
3.2.3 Engine friction model 41
3.3 Turbocharger Model 43
3.3.1 Turbocharger performance maps 43
3.3.2 Dynamic turbocharger model 54
3.4 Dynamic Engine Model 55
3.5 Particulate Calculation 59
3.6 Summary 60
4. EXPERIMENTAL APPARATUS 62
4.1 Engine Test Setup 62
4.2 Dilution Tunnels 65
4.3 Dilution Air System 68
4.4 Particulate Matter Measurements 70
4.4.1 Particulate sampling system 70
4.4.2 Particulate weighing chamber 74
4.5 Data Acquisition System 75
5. EXPERIMENTAL PROCEDURE AND DATA ANALYSIS . . . 77
5.1 Steady State Test Procedures 77

5.2 EPA Transient Test Procedures 80
5.3 Discrete Transient Cycle Tests 82
5.4 Procedure for Soluble Hydrocarbon Extraction 83
5.5 Data Analysis 84
5.5.1 Turbocharger performance 84
5.5.2 Calculation of particulate emission from measurements 85
5.5.3 Statistical analysis 88
6. RESULTS AND DISCUSSION 91
6.1 Model's Capability of Predicting Engine Performance Parameters . . 92
6.1.1 Boost pressure and temperature 92
6.1.2 Back pressure and temperature 101
6.1.3 Turbocharger speed 109
6.2 Model's Capability of Predicting Equivalence Ratio 116
6.3 Impact of EPA Transient Cycle Schedule on Particulate Emissions . . 128
6.3.1 Distributions of engine speed and equivalence ratio over an EPA transient cycle schedule 130
6.3.2 Discussion of trends of particulate emission 133
6.4 Model's Capability of Predicting Transient Particulate Emission . . . 138
6.4.1 Comparison of model prediction and measured transient particulate emissions during the EPA transient cycle 140
6.4.2 Comparison of model predictions and measured particulate emissions during four segments of the EPA transient cycle 142
7. CONCLUSIONS 146
7.1 Summary 146

7.2 Recommendations for Future Work 149

REFERENCES 151

APPENDIX A. DIFFERENTIAL EQUATIONS OF COMBUSTION MODEL 159

APPENDIX B. CALIBRATION OF PRESSURE TRANSDUCERS 161

APPENDIX C. CIRCUIT FOR THE LIGHT DETECTOR 163

APPENDIX D. FREQUENCY-TO-VOLTAGE CONVERTER CALIBRATION 165

D.1 60 Hz Frequency-to-Voltage Converter Calibration 165

D.2 1300 Hz Frequency-to-Voltage Converter Calibration 168

APPENDIX E. CALIBRATION OF THE DILUTION AIR SYSTEMS 170

E.1 Primary Dilution Air System Calibration 170

E.2 Secondary Dilution System Calibration 170

APPENDIX F. SAMPLING SYSTEM LEAK TEST 173

APPENDIX G. FILTER WEIGHING PROCEDURE 176

APPENDIX H. DIESEL FUEL FLOW RATE EQUATION AT STEADY-STATE CONDITIONS 180

LIST OF TABLES

Table 3.1: Polynomial coefficients for compressor pressure ratio and efficiency 48

Table 3.2: Polynomial coefficients for particulate emission 60

Table 4.1: John Deere 4276T four cylinder engine specifications 63

Table 4.2: Computer recorded measurements 76

Table 6.1: Comparison of model-predicted and measured boost pressures and temperatures 100

Table 6.2: Comparison of model-predicted and measured back pressures and turbine inlet temperatures 110

Table 6.3: Comparison of model-predicted and measured turbocharger speeds 115

Table 6.4: Comparison of model-predicted and measured air and fuel flow rates and experimental-calculated equivalence ratios 129

Table 6.5: Distributions of speed and equivalence ratio over an EPA transient cycle 130

Table 6.6: Distributions of speed and equivalence ratio over three different segments of an EPA transient cycle 132

Table 6.7: Soluble hydrocarbon extraction analysis 137

Table 6.8: Predicted and measured particulate emissions during EPA transient cycles 140

Table 6.9: Distribution of the particulate emission over the predicted equivalence ratios 142

Table 6.10: Predicted and measured particulate emissions over four segments of EPA transient cycles 143

Table B.1: Data for pressure transducers 162

Table G.1: Statistical data of reference filters 178

LIST OF FIGURES

Figure 2.1: Processes leading to the production of diesel particulates . . 10

Figure 2.2: Schematic diagram of the EPA-specified exhaust emissions sampling system (PDP-CVS) 16

Figure 3.1: Schematic of engine and turbocharger 28

Figure 3.2: Flow chart of engine model 30

Figure 3.3: Control volume for engine analysis 34

Figure 3.4: Compressor performance map from Garrett 45

Figure 3.5: Compressor performance map from tests 46

Figure 3.6: Combined compressor performance map 49

Figure 3.7: Turbine performance map from Garrett 52

Figure 3.8: Step input to the speed reference command of dynamometer 57

Figure 4.1: Schematic diagram of the primary and secondary dilution tunnels 66

Figure 4.2: Schematic diagram of particulate sampling system 71

Figure 4.3: Variations of the secondary dilution air flow rate 72

Figure 5.1: Reference speed and torque trajectories for the transient cycle 81

Figure 6.1: Comparison of model-predicted and measured boost pressures over the EPA transient cycle 94
Figure 6.2: Linear regression analysis on boost pressures 95
Figure 6.3: Comparison of model-predicted and measured boost pressure over the third segment of the EPA transient cycle 97
Figure 6.4: Comparison of model-predicted and measured boost temperature over the third segment of the EPA transient cycle . . . 98
Figure 6.5: Comparison of model-predicted and measured back pressures 102
Figure 6.6: Comparison of model-predicted and measured back pressure over the second segment of the EPA transient cycle 103
Figure 6.7: Linear regression analysis on back pressures 104
Figure 6.8: Comparison of model-predicted and measured turbine inlet temperatures 106
Figure 6.9: Comparison of model-predicted and measured turbine outlet temperatures 107
Figure 6.10: Comparison of model-predicted and measured turbocharger speeds over the EPA transient cycle 111
Figure 6.11: Linear regression analysis on turbocharger speeds 112
Figure 6.12: Comparison of model-predicted and measured turbocharger speeds over the second segment of the EPA transient cycle . 114
Figure 6.13: Comparison of model-predicted and experimental-calculated equivalence ratios 117
Figure 6.14: Linear regression analysis on equivalence ratios 118

Figure 6.15: Comparison of model-predicted and experimental- calculated equivalence ratios over the fourth segment of the EPA transient cycle 120
Figure 6.16: Comparison of model-predicted and measured air flow rates over the EPA transient cycle 121
Figure 6.17: Comparison of model-predicted and measured air flow rates over the fourth segment of the EPA transient cycle 122
Figure 6.18: Linear regression analysis on air flow rates 123
Figure 6.19: Comparison of model-predicted and measured fuel flow rates over the EPA transient cycle 124
Figure 6.20: Comparison of model-predicted and measured fuel flow rates over the fourth segment of the EPA transient cycle 125
Figure 6.21: Linear regression analysis on fuel flow rates 127
Figure 6.22: Particulate emissions vs. equivalence ratio ranging from 0.05 to 1.10 134
Figure 6.23: Particulate emissions vs. equivalence ratio ranging from 0.05 to 0.60 135
Figure 6.24: Particulate emissions vs. equivalence ratio ranging from 0.60 to 1.10 136
Figure 6.25: Cyclic particulate emission vs. equivalence ratio 139

Figure C.1: Circuit diagram for the light detector 164

Figure D.1: Calibration line for the 60Hz frequency-to-voltage converter . 166
Figure D.2: Sampling volume flow rate vs. voltage 167

Figure D.3: Calibration line for the 1,300 Hz frequency-to-voltage converter 168

Figure E.1: Calibration curve for secondary dilution air system 172

Figure F.1: Normal leak test results 175

Figure G.1: Temperature in the weighing chamber 177

Figure G.2: Relative humidity in the weighing chamber 177

Figure H.1: Diesel fuel flow rate as the function of engine speed and rack position 182

ACKNOWLEDGEMENTS

I am most grateful for the guidance and counsel that Dr. Jon H. Van Gerpen has generously provided throughout my research work. His dedication and attention to detail will always serve as a model for my own work in the future. I consider him to be a mentor and a friend.

I also extend my appreciation to Drs. Howard N. Shapiro, Robert C. Brown, Stephen J. Marley, and Ambar K. Mitra, for their patience and support as members of my graduate program of study committee.

I gratefully appreciate the friendship and support of Taner Tuken who was a graduate student during the course of my study at Iowa State University.

I wish to thank James Dautremont, Gaylord Scandrett, and Robert Steed for their technical support and assistance. The computer consulting services offered by Frank Poduska are greatly appreciated. I would also like to acknowledge the assistance provided by William Carr, Darren Herum, and Tryg Tow.

Finally, and most importantly, I want to thank my family for the tremendous support and love they have given me. My wife Fengling not only helped with drawing the diagrams, but also worked "overtime" at home during my absences to complete my experimental work and during the many hours I spent analyzing data and writing the dissertation. My daughter Angela often accompanied me to my office. Her

company and silly antics brought many smiles to my face, often when I needed them the most.

1. INTRODUCTION

1.1 The Need for this Investigation

Internal combustion engines have more than a century of history going back to the spark-ignition engine of Otto (1876) and the compression-ignition engine of Diesel (1892) [1]. Because of their simplicity, ruggedness and high power to weight ratio, these two types of engine have found wide application in land, sea, and air transportation as well as for stationary power generation. During the past three decades, new forces for change have become important and now significantly affect engine design and operation. The three most important forces are the need to control the automotive contribution to urban air pollution, the need to reduce automotive fuel consumption, and the need to compete in the global marketplace.

For the last half century, the diesel engine has been a popular choice for heavy- and medium-duty applications due to its proven superiority in fuel economy over the spark-ignition engine. In addition, most diesel engines have lower levels of unburned hydrocarbons and carbon monoxide emitted from their exhaust than comparable sized spark-ignition engines without after-treatment. The two types of engines emit comparable levels of nitrogen oxides. However, diesel engines emit a much greater quantity of particulate matter than spark-ignition engines.

Emission standards for passenger cars, trucks, and buses were introduced first in

California, then nationwide in the United States, starting in the early 1960s. Particulate emission control was first proposed in 1975 primarily for health and aesthetic reasons. The Environmental Protection Agency (EPA) started regulating diesel exhaust particulate matter from light duty vehicles in 1987. Since then, the amount of particulate matter emission permitted by the EPA has been regularly reduced. Current regulations allow 0.335 g/bkW-hr[1] (0.25 g/bhp-hr)[2] of particulate matter emission both for urban bus and truck engines until 1993. The 1993 and 1994 urban bus particulate standards are 0.134 g/bkW-hr (0.10 g/bhp-hr) and 0.067 g/bkW-hr (0.05 g/bhp-hr) respectively. For trucks, the proposed 1994 particulate standards are 0.134 g/bkW-hr (0.10 g/bhp-hr) [2]. To determine whether or not the engines meet the EPA standard, they are run over an EPA transient cycle while particulate matter is collected from the exhaust gas. The EPA transient cycle is a prescribed series of engine speeds and torques that simulates the driving conditions in both the New York and Los Angeles areas. The EPA also specifies that the temperature of the diluted exhaust gas should be lower than 325 K [3] when it enters the collection filter. This regulation ensures the diesel exhaust has been sufficiently mixed with air and that the actual exhaust-atmospheric air mixing process is simulated.

The future diesel emission standards for heavy-duty buses and trucks are a formidable challenge for engine manufacturers. Across a broad front of interrelated technical areas, a number of potential emission reduction strategies must be investigated within the regulatory time limits. These include: fuel quality, lubricant modifications, turbocharger response, turbocharger matching, transient response, control

[1] g/bkW-hr stands for grams per brake kilowatt-hour.

[2] g/bhp-hr stands for grams per brake horsepower-hour.

of the diesel combustion process, electronic engine control, heat rejection, catalytic converters, and particulate traps. In addition, the economic impact of all these engineering frontiers has to be considered.

To run a transient cycle, it is necessary to have a computer-controlled engine dynamometer and a sophisticated electronic control system. Since the diluted exhaust gas must be lower than 325 K, the dilution system becomes very large and the size of the equipment directly affects the cost. It is clear that conducting the EPA transient test is very expensive.

Computer models provide one option for evaluating engine particulate emission over the transient cycle without having to run expensive tests. Since the amount of particulate matter emission from a diesel engine depends mainly on fuel to air ratio and speed, steady-state measurements could be used to develop a functional relationship between the particulate emission and these engine operating parameters. If this were combined with a computer model which could predict the instantaneous engine fuel-air ratio over the transient cycle, the total amount of particulate matter emitted over the EPA transient cycle could be estimated.

A model of this type would rely on particulate emission data collected during steady-state tests, but it has the advantage of easily predicting the particulate emissions over different transient cycles. The flexibility of the model is beneficial for understanding the engine's transient response and controlling the particulate emission. Also, conducting the steady-state tests is much simpler than running the transient test. No sophisticated engine dynamometer is required and the engine speed and torque can be manually controlled at desired settings. The steady-state tests also do not require an exhaust sampling system capable of handling the full engine exhaust

flow. A dilution mini-tunnel which processes only a fraction of the engine exhaust can be used for steady-state particulate measurements [4, 5, 6, 7]. This type of model, combined with the steady-state tests, could provide an economic way to predict the particulate emission for transient cycles.

1.2 Research Goals

Very few attempts have been made to provide models for predicting diesel engine particulate emission during transient cycles. The objective of this study was to develop such a model.

The goals of the research were to:

1. develop an engine model to predict the instantaneous engine fuel-to-air ratios over a transient cycle;
2. predict the engine particulate emission for different transient cycles, based on the model-predicted engine fuel to air ratio and measured steady-state particulate emission data; and
3. verify the model using experimental data obtained from transient testing.

1.3 Dissertation Organization

The organization of this dissertation is given as follows. Chapter 1 provides a general introduction to the problem of predicting diesel engine particulate emissions. Chapter 2 provides a literature review on diesel engine combustion and particulate emission, on particulate measurements, and on models predicting particulate emission. Chapter 3 is devoted to the development of the computer model, which consists

of a quasi-steady-state engine combustion model, a dynamic turbocharger model, and a dynamic engine model. The experimental set-up for the tests is presented in Chapter 4. Chapter 5 covers the procedures for the steady-state tests, the transient tests, and discrete transient cycle tests. Chapter 6 discusses comparisons between model predictions and experimental data. The conclusions are summarized in Chapter 7. Appendices provide additional details on the important differential equations for the model, the design of the experimental apparatus, and the calibration of the equipment.

2. LITERATURE REVIEW

This literature review is divided into three sections. The first section is a review of diesel combustion and emission processes. The second section is a review of particulate measurements and the last section is a review of recent diesel particulate emission modeling.

2.1 Combustion and Emissions in Diesel Engines

2.1.1 Combustion

The diesel combustion process is an extremely complex phenomenon. It is an unsteady, heterogeneous, three-dimensional combustion process. It involves the burning of a liquid fuel spray under transient operating conditions [8]. Although an adequate conceptual understanding of diesel engine combustion has been developed, to date a quantitative evaluation for the process is still lacking [1].

The fuel and air are not premixed initially in the compression-ignition or diesel engine. In the diesel engine, air alone is compressed and raised to a high temperature and pressure on the compression stroke. One or more jets of fuel, usually at high velocity, are introduced into the combustion chamber toward the end of the compression stroke, just before the desired start of combustion. The fuel vaporizes, mixes with the high-temperature and high-pressure turbulent air, and undergoes chemical

pre-combustion reactions. The fuel does not ignite immediately. There is a time period called the ignition delay, during which the fuel undergoes heating, vaporization, mixing and the pre-reactions. The duration of this delay depends on the engine design and the fuel type [9].

After the delay period, usually a few degrees of crankshaft rotation, spontaneous ignition will occur at regions where the mixture has fuel-air ratios close to stoichiometric. The cylinder pressure and temperature are increased due to the rapid combustion of the physically and chemically prepared charge. The resulting compression of the unburned portion of the fuel-air mixture shortens the delay for that mixture. The rate for the subsequent combustion depends on how fast the air is entrained into the fuel rich zones and a combustible mixture formed [10, 11, 12, 13].

2.1.2 Diesel emissions

In the diesel engine, the pollutants come from three sources: the exhaust pipe, the crankcase breather, and the fuel tank breather. The exhaust pipe is the primary source with from 65 to 85 percent of the diesel engine's pollutants passing through it.

The ideal exhaust gas should contain only nitrogen, oxygen, water vapor, and carbon dioxide. Due to the nature of the diesel combustion discussed in Section 2.1.1, the exhaust gas also contains particulates of solid carbon, unburned hydrocarbons, oxides of nitrogen, carbon dioxide, carbon monoxide and traces of alcohols, aldehydes, ketones, phenols, acids, esters, ethers, epoxides, peroxides, and other oxygenates. Currently, there are only four regulated exhaust constituents. These pollutants are oxides of nitrogen (NO_x), unburned hydrocarbons (HC), carbon monoxide (CO),

and particulate matter (PM) which includes soot, or solid carbon, sulfates, and condensed hydrocarbons, sometimes called the soluble organic fraction (SOF) [3].

The nature of the mixing controlled combustion process is important in understanding the sources of the air pollutants. In the diesel engine, the fuel is injected into the combustion chamber just before the end of the compression stroke, so throughout most of the critical parts of the cycle the fuel distribution is nonuniform. The pollutant formation processes are strongly dependent on the fuel distribution and how that distribution changes with time due to mixing. The fuel spray and air entrainment region is divided into the fuel-rich zone, where soot formation occurs, the intense reaction zone, which is responsible for the heat release and NO_x formation, and the lean outer zone, which is the source of most of the unburned hydrocarbon formation due to flame quenching and in which most of the soot oxidation takes place. Since this dissertation is primarily concerned with diesel particulate emission, the sources of NO_x, HC, and CO emissions will not be discussed here. Further information on these species is provided in reference [1].

2.1.3 Particulate matter

Particulate matter is defined by the EPA as any diesel exhaust substance other than water that can be collected by filtering the diluted exhaust at or below 325 K [3]. The material collected on the filter is generally classified into three parts: solid carbon material or soot, sulfate, and the soluble organic fraction (SOF) that is composed of unburned fuel and lubrication oil, and their partial oxidation products [14]. Needham et al. [15] presented measurements of the particulate composition from 16 heavy-duty turbocharged diesel engines in their literature review. They found that soot makes

up 41.0% of the total particulate emission, unburned oil is 25.0%, sulfate and water are 14.0%, unburned fuel is 7.0%, and unaccounted for substances are 13.0%.

This section discusses the particulate formation processes including soot formation, soot oxidation, and adsorption and condensation of hydrocarbons. Most of the information available on the fundamentals of soot formation in combustion comes from studies in simple premixed and diffusion flames, stirred reactors, shock tubes, and constant-volume combustion bombs. However, these studies are not able to explain the soot formation process in diesel engines due to the unique characteristics of diesel combustion—the high gas temperatures and pressures, the complex fuel composition, the dominance of turbulent mixing, the unsteady nature of the process, and the three-dimensional geometry. Therefore, soot formation in the diesel engine is poorly and incompletely understood.

The following conclusions are primarily derived from a review of the technical literature written by Haynes and Wagner [16]. Figure 2.1 shows the processes involved in particulate formation. Soot formation takes place in the diesel combustion environment at temperatures between about 1000 and 2800 K, at pressures of 50 to 100 bar, and with sufficient air overall to fully burn the fuel. Equilibrium considerations indicate that soot formation should occur when the carbon/oxygen ratio in the fuel-oxidizer mixture exceeds unity. However, it is generally recognized that soot formation is a nonequilibrium process. Experimentally observed critical C/O ratios range from about 0.5 to 0.8. The time available for the formation of solid soot particles from a fraction of the fuel (containing 12 to 22 carbon atoms) is on the order of milliseconds.

The production of diesel particulates can be divided into two stages: particle

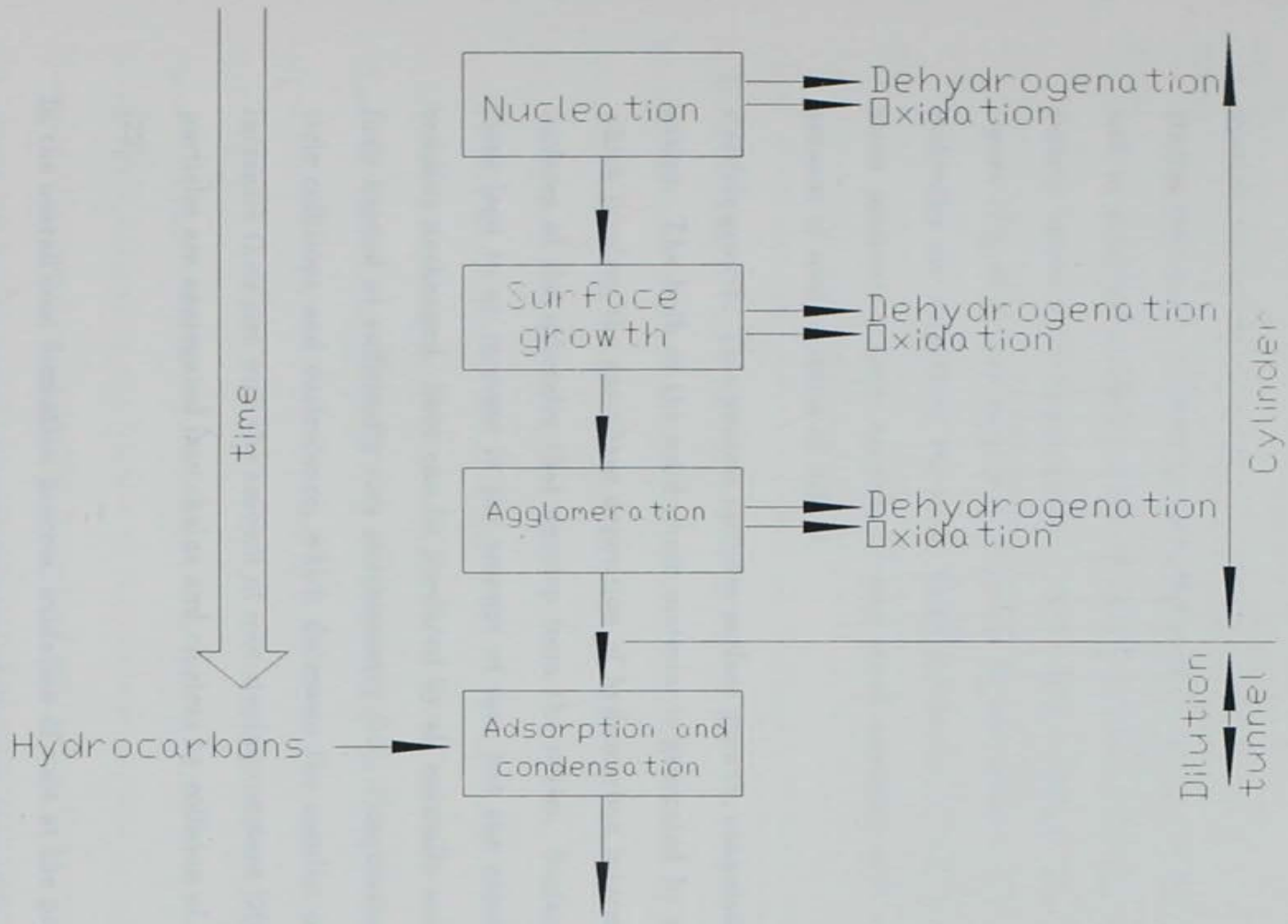

Figure 2.1: Processes leading to the production of diesel particulates[17]

formation and particle growth. These two stages are described as follows.

1. Particle formation: The particle formation process is also called nucleation. During this stage, the first condensed-phase material arises from the oxidation and/or pyrolysis products of fuel molecules. These products typically include various unsaturated hydrocarbons, particularly acetylene and its higher analogues ($C_{2n}H_2$), and polycyclic aromatic hydrocarbons. These two types of molecules are considered the most likely precursors of soot in flames. Nucleation produces a large number of very small particles with an insignificant amount of soot in terms of weight.

2. Particle growth: This process includes surface growth, coagulation, and aggregation. The bulk of the solid-phase material is generated by surface growth, which involves the gas-phase deposition of hydrocarbon intermediates on the surfaces of the spherules that develop from the nuclei. Surface growth reactions lead to an increase in the amount of soot but the number of particles remains unchanged. Soot can be produced by all normally used hydrocarbon fuels burned at sufficiently rich stoichiometry [19]. Coagulation involves particle collisions and coalescence, which decreases the number of particles and increases their size with the amount of soot staying constant [20, 21]. Then the particles are aggregated into chains and clusters by collision of larger particles [22].

In the overall soot formation process, oxidation of soot at the precursor, nuclei, and particle stages can occur. A large fraction of the soot formed is oxidized within the cylinder before the exhaust process commences. The soot oxidation process in

the diesel cylinder is kinetically controlled since particle sizes are in the 0.01 to 1.0 μm diameter range [21]. There are many species in or near the flame that could oxidize the soot such as O_2, O, OH, CO_2. The eventual emission of soot from the engine will depend on the balance between the processes of formation and burn-out [17, 16, 23].

The final process in the particulate formation sequence is adsorption and condensation of hydrocarbons. This occurs primarily after the cylinder gases have been exhausted from the engine, as these exhaust gases are diluted with air [24]. In the standard particulate mass emission measurement process this occurs in a dilution tunnel which simulates the actual atmospheric dilution process. The measurement involves filtering a diluted exhaust gas sample to remove the particulate. After equilibrating the filter at temperature and humidity controlled conditions to remove water, the particulate mass is obtained by weighing. In the prescribed EPA procedure, the filter temperature must not exceed 325 K.

The total particulate mass is partitioned into the insoluble organic fraction (IOF), the soluble organic fraction (SOF), and the sulfate. The IOF consists mainly of carbon soot generated during combustion and is not affected by the dilution process. The SOF is controlled by both adsorption and condensation, which occur during the dilution process. Adsorption involves the adherence of molecules of unburned hydrocarbons to the surfaces of the soot particles by chemical or physical forces. This depends on the fraction of the available particle surface area occupied by hydrocarbons and on the partial pressure of the gaseous hydrocarbons that drives the adsorption process. Condensation will occur whenever the vapor pressure of the gaseous hydrocarbon exceeds its saturated vapor pressure. High exhaust concentra-

tions of hydrocarbons are the conditions where condensation is likely to be most significant, and the hydrocarbons most likely to condense are those of low volatility. Sources of low-volatility hydrocarbons are the high-boiling-point fraction of the fuel, unburned hydrocarbons that have been pyrolyzed but not consumed in the combustion process, and the lubricating oil [17]. The adsorbed and condensed high molecular weight organic compounds include: unburned hydrocarbons, oxygenated hydrocarbons(ketones, esters, ethers, organic acids), and polynuclear aromatic hydrocarbons. The condensed material also includes inorganic species such as sulfur dioxide, nitrogen dioxide, and sulfuric acids (sulfates) [17, 18].

Both soxhlet and sonification methods are used to extract the organic fraction from particulate samples. Two commonly used solvents are methylene chloride (dichloromethane) and a benzene-ethanol mixture. Typically 15 to 30 mass percent is extractable, though the range of observations is much larger (approximately 25 to 75 percent) [25]. Thermogravimetric analysis (weighing the sample as it is heated) produces comparable results [14].

2.2 Particulate Emission Measurements

The future of diesel engines, while brightened by significant fuel economy advantages over gasoline engines, is partly clouded by their higher particulate emissions. Increased attention to this problem has led to appreciable reductions in particulate emissions. As emission levels are further reduced there is a need to determine the origin of the remaining particulate emissions in terms of engine operating mode. This section presents the methods used to measure soot and particulate emissions, both in-cylinder and in the exhaust.

2.2.1 In-cylinder measurements of particulate

Starting from the middle of the 1970s, researchers have developed numerous methods to measure soot emission from an engine cylinder. These methods can be divided into two categories: the direct sampling method and optical methods. Direct sampling means the combustion products are directly sampled from the cylinder. Optical methods have been applied to measure the radiation properties of the combustion products in order to study the formation and the oxidation processes of soot particles.

The direct sampling method has been extensively used at the University of Minnesota [26, 27, 21, 28, 29, 30]. Direct sampling experiments, which are also called blowdown or dumping experiments, were used to sample the entire contents of the cylinder during combustion. The method allows the contents of the cylinder to rush out into a sample bag where they are quenched and diluted. Then they were analyzed for chemical composition or aerosol properties.

Norris-Jones et al. [31] used a direct sampling method to study the formation of particulates in the cylinder of a direct injection diesel engine in combination with a high speed combustion photography technique. The direction and location of a sampling probe could be changed so that a comprehensive map of in-cylinder particulate formation could be established. The products of combustion were sampled through a glass fiber filter and the particulate density in the cylinder was determined by thermogravimetric analysis. Lida and Sato [32] applied a direct sampling method combined with a freezing technique to study particulate shape, structure, and size distribution in the diesel cylinder. Sampled gas was introduced to a freezing dilution mini-tunnel and cooled rapidly to the temperature of about 343 K with low temper-

ature air at 153 K, which had evaporated from liquid air. By the thermophoresis effect, the particulates in the diluted gas were caught on a frozen sampling mesh, kept at or below 153 K, located downstream of the freezing dilution mini-tunnel. This method was expected to preserve the original chemical and physical properties of the particulates in the combustion chamber.

Although the direct sampling techniques provide useful information, they have several defects such as disturbing the flow field when sampling probes are used, difficulties in measuring the soot concentration near the piston surface except at around top dead center, and giving poor time resolution due to a rather long valve opening duration. To eliminate these problems, researchers have applied optical methods to investigate in-cylinder soot characteristics. The Two-Color Method was used by Matsui et al. [33, 34] and Yan et al. [35]. The method determines the flame temperature and the emissivity of the luminous flame by measuring radiation emitted by soot particles at two wavelengths. The soot concentration in the cylinder can be expressed as a function of the KL factor, where K is the absorption coefficient and L is the flame thickness along the optical path. K and L can be determined from the experiments. The soot concentration in the combustion chamber can be converted into a concentration under atmospheric conditions. Other optical methods such as extinction and scattering were used by Wersborg and Haynes[36, 37, 38].

2.2.2 Measurement of particulate matter

According to the specifications in the Code of Federal Regulations, the particulate matter should be measured with a full-scale EPA-specified system [3]. A schematic diagram of this system is shown in Figure 2.2. This system is called a pos-

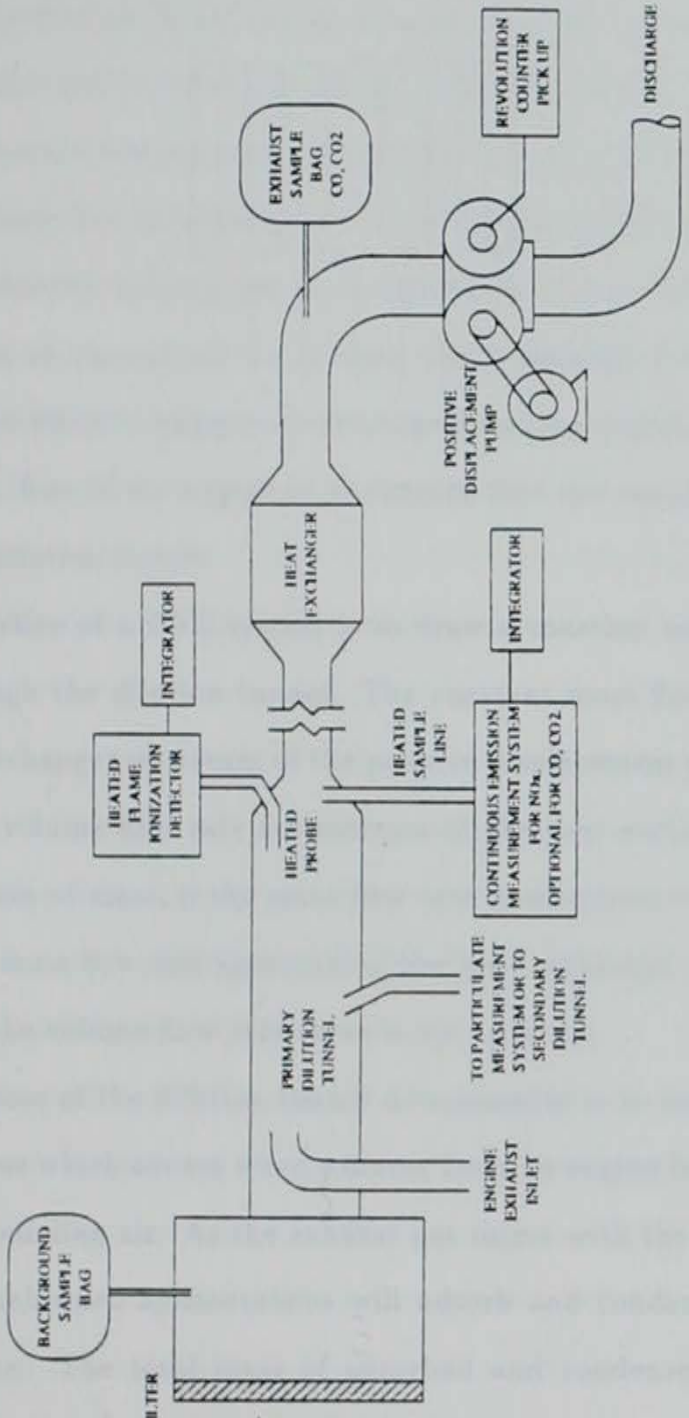

Figure 2.2: Schematic diagram of the EPA-specified exhaust emissions sampling system (PDP-CVS) [39]

itive displacement pump-constant volume sampler (PDP-CVS). PDP-CVS systems maintain constant mass flow through the measurement system even when the engine exhaust flow rate and temperature change. They do this by using a heat exchanger to maintain a constant temperature and pressure through a positive displacement pump. The total volume flow is measured by counting the pump revolutions. Proportional sampling is achieved by sampling at a constant flow rate. The positive displacement pump, located at the exit of the system, draws ambient air through a filter into a dilution tunnel where it mixes with the exhaust of the engine being tested. Since the entire exhaust flow of the engine is introduced into the tunnel, the tunnel is termed a "full-flow" dilution tunnel.

The objective of a CVS system is to draw a constant mass flow rate of diluted exhaust through the dilution tunnel. The constant mass flow rate can be achieved by the heat exchanger upstream of the positive displacement pump because the temperature and volume flow rate downstream of the heat exchanger are constant. By the conservation of mass, if the mass flow rate downstream of the heat exchanger is constant, the mass flow rate upstream of the heat exchanger should also be constant even though the volume flow rate there is not constant.

The purpose of the dilution tunnel measurement is to simulate the atmospheric dilution process which occurs when exhaust from an engine leaves a stack and mixes with the surrounding air. As the exhaust gas mixes with the atmosphere and cools, some of the unburned hydrocarbons will adsorb and condense onto the surface of the particulate. The total mass of adsorbed and condensed hydrocarbons is the soluble organic fraction (SOF) of the particulates. The dilution tunnel is intended to collect and measure any particulate material, either solid or liquid, which would

be present following such a dilution process. Any material collected on a filter under these conditions is defined as "particulate." Sometimes a secondary dilution tunnel is used to achieve the correct temperature reduction and increase the length of mixing process.

The particulate sample is collected by passing a portion of the diluted exhaust through a filter. The best filters have been determined through experience to be Teflon-coated fiberglass [40, 41]. The flow rate of diluted exhaust passing through the filter must be a constant mass fraction of the total diluted exhaust flow rate so that the amount and type of particulate emitted by the engine during the test will be accurately represented on the filter. The particulate sample must be taken upstream of the heat exchanger otherwise a large amount of the particulate matter would be lost on the surfaces of the heat exchanger and the hydrocarbons would be condensed and deposited before sufficiently mixed with atmospheric air.

It is clear that a PDP-CVS system is very expensive. They can not always be built in a given engine laboratory because of its needs, size, and budget. Hence, researchers have often simplified the EPA dilution tunnels and developed their own dilution tunnel systems for their purposes.

Harrington and Yetter built a particulate measurement system suitable for steady-state tests on small, single cylinder engines [5]. A fraction of the engine exhaust was admitted to a dilution mini-tube. The tube flow rate could be held constant for a five minute steady-state test. The experimental results showed that the dilution mini-tube design could provide particulate mass measurements that agree to within 10% of those made with a full-flow dilution tunnel. Thus, this simplified dilution tunnel design meets the needs of its designers for much less money and space than

a complete full-flow EPA-type system. Cornetti et al. [7] used a similar dilution mini-tunnel for tests of the European 13-mode cycle. Their repeatability test results showed that an average coefficient of variation (the standard deviation divided by the mean) was equal to or less than five percent. Comparing both the mini-tunnel system and the EPA system on a mode to mode basis, there were no significant differences for total particulate and volatiles. However, these dilution mini-tunnel systems were not adequate for transient tests because the system could not maintain a constant sampling fraction from the engine exhaust.

Suzuki et al. [6] set up a dilution mini-tunnel for particulate measurements during transient operating cycles. A fraction of the total exhaust gas was drawn into the tunnel by an air ejector. The system was capable of drawing a roughly constant fraction of the total exhaust into the tunnel. Thus, transient tests could be performed with this system. Statistical analysis has shown that the mini-tunnel measurements were directly proportional to the full-flow tunnel measurements with a correlation coefficient of 0.998. The particulate matter measured in the mini-tunnel was about 10% lower than that measured in the full-flow tunnel. The system retained many of the features of the EPA system but with smaller size and lower cost. Hirakouchi et al. [42] developed a multi-tube type of dilution mini-tunnel to measure exhaust emissions for both steady-state and transient mode operating conditions. The size of their mini-tunnel was reduced to approximately 20% of the full-flow dilution tunnel. The correlation coefficient for particulate measurements from the two tunnels was greater than 0.97.

The dilution tunnel built in the ISU engine laboratory is a full-flow dilution tunnel. The tunnel was originally designed to investigate the effect of alcohol fumigation

on diesel engine emissions. The present research was to use the tunnel to measure the particulate matter from both steady-state and transient tests. The nominal dilution ratio was kept the same for both tests at the same operating conditions because the dilution air flow rate was constant. The particulate sampling flow rate was also constant. Since the objective for both cases was not to try to determine whether or not the engine met the EPA emission standards, an EPA-type system was not essential. In addition, the design of the tunnel was greatly constrained by factors of cost and space. The details of the design appear in Section 4.2.

2.3 Modeling Particulate Emission

As discussed in Section 2.1.3, the processes leading to the net production of diesel particulates include nucleation, surface growth, and agglomeration, which take place in the engine cylinder, and adsorption and condensation of hydrocarbons in the dilution tunnel. The oxidation of soot can occur simultaneously with the first three processes. Although researchers have developed numerous mathematical models to predict particulate emission, the mechanisms of particulate production are still far from being understood.

This section presents: (1) the models which simulate the processes of soot formation and soot oxidation; (2) the models which predict transient particulate emission; and (3) the models which predict engine performance parameters.

2.3.1 Modeling steady particulate emission

Khan and Greeves modeled the overall soot production process, including the formation and oxidation of soot precursors, nucleation, and heterogeneous particle

growth, by an Arrhenius exponential expression [43, 44]. Following formation, the particles were assumed to undergo coagulation or agglomeration in accordance with the Whytlaw-Gray equation [45]. The surface oxidation process alone could be expressed according to global kinetic equations [43, 44, 46].

Mehta et al. [47] developed a sophisticated computer model, which simulated both soot formation and soot oxidation processes, for predicting in-cylinder and exhaust soot emissions from direct injection engines. The authors used a two-dimensional, multi-zone, phenomenological spray mixing combustion model to predict flame temperature, equivalence ratio, and engine cylinder pressure. The equivalence ratio here is defined as the ratio of the actual fuel-to-air ratio to the stoichiometric fuel-to-air ratio. Compared with the experimental measurements which came from three sources at various engine design and operating conditions, the model predicted the in-cylinder and exhaust soot concentration reasonably well. The effects of injection timing, fueling rate, and swirl ratio on the soot emissions were also investigated by the model.

These models predict the soot emission without running the engine and can be used to investigate the effects of engine design parameters and fuel and oil properties on the particulate emissions for steady-state conditions. However, these models are so complex that they can not be used to predict the particulate emissions during transient cycles. They would require excessive computer time if applied over large numbers of engine cycle events.

2.3.2 Modeling transient particulate emission

Callahan et al. [48] have developed an empirically-based model which can predict particulate and gaseous emissions during transient cycles. The model can be broken up into two components. The first component consists of the average effect, the emission level due to an average speed and torque. The second component reflects deviations from the average effect due to the rate of speed and torque changes. The model was developed in such a way that the emission level predicted by the model for a transient segment results from the combination of two terms. The first component is based on the average and the second effect contains rate of change information. A regression analysis was performed to determine the effects of changes in speed and torque and the rate of change of speed and torque on the emissions, which were sampled for discrete segments of 27 transient cycles. For each transient cycle, there were four distinct segments. The first segment was a transient portion in which torque and speed varied. Then, the torque and the speed were held constant in the second segment. The third segment was another transient, followed by the fourth segment, a steady-state segment. The coefficients of determination for the prediction of emission values by the model were 0.9611 for NO_x, 0.9152 for HC, 0.9081 for CO, and 0.8090 for particulates.

Callahan and co-workers [49] continued their research and developed another version of the model. The differences from the previous work were as follows. First of all, the test matrix was modified so that it represented 120 individual discrete segments of transient cycles. Second, the effects of the independent variables were better defined and normalized. Third, the relative error between the reference work and the actual work from the engine was considered, which resulted in a total of 15

independent variables. With the new model, the coefficients of determination were changed into 0.9656 for NO_x, 0.8964 for HC, 0.8887 for CO, and 0.9123 for particulates. The capability of predicting particulate matter by the model was considerably improved.

Abe et al. [50] investigated the particulate emissions from two diesel powered passenger cars by calculation and experiment. The estimation of the particulate emissions was based on the assumption that the exhaust gas particulate concentration is determined by the engine speed and the vehicle traction force. The exhaust particulate concentration was expressed as a function of the engine speed and traction force, which was developed from steady-state tests. There were three weighting factors applied to three zones of the engine load: loads below 20%, loads between 20% and 80%, and loads greater than 80% of the rated load. The objective was to apply particulate emission characteristics obtained during steady engine operation to transient engine operation. The total particulate matter emission in a given distance of a driving pattern was estimated relatively well by the model although no statistical information was provided.

The effect of engine load on the particulate emissions has been considered for the models mentioned above. However, the load is not as useful as the equivalence ratio for predicting the particulate emission. The key is that there exists a turbocharger "lag" when the rack position of the engine fuel pump quickly changes to increase the engine torque. The increase in fuel supply to the engine does not result in an instantaneous response of the turbocharger, due to its inertia and the compressibility of the exhaust gas line from the engine. The air mass flow rate initially remains constant, resulting in a rich fuel-air ratio. Too rich a mixture causes poor combustion,

high soot and HC emissions, and a slow increase in engine torque output. Hence, in some cases the engine has the same torque output but different equivalence ratios. It is appropriate to investigate the effect of the engine equivalence ratio rather than the engine load on the particulate emission because the engine load is too ambiguous to be used in this case. In view of this fact, the computer model developed in this study considers the effects of equivalence ratio and speed on particulate emission.

2.3.3 Modeling engine performance

Since the instantaneous equivalence ratio is extremely difficult to measure accurately under transient conditions, researchers have been working for decades to develop models to predict the transient response of a turbocharged diesel engine. The existing models can be classified as linear, quasi-linear, and non-linear models.

The linear models are based on either continuous control [51] or sampled-data concepts [52]. But the models generally cannot represent the true non-linearity of the engines. Benson et al. [53] developed a quasi-linear model which linked steady-speed experimental data representing engine thermodynamics and gas flow with dynamic models for the mechanical components. The major disadvantage of quasi-linear models is their heavy reliance on experimental data. Watson and Marzouk [54] developed their non-linear mathematical model to predict the transient response of a turbocharged diesel engine by using the quasi-steady "filling and emptying" concept. The model was capable of continuously evaluating the dynamic interactions of engine components. Good agreement between predicted and measured engine performance was obtained.

Although the non-linear models are capable of accurate performance prediction

under both steady and transient conditions, the computing time and cost for running the simulations are significant. Diesel engine manufacturers still prefer to use quasi-linear models. Tsai and Goyal [55] used their improved quasi-linear model for control analysis and design. The improved model had the capability of predicting engine transient response over a broad operating range. The engine combustion model was based on Borman [56] and McAulay et al. [57]. The mass rate of burning was obtained using a semi-empirical equation. The performance of the compressor and the turbine were derived from steady-state performance charts. The turbocharger dynamics dealt with turbocharger speed, acceleration, and deceleration. Srivastava's model [58] was used to calculate the turbocharger speed at the next time step. The engine load was both speed and time-dependent. The governor dynamics were represented by a second order differential equation based on a single mass, single degree of freedom system including centrifugal forces. Finally, the fueling rate was interpolated using the two-dimensional coordinates, the engine speed and the rack position. Tsai and Goyal compared their quasi-linear model to a non-linear model and found good agreement of the computational results.

Despite the fact that the transient models have been reported in the literature, there is a scarcity of models that predict engine performance over the EPA transient cycle. It would be impractical to run most of the existing models over a 1,200 second cycle because of excessive computation time. During the development of the author's model, both simplicity and accuracy were emphasized.

3. DEVELOPMENT OF THE ENGINE MODEL

This chapter covers the development of the overall engine model. The chapter is divided into six sections. The first section gives an introduction to the engine model. Models for the engine energy and mass flows are presented in the second section. The turbocharger model and the dynamic engine model are discussed in the third and fourth sections. The fifth section shows how particulate emission is calculated over a transient cycle. Finally, the sixth section gives a summary of the model.

3.1 Introduction

3.1.1 Overview of the engine model

The purpose of developing an engine model was to predict particulate emission during transient cycles. As discussed in Sections 1.1 and 2.3.3, the particulate emission primarily depends on the overall equivalence ratio and the engine speed. The relationship between the particulate emission and the overall equivalence ratio and speed can be established. The term overall equivalence ratio is defined as the equivalence ratio based on the fuel and air flow rates into the engine. Thus, to predict particulate emission, the model must have the capability of predicting instantaneous overall equivalence ratio during a transient cycle.

Since the overall equivalence ratio is determined by the rates of actual fuel and

air flow to the engine, the model must have the ability to predict these quantities. The amount of fuel that enters the engine combustion chamber depends on the torque required for a testing schedule such as the EPA transient cycle. The turbocharger characteristics determine the amount of air entering the engine. Since it is the hot, pressurized exhaust gas that drives the turbocharger, the combustion process affects the operating conditions of the turbocharger. Hence, it is essential for the engine model to have a sub-model to simulate the engine combustion processes combined with a sub-model for the turbocharger characteristics. In addition, in order to simulate transient operation, the model must properly account for the engine and turbocharger dynamics.

The engine and turbocharger to be simulated is shown in Figure 3.1. The number of stations and the symbols are defined as follows:

1 = the compressor inlet,

2 = the compressor outlet,

3 = the turbine inlet,

4 = the turbine outlet,

C = the compressor,

T = the turbine,

$\dot{m}_a$=the rate of air flow entering the engine,

$\dot{m}_f$=the rate of fuel flow entering the engine,

$\dot{m}_{out}$=the rate of the exhaust gas exit the engine, which is equal to the sum of $\dot{m}_a$ and $\dot{m}_f$ if minor losses are neglected,

P_{shaft}=the power output from the engine shaft, and

$\dot{Q}$=the heat transfer between the engine and the surroundings.

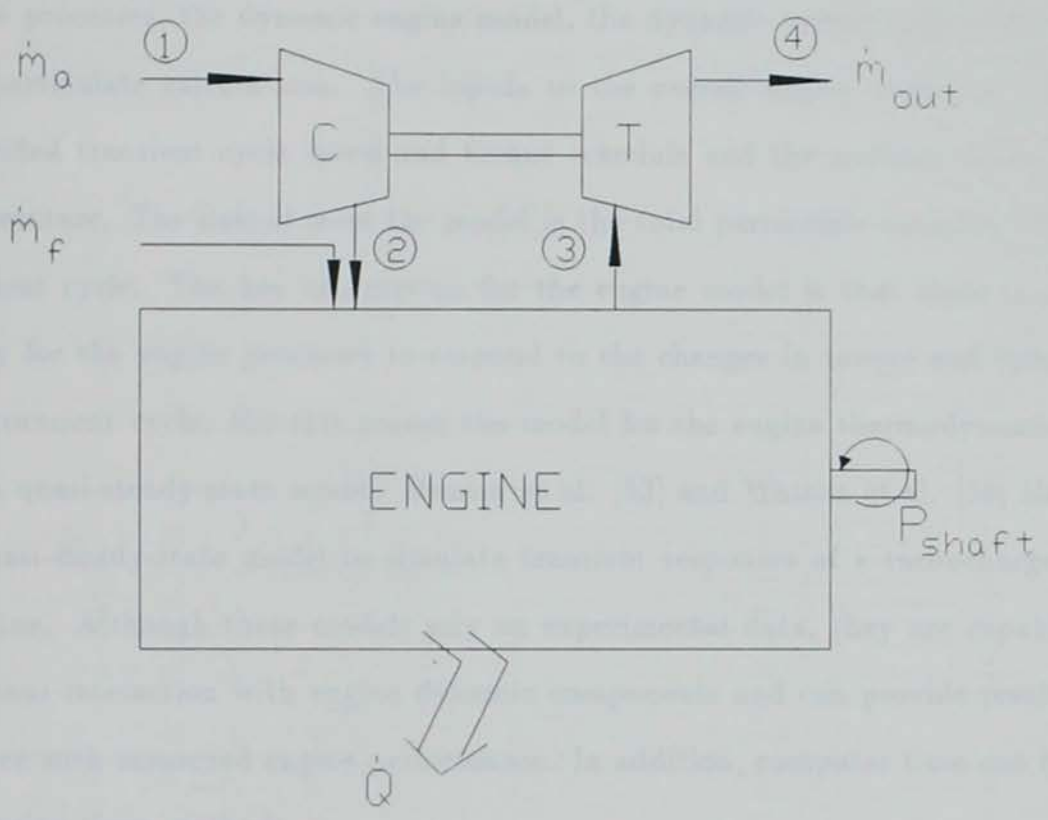

Figure 3.1: Schematic of engine and turbocharger

3.1.2 Strategies of the engine model

Figure 3.2 shows the flow chart of the engine model. It can be seen that the engine model is composed of the turbocharger performance maps, the sub-model for the engine processes, the dynamic engine model, the dynamic turbocharger model, and the particulate calculations. The inputs to the overall engine model are the EPA specified transient cycle speed and torque schedule and the ambient pressure and temperature. The output from the model is the total particulate emission over the transient cycle. The key assumption for the engine model is that there is no time delay for the engine processes to respond to the changes in torque and speed over the transient cycle. For this reason the model for the engine thermodynamics is called a quasi-steady-state model. Benson et al. [53] and Watson et al. [54] also used a quasi-steady-state model to simulate transient responses of a turbocharged diesel engine. Although these models rely on experimental data, they are capable of continuous interaction with engine dynamic components and can provide results which agree with measured engine performance. In addition, computer time can be saved by using these methods.

Figure 3.2 also illustrates the initial values for the overall engine model, the inputs and outputs to and from each individual model, and the loops for iterations each individual model. It is noted that the initial value for the dynamic turbocharger model was ω_0, which is the turbocharger angular velocity when the engine is run at the first data point specified by the testing schedule. For this study, ω_0 was determined from an experimental measurement. The following discussion of Figure 3.2 describes the flow path of the model computation.

To start the engine model, initial estimates for the air and fuel flow rates are as-

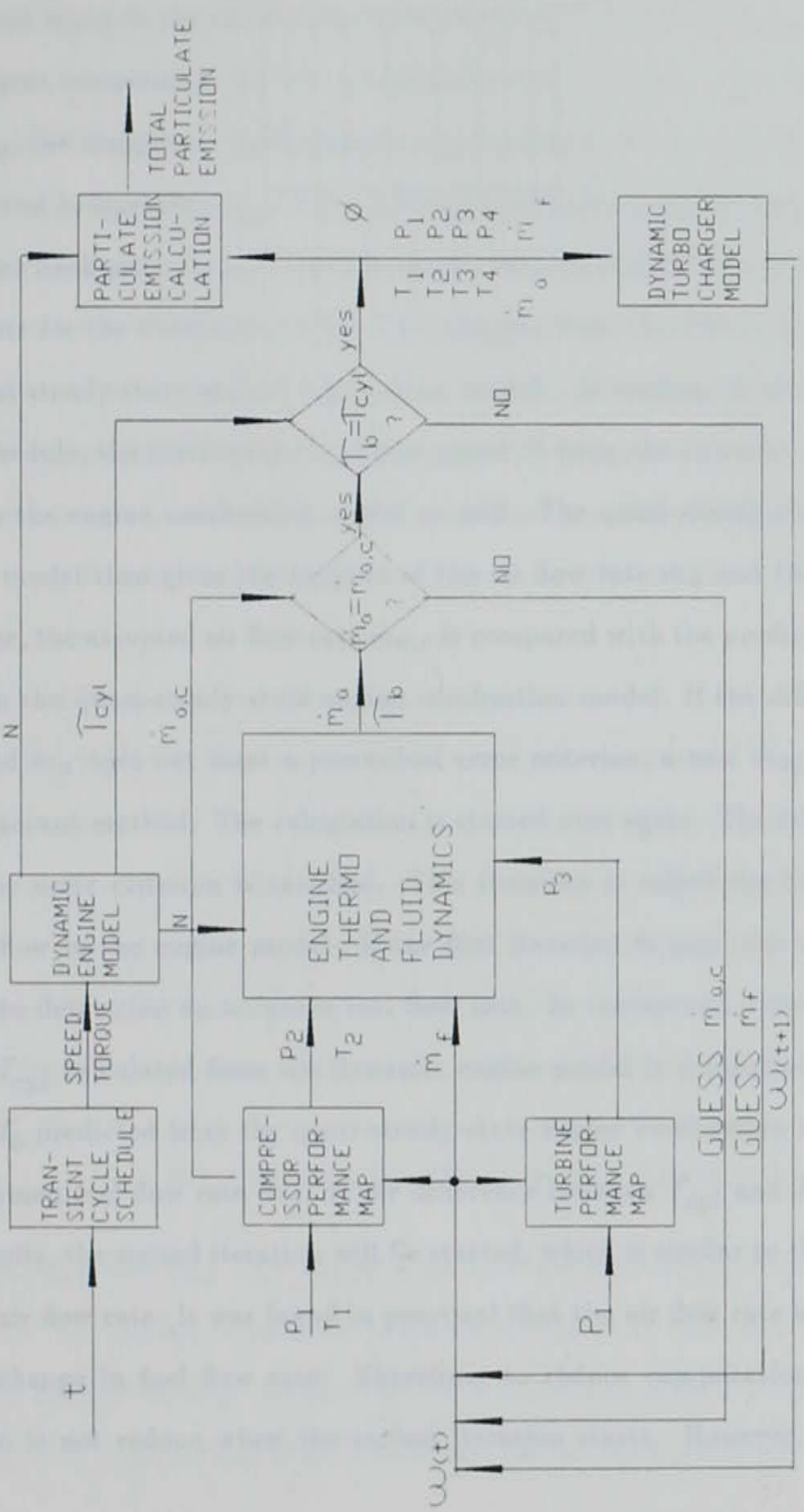

Figure 3.2: Flow chart of engine model

sumed and input to the simulation. With the inputs of the atmospheric pressure p_1, the ambient temperature T_1, the assumed air flow rate $\dot{m}_{a,c}$, and the turbocharger speed ω_0, the compressor performance map generates the outputs of the boost pressure p_2 and temperature T_2. The turbine performance map generates an output of the engine back-pressure p_3 with an assumed value of the fuel flow rate in addition to the inputs for the compressor map. The outputs from the turbocharger maps enter the quasi-steady-state engine combustion model. According to the EPA transient cycle schedule, the instantaneous engine speed N from the dynamic engine model is input to the engine combustion model as well. The quasi-steady-state engine combustion model then gives the outputs of the air flow rate $\dot{m}_a$ and the torque $\mathcal{T}_b$. At this stage, the assumed air flow rate $\dot{m}_{a,c}$ is compared with the predicted air flow rate $\dot{m}_a$ from the quasi-steady-state engine combustion model. If the difference between $\dot{m}_{a,c}$ and $\dot{m}_a$ does not meet a prescribed error criterion, a new $\dot{m}_{a,c}$ is assumed by using a secant method. The calculation is started over again. The iteration will stop when the error criterion is satisfied. This iteration is called the first iteration for the air flow in the engine model. If the first iteration is past, the second iteration follows to determine an accurate fuel flow rate. In the second iteration, the engine torque $\mathcal{T}_{cyl}$ calculated from the dynamic engine model is compared with the brake torque $\mathcal{T}_b$ predicted from the quasi-steady-state engine combustion model, based on the assumed fuel flow rate $\dot{m}_f$. If the difference between $\mathcal{T}_{cyl}$ and $\mathcal{T}_b$ is beyond the error limits, the second iteration will be started, which is similar to the first iteration for the air flow rate. It was found in practical that the air flow rate was not sensitive to the change in fuel flow rate. Therefore, to reduce computation time, the first iteration is not redone when the second iteration starts. However, to finish either

the first or the second iteration, the quasi-steady-state engine model will be called as many times as needed to meet the specified error criteria set for the air flow rate and the torque. The final air and fuel flow rates, which come from the quasi-steady-state engine model, are used to calculate the instantaneous overall equivalence ratio, ϕ.

The particulate emission is calculated with the provided values of the engine equivalence ratio and speed. Using steady-state tests, a function was developed to calculate the particulate emission with the independent variables of equivalence ratio and engine speed. If the instantaneous engine speed and equivalence ratio are known, the function can be used to calculate the instantaneous particulate emission. The total particulate emission is then obtained by integration over the period of the transient cycles.

After finishing the two iterations, the pressures and temperatures at the four stations denoted by 1, 2, 3, and 4 are known. Also the air and fuel flow rates have been determined. The new turbocharger speed $\omega(t+1)$ can be determined by the dynamic turbocharger model. Up to now, one time step has been completed. Then the time is advanced and the computer program continues. The simulation will be terminated when the transient cycle schedule is over.

The following are detailed discussions of the sub-models of the engine model.

3.2 Models for the Engine Processes

Generally speaking, the engine processes are extremely complex and difficult to model. The processes produce property variations in both space and time. Researchers usually simplify the processes with reasonable assumptions for their particular purposes. This section presents a model for the thermodynamic processes in the

engine cylinder, a model for the intake and exhaust flows which relate to the thermodynamic processes, and a model for calculating the engine friction to which part of the work generated during the thermodynamic processes goes. The most important parameter output from the model for this study is the engine overall equivalence ratio, which is one of the independent variables to determine the particulate emission from the engine. A single-zone thermodynamic model was used to simulate the in-cylinder processes. The entire mass in the cylinder was characterized by a single temperature, pressure, density, and equivalence ratio. For the purpose of predicting the equivalence ratio, it is not required to have a sophisticated multi-zone model, which require large amounts of computer time. Although the single-zone model is simple, it can accurately predict engine performance parameters.

3.2.1 Model for thermodynamic processes in the cylinder

Single-zone models such as that proposed by Krieger and Borman [59] have been widely used for studying diesel combustion processes. They are based with empirical relations to quantify the individual processes that occur in an engine. Based on Van Gerpen's report [60], this section presents the governing equations for a single-zone model for the diesel engine thermodynamic processes.

The equations are developed from the control volume illustrated schematically in Figure 3.3. The model considers the four processes of the four stroke cycle including exhaust, intake, compression, and expansion. The calculation begins at the time when the exhaust valve is opened. To finish a complete cycle, the time advances by an amount corresponding to 720° of crankshaft rotation. In most analyses involving engine processes it is convenient to use crank angle as the independent variable in

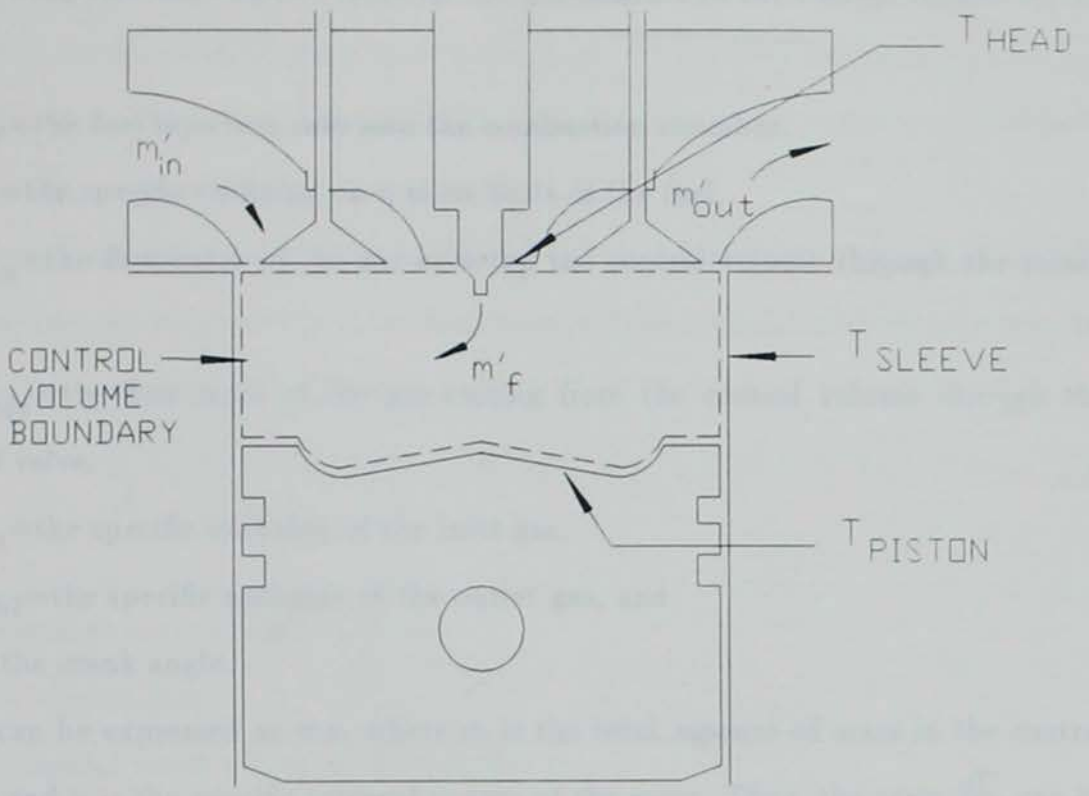

Figure 3.3: Control volume for engine analysis

place of time, although they are related through the engine speed. No blow-by losses are considered in the present analysis.

Neglecting kinetic and potential energy effects, the rate form of the first law of thermodynamics with respect to the change in crank angle can be written as

$$\frac{dU}{d\theta} = Q' - W' + m'_f h_f + m'_{in} h_{in} - m'_{out} h_{out} \tag{3.1}$$

where

U=the total internal energy of the mass contained within the control volume,

Q'=the net rate of heat transfer into the control volume,

W'=the rate that work is done by the gas mixture in the control volume on the piston,

m'_f=the fuel injection rate into the combustion chamber,

h_f=the specific enthalpy on a mass basis of the fuel,

m'_{in}=the flow rates of the gas entering the control volume through the intake valve,

m'_{out}=the flow rates of the gas exiting from the control volume through the exhaust valve,

h_{in}=the specific enthalpy of the inlet gas,

h_{out}=the specific enthalpy of the outlet gas, and

θ=the crank angle.

U can be expressed as mu, where m is the total amount of mass in the control volume and u is the specific internal energy of the mass. Thus, the term $\frac{dU}{d\theta}$ can be written as

$$\frac{dU}{d\theta} = m\left(\frac{du}{d\theta}\right) + um' \tag{3.2}$$

A mass balance on the cylinder yields the following equation.

$$\frac{dm}{d\theta} = m'_{in} + m'_f - m'_{out} \tag{3.3}$$

where m is the total mass contained in the cylinder.

Also, the work term W' can be expressed as the product of the pressure p and the differential rate of change in cylinder volume $p\frac{dV}{d\theta}$. Here, $\frac{dV}{d\theta}$ is only a function of the geometry of the cylinder, the crank, and the connecting rod mechanism [61]. Hence, Eq. 3.1 becomes

$$m\left(\frac{du}{d\theta}\right) + um' = Q' - p\left(\frac{dV}{d\theta}\right) + m'_f h_f + m'_{in} h_{in} - m'_{out} h_{out} \tag{3.4}$$

This equation can be solved to obtain the pressure, temperature, and equivalence ratio in the cylinder at all times during the cycle. This allows the engine power and efficiency to be determined. Because this equation has many unknowns, additional equations are required before it can be solved.

The widely used Annand correlation [62] was employed with appropriate wall temperatures to calculate the heat transfer rate. The Annand heat transfer correlation was incorporated in the form

$$\frac{Q'}{A} = \left(\frac{1}{6N}\right)\left[0.49\frac{k}{B}(R_e)^{0.7}(T - T_w) + b(T^4 - T_w{}^4)\right] \tag{3.5}$$

where

A=surface area of heat transfer,

B=cylinder bore,

k=thermal conductivity of the cylinder gas,

T=bulk cylinder temperature,

T_w=cylinder wall temperature,

b=$3.267 \times 10^{-3}\ Watts/m^2 - K^4$,

N=engine speed, rpm, and

R_e=Reynolds number based on the cylinder diameter.

The surface area for heat transfer was divided into three regions, and each region was assigned a characteristic temperature. The three regions were the head surface, the piston surface, and the cylinder sleeve. The head and piston surface areas are constant, but the sleeve area depends on the piston position.

The state of the gas in the control volume is dependent on the pressure p, temperature T, and equivalence ratio ϕ. The thermodynamic properties, such as the gas constant R and the specific internal energy u, are fixed by p, T, and ϕ. Thus,

differentiating R and u with respect to crank angle yields

$$\frac{du}{d\theta} = \frac{\partial u}{\partial p}\frac{dp}{d\theta} + \frac{\partial u}{\partial T}\frac{dT}{d\theta} + \frac{\partial u}{\partial \phi}\frac{d\phi}{d\theta} \tag{3.6}$$

and

$$\frac{dR}{d\theta} = \frac{\partial R}{\partial p}\frac{dp}{d\theta} + \frac{\partial R}{\partial T}\frac{dT}{d\theta} + \frac{\partial R}{\partial \phi}\frac{d\phi}{d\theta} \tag{3.7}$$

The partial derivatives of R and u with respect to p, T, and ϕ are thermodynamic properties and can be calculated at the instantaneous state.

Another independent relation is provided by differentiating the ideal gas equation as follows

$$p\frac{dV}{d\theta} + V\frac{dp}{d\theta} = mR\frac{dT}{d\theta} + mT\frac{dR}{d\theta} + RT\frac{dm}{d\theta} \tag{3.8}$$

The equivalence ratio in the cylinder changes because of the addition of air from the intake manifold, fuel from the fuel injector, and back-flow from the exhaust manifold. The derivative of the equivalence ratio can be expressed as [63]

$$\frac{d\phi}{d\theta} = \frac{1 + f_s\phi}{m}\left(m'_{in}\frac{\phi_{in} - \phi}{1 + f_s\phi_{in}} - m'_{out}\frac{\phi_{out} - \phi}{1 + f_s\phi_{out}} + \frac{m'_f}{f_s}\right) \tag{3.9}$$

where

f_s=the stoichiometric fuel to air ratio on a mass basis,

ϕ_{in}=the inlet gas equivalence ratio, and

ϕ_{out}=the outlet gas equivalence ratio.

f_s was found by solving a stoichiometric reaction equation. The stoichiometric reaction is defined such that the only combustion products are carbon dioxide, water, and nitrogen. The fuel used for this study was $C_{13.78}H_{24.26}$ [64]. The reaction is represented by the chemical reaction:

$$\epsilon C_{13.78}H_{24.26} + (0.21O_2 + 0.79N_2) \rightarrow \nu_1 CO_2 + \nu_2 H_2O + \nu_3 N_2 \tag{3.10}$$

Solving Eq. 3.10 yields f_s=0.06940.

The model assumes that fuel burns instantaneously to equilibrium combustion products as soon as it enters the cylinder. This means that the fuel injection rate, m'_f, really corresponds to an apparent fuel mass burning rate. This assumption has been used by Krieger and Borman [59] and Van Gerpen and Shapiro [60]. Watson et al. [65] developed a function for the apparent mass burning rate based on experimental data. This function was modified slightly and uses five constants, C_1 through C_5 [66].

For $\theta \geq C_2$:

$$m'_f = m_f \left[C_1 PR(\theta) + (1 - C_1) DI(\theta)\right] \tag{3.11}$$

where

m_f=the total fuel injected over a cycle,

$PR(\theta)$=the premixed portion of the burning rate, and

$DI(\theta)$=the diffusion portion of the burning rate.

$PR(\theta)$ is defined as

$$PR(\theta) = \frac{5000}{C_3}(C_4 + 1) y^{C_4} \left[1 - y^{(C_4+1)}\right]^{4999} \tag{3.12}$$

and $DI(\theta)$ is expressed as

$$DI(\theta) = \frac{6.9076}{C_3}(C_5 + 1) y^{C_5} \left[\exp^{-6.9076 y^{(C_5+1)}}\right] \tag{3.13}$$

Here, y is defined as

$$y = \frac{\theta - C_2}{C_3} \tag{3.14}$$

The values of the five constants determine the particular characteristics of the mass burning rate function as follows. The values of the parameters used in the

model are shown in parentheses.

C_1=the fraction of fuel burned in premixed portion (0.20),

C_2=the parameter for specifying start of combustion (715°),

C_3=the parameter for specifying duration of combustion (55°),

C_4=the shape parameter for premixed burning (0.35), and

C_5=the shape parameter for diffusion burning (1.0).

After manipulating the governing equations, six ordinary differential equations were developed. The equations involve fuel burning rate, cylinder mass, the rate of heat transfer, and the rates of the changes in equivalence ratio, cylinder pressure, and cylinder temperature. These equations are presented in Appendix A.

Following the assumption that the contents of the engine cylinder are at equilibrium at all times, the gas properties used in the model were determined from a version of the FORTRAN subroutine PER developed by Olikara and Borman [67]. However, in a time study of the diesel simulation it was determined that the simulation program was spending about 80% of its time calculating the properties [60]. Therefore, the program was modified to reduce the amount of time spent in property evaluation. A new property routine, PEREZ, was developed that assumes the combustion products consist of oxygen, nitrogen, carbon dioxide, and water vapor under lean conditions and oxygen, nitrogen, carbon dioxide, carbon monoxide and hydrogen under rich conditions.

The differential equations of the model were integrated by using the subroutine LSODE. LSODE uses a very efficient implicit numerical procedure [68]. The combined program was run on a DEC 3100 work-station.

The inputs for the thermodynamic model are intake manifold temperature T_2,

intake manifold pressure p_2, exhaust manifold pressure p_3, engine speed N, and assumed fuel flow rate $\dot{m}_f$. The outputs from the model are air flow rate, equivalence ratio, the indicated work W_i generated during the compression and expansion processes, and the pumping work W_p required for accomplishing the exhaust and intake processes.

3.2.2 Model for the intake and exhaust flows

The model for the intake and exhaust flows assumes that the mass leaving a system has the same properties as the system. For example, the mass leaving the cylinder has the same properties as the mass in the cylinder. This assumption implies that the contents of the system are always perfectly mixed. According to this assumption, the mass leaving the intake manifold entering the cylinder has the properties of air. But if there is back-flow from the exhaust manifold to the cylinder, the equivalence ratio of the mixture entering the cylinder is assumed to be that based on the total fuel and air flow rates into the engine, which is the exhaust equivalence ratio.

It is possible that a back flow in the system can occur during either the intake of exhaust processes. The back-flow is checked by comparing the pressure differences across the valves. If the pressure in the intake manifold is less than that in the cylinder, the gas in the cylinder flows back into the intake manifold. If the pressure in the exhaust manifold is greater than that in the cylinder, the gas in the exhaust manifold returns to the cylinder. Both of these cases are considered to be back-flows.

The intake and exhaust valve flow areas were tabulated according to data from the engine manufacturer. There were 28 and 32 data points for the intake and

exhaust valve flow areas, respectively. A cubic spline was fit to these data to allow interpolation between tabulated values [69, 70].

After determining the gas flow direction and the flow area, the rate of the mass flow entering or leaving the cylinder can be calculated. If the flow is choked, the flow rate depends only on the upstream conditions. Otherwise, the flow rate depends on both the upstream and downstream conditions. A subroutine was developed to calculate the temperature, velocity, and Mach number of the exit flow by assuming constant specific heats and an isentropic process. The inputs to the subroutine are the temperature, pressure, and equivalence ratio of the entering flow and the pressure of the exit flow. The subroutine also determines the temperature, pressure, and velocity at the section where the Mach number is 1.0. A discharge coefficient for the flow was assumed to be a constant of 0.7. Thus, the actual flow rate is the product of the discharge coefficient and the isentropic flow. The outputs from the subroutine are the intake flow rate m'_{in} and m'_{out} which enter the engine thermodynamic model as discussed in Section 3.2.1.

3.2.3 Engine friction model

The engine friction model was developed to predict the friction of the power generated from the combustion which is not available at the engine output shaft. As discussed in Section 3.2.1, the engine indicated work W_i and pumping work W_p could be determined from the engine thermodynamic model for the given inputs. The sum of the work done by the gas on the piston during the compression and expansion cycle, W_i and the work done during the intake and exhaust cycle, W_p must be equal

to the sum of the brake work, W_b and the work to overcome friction, W_f.

$$W_i + W_p = W_b + W_f \tag{3.15}$$

Engine brake work output W_b can be calculated with Eq. 3.15 if the friction work W_f during the processes is known.

The engine brake, or output, torque can be calculated using the equation $W_b = \mathcal{T}_b/(4\pi)$. $\mathcal{T}_b$ is the torque required to obtain the engine shaft torque $\mathcal{T}_{shft}$ which is specified by a test schedule. If the engine is run at a steady-state condition, $\mathcal{T}_b$ is equal to $\mathcal{T}_{shft}$. If there is a speed transition, either acceleration or deceleration, $\mathcal{T}_b$ is either larger than $\mathcal{T}_{shft}$ of less than $\mathcal{T}_{shft}$. The reason for this is explained in Section 3.4.

Van Gerpen [60] used an empirical equation for calculating the friction mean effective pressure $FMEP$, which is defined as

$$FMEP = \frac{W_f}{V_d} \tag{3.16}$$

where V_d is the cylinder displacement volume.

The empirical equation for $FMEP$ was found to be

$$FMEP = c_0 + c_1 \bar{V}_p + c_2 \bar{V}_p^2 \tag{3.17}$$

where

$FMEP$=friction mean effective pressure, Pa,

$\bar{V}_p$=mean piston speed, m/sec, and

c_0, c_1, and c_2=coefficients from experiment.

c_0, c_1, and c_2 were chosen to be 8.93936×10^4, 0.10674, and 1.16501×10^{-6}. The $FMEP$'s calculation with Eq. 3.17 were validated by experimental results and the differences were within 4% of the experimental values of $FMEP$.

If the calculated $FMEP$ is known, the value of W_f can be determined from Eq. 3.16. Hence, W_b in Eq 3.15 can be calculated. The inputs for the model are engine speed, engine bore and stroke. The output from the model is the friction mean effective pressure.

3.3 Turbocharger Model

Since the engine was turbocharged, it was necessary to have a turbocharger model to predict the performance characteristics of the turbocharger, such as flow rates, pressure ratio, angular velocity, and efficiency. This section is divided into two parts. The first part presents the compressor and turbine performance maps and the second part covers the dynamic turbocharger model.

3.3.1 Turbocharger performance maps

As discussed later in Section 5.1, a series of steady-state tests were conducted to determine the turbocharger characteristics. This section shows how turbocharger performance maps were generated from the tests.

3.3.1.1 Compressor performance map During the steady-state engine tests, air flow rate, turbocharger speed, and temperatures and pressures at compressor inlet and outlet were measured. The data were grouped into four variables, corrected mass flow rate $\frac{\dot{m}_{in}\sqrt{T_1/T_{ref}}}{p_1/p_{ref}}$, pressure ratio $\frac{p_2}{p_1}$, corrected compressor speed $\frac{N_{tc}}{\sqrt{T_1/T_{ref}}}$, and efficiency η_c, which will be discussed in Section 5.5. N_{tc} denotes the turbocharger speed. T_1 is the compressor inlet temperature. p_1 and p_2

are the compressor inlet and outlet pressures. The reference temperature T_{ref} and pressure p_{ref} were chosen to be 298 K and 1 bar. Calculations for the variables were straight-forward except for η_C. The efficiency of a compressor can be defined as the work required for isentropic compression divided by the actual work required to achieve the same pressure ratio. η_C is calculated from the following equation by assuming constant specific heats.

$$\eta_C = \frac{\left(\frac{p_2}{p_1}\right)^{\gamma-1/\gamma} - 1}{\frac{T_2}{T_1} - 1} \tag{3.18}$$

where

γ=the ratio of constant pressure specific heat to constant volume specific heat, C_p/C_v, and

T_2=the compressor outlet temperature.

As discussed later in Section 5.5, the mass flow rate and compressor speed were selected as independent variables and the other parameters became dependent variables. In other words, the pressure ratio is a function of the mass flow rate and the turbocharger speed and so is the efficiency. The reason for this is as follows. The mass flow rate is the variable which must match the rate given by the engine thermodynamic model. If it was chosen as an independent variable, computer time could be reduced. Choosing the turbocharger speed as an independent variable was necessary because it is an initial value input to the model.

Figure 3.4 shows the compressor performance map generated by the Research Division of Garrett Automotive. It is believed that the turbocharger was tested on a test stand because the turbocharger on the engine used for this study only operated over a very limited region of the performance map given in Figure 3.4. Figure 3.5

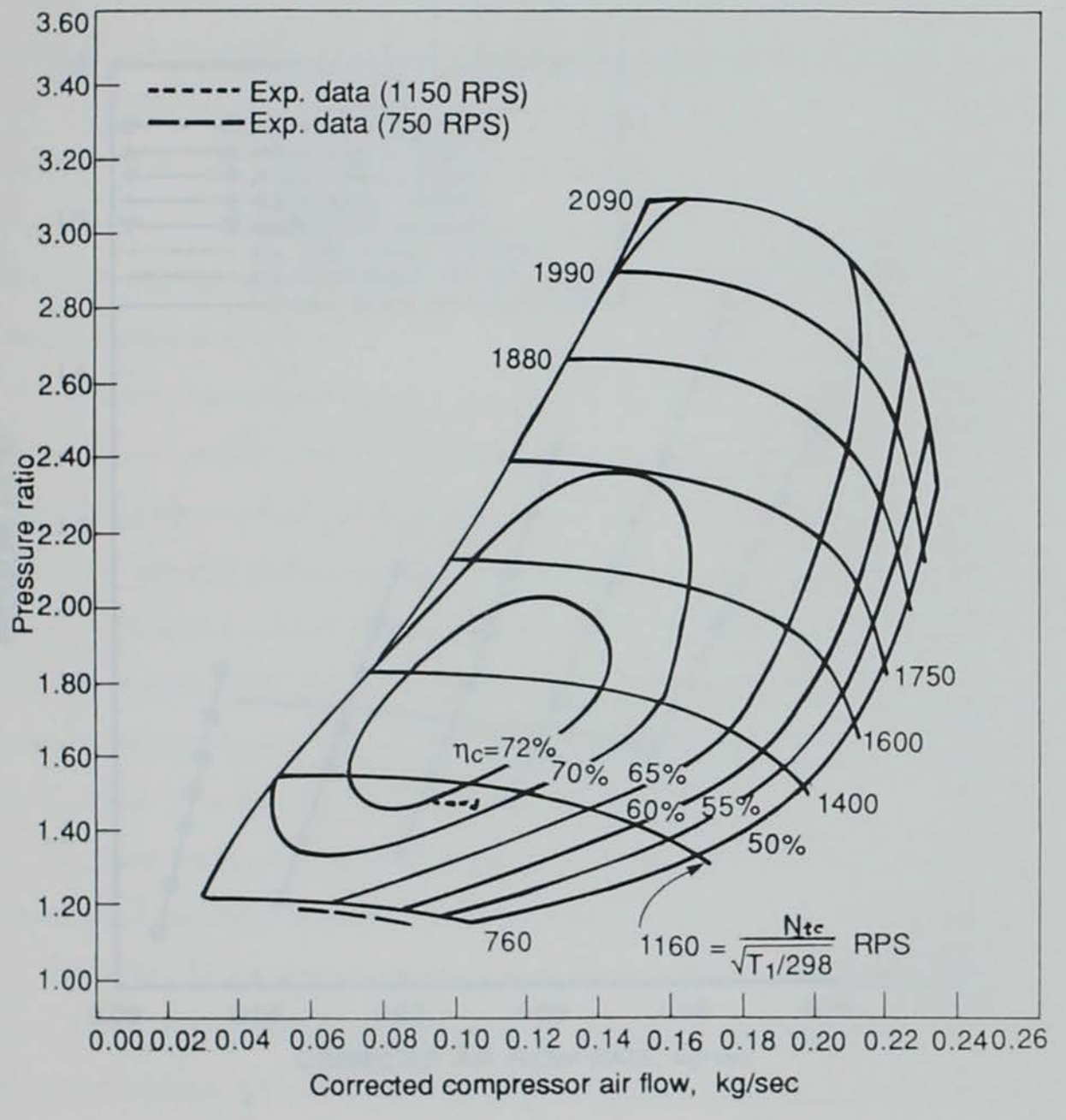

Figure 3.4: Compressor performance map from Garrett

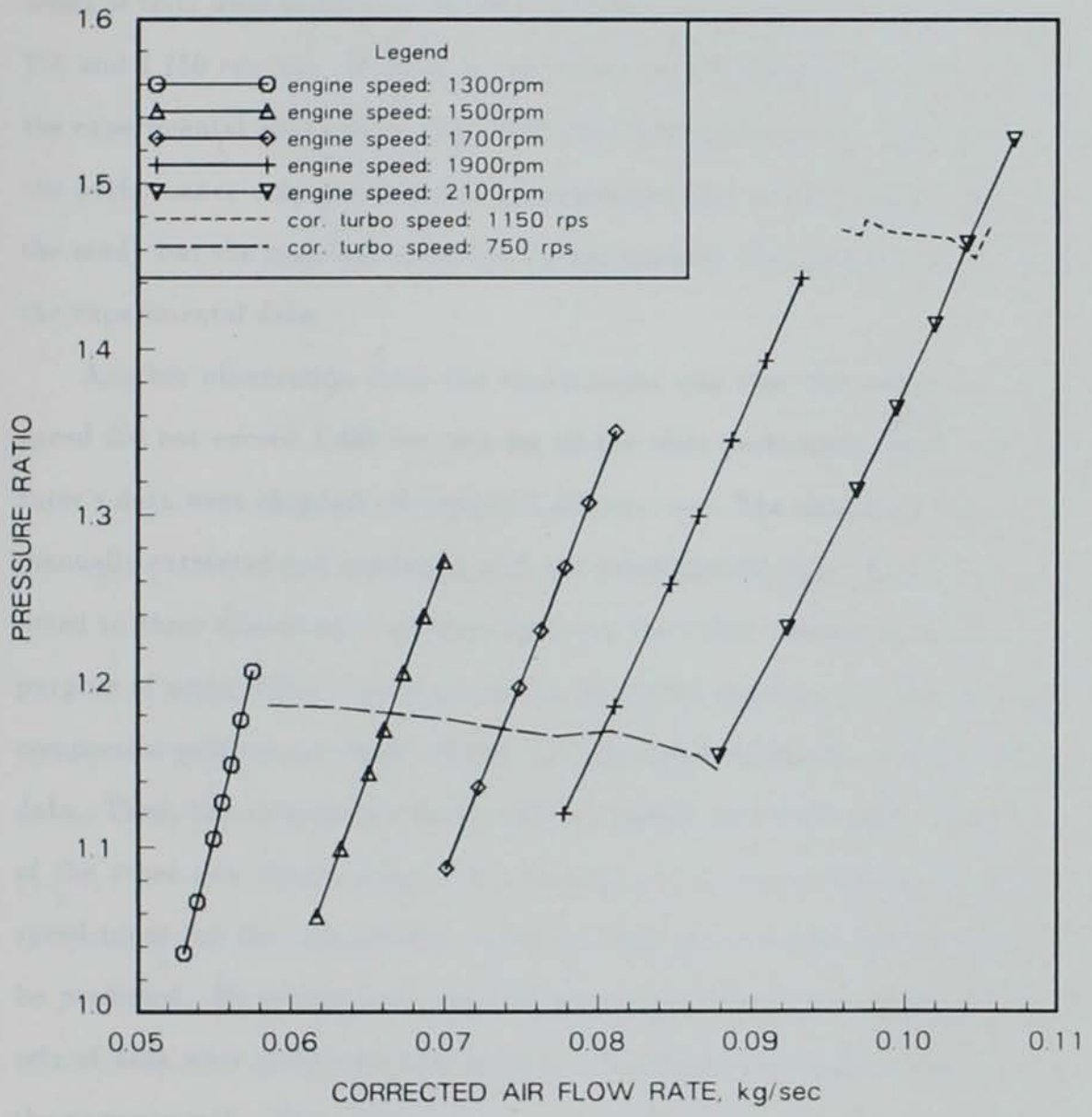

Figure 3.5: Compressor performance map from tests

shows the operating range of the compressor used for this study. If the data in Figure 3.5 were plotted on Figure 3.4, they would only be shown in the lower left corner. To verify if the experimental data match the data shown on Figure 3.4, a series of tests were performed by keeping the corrected compressor speed constant at 750 and 1,150 *rev/sec*. These data are shown on the Figure 3.4. It can be seen that the experimental data agreed fairly well with those given by the manufacturer. Since the performance map given by the manufacturer had a wider range, it was used for the study but the map was extended further towards the lower left corner by adding the experimental data.

Another observation from the experiments was that the corrected compressor speed did not exceed 1,400 *rev/sec* for all the tests performed. Thus, the manufacturer's data were chopped off beyond 1,400 *rev/sec*. The data from Figure 3.4 were manually extracted and combined with the experimental data. These data were then fitted to three dimensional surfaces by using the IMSL subroutine SURF [71]. The purpose of using SURF was to generate a fine mesh and improve the accuracy of the compressor performance map. SURF initially needs the inputs of three dimensional data. Then, the subroutine can be used to predict the third value based on inputs of the other two known values. For example, if the corrected mass flow rate and speed input are the independent variables, then the pressure ratio or efficiency can be predicted. By setting the corrected compressor speed at 12 different values, 12 sets of data were generated and fitted to 12 second order polynomials to calculate the pressure ratio. The pressure ratio can be calculated using Eq. 3.19 as follows.

$$\frac{p_2}{p_1} = a_0 + a_1 \dot{m}_{cor} + a_2 \dot{m}_{cor}^2 \tag{3.19}$$

where

Table 3.1: Polynomial coefficients for compressor pressure ratio and efficiency

Corrected Speed rps	p_2/p_1			η_c
	a_0	a_1 $1/(kg/sec)$	a_2 $1/(kg/sec)^2$	
400.0	1.0325	-0.1038	0.2167	0.1667
450.0	1.0527	-0.3645	1.2722	0.2083
500.0	1.0700	-0.4381	1.2240	0.2917
550.0	1.0810	-0.4174	1.7713	0.3333
650.0	1.0796	0.3922	-2.0725	0.4167
750.0	1.2571	-1.4461	2.4175	0.4583
900.0	1.3911	-2.4880	8.3353	0.4650
950.0	1.4399	-2.3969	7.8738	0.4833
1000.0	1.4384	-1.6483	4.9576	0.4875
1100.0	1.3763	0.6078	-2.2513	0.5000
1150.0	1.4749	0.0151	-0.4469	0.5167
1400.0	1.4777	6.9002	-33.368	0.5250

$\dot{m}_{c,cor}$=the corrected compressor mass flow rate, kg/sec, and

a_0, a_1, and a_2=the polynomial constants listed in Table 3.1.

The coefficients of the polynomials are listed in Table 3.1 and the curves are shown in Figure 3.6. The 12 corrected speeds were, from the bottom to the top of the figure, 400, 450, 500, 550, 650, 750, 900, 950, 1000, 1100, 1150, and 1400 rev/sec. If the speed was between these speeds, an interpolation technique was used to calculate the pressure ratio.

It can be seen that the shape of the top curve in Figure 3.6 is different from those of the others. The reason for this is that the data for the top curve was exclusively extracted from Figure 3.4, while the data for the other curves were the combinations from Figure 3.4 and Figure 3.5. The compressor efficiency was found to be independent of the corrected compressor mass flow rate and only varied with

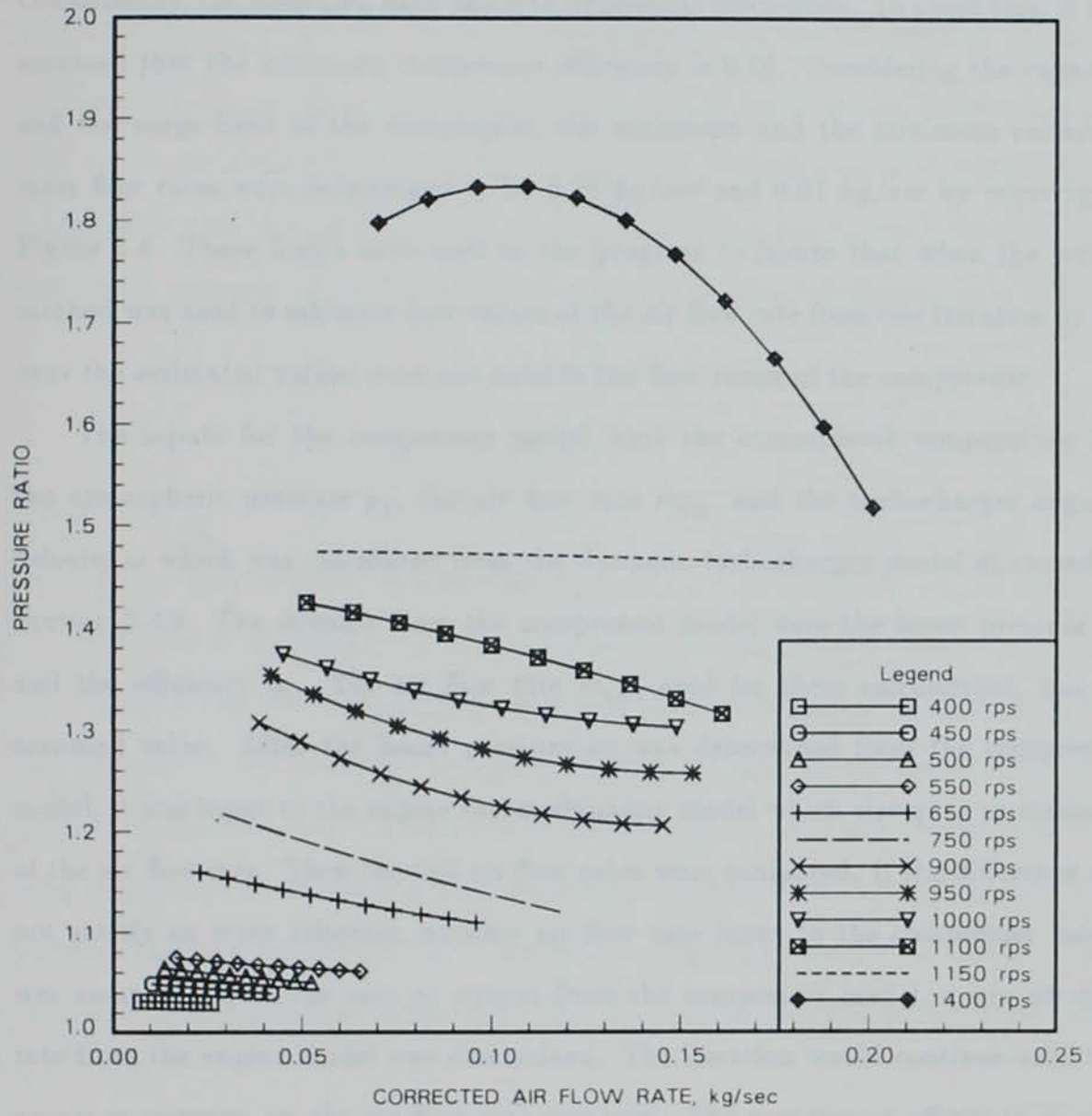

Figure 3.6: Combined compressor performance map

changes in the corrected compressor speed as shown in Table 3.1.

At low pressure ratios, the exit temperature measurement on the turbocharger is very difficult because the temperature change across the compressor is so small. Occasionally, the measured data can give impossible efficiencies. To avoid this, it was assumed that the minimum compressor efficiency is 0.16. Considering the capacity and the surge limit of the compressor, the maximum and the minimum corrected mass flow rates were determined to be 0.20 kg/sec and 0.01 kg/sec by referring to Figure 3.4. These limits were used in the program to insure that when the secant method was used to estimate new values of the air flow rate from one iteration to the next the estimated values were not outside the flow range of the compressor.

The inputs for the compressor model were the atmospheric temperature T_1, the atmospheric pressure p_1, the air flow rate $\dot{m}_{in}$, and the turbocharger angular velocity ω which was calculated from the dynamic turbocharger model discussed in Section 3.3.2. The outputs from the compressor model were the boost pressure p_2 and the efficiency η_C. The air flow rate $\dot{m}_{in}$, used for these calculations, was an assumed value. After the boost pressure p_2 was determined from the compressor model, it was input to the engine thermodynamic model which also gave an estimate of the air flow rate. Then the two air flow rates were compared. If the difference did not satisfy an error criterion, another air flow rate input to the compressor model was assumed. With the new p_2 output from the compressor model, a new air flow rate from the engine model was determined. The iteration would continue until the accuracy criterion on the air flow rate was met. The compressor efficiency η_C was then used to calculate the boost temperature T_2 with Eq. 3.18.

3.3.1.2 Turbine performance map The turbine performance map was generated using the same technique as that employed for setting up the compressor performance map. The four parameters were corrected mass flow rate $\frac{\dot{m}_{out}\sqrt{T_3/T_{ref}}}{p_3/p_{ref}}$, pressure ratio $\frac{p_3}{p_4}$, corrected turbine speed $\frac{N_{tc}}{\sqrt{T_3/T_{ref}}}$, and efficiency η_t. T_3 is the turbine inlet temperature. p_3 and p_4 are the compressor inlet and outlet pressures. The definition of the turbine efficiency is the ratio of the actual work output to the work which could be obtained from an isentropic expansion between the same inlet and outlet pressures of the turbine. The equation used to calculate η_t is as follows.

$$\eta_t = \frac{\frac{T_4}{T_3} - 1}{\left(\frac{p_4}{p_3}\right)^{\gamma-1/\gamma} - 1} \tag{3.20}$$

where

T_4=the turbine outlet temperature, and

γ=the ratio of constant pressure to constant volume specific heats, C_p/C_v.

Figure 3.7 shows the turbine performance map generated by the Research Division of Garrett Automotive. The figure was directly used for the model. The main reason for this was that the range of the experimental data was too narrow to be used to generate an accurate performance map. Additionally, the temperature measurement for the turbine is even more difficult than that for the compressor. The turbine inlet temperature varies with time and spatial location within the turbine inlet scroll.

It can be seen from Figure 3.7 that the pressure ratio and the corrected mass flow rate can be expressed as functions of the corrected turbine speed $\frac{N_{tc}}{\sqrt{T_3/T_{ref}}}$ (rev/min). Third order polynomials were fit to data extracted from the map. They

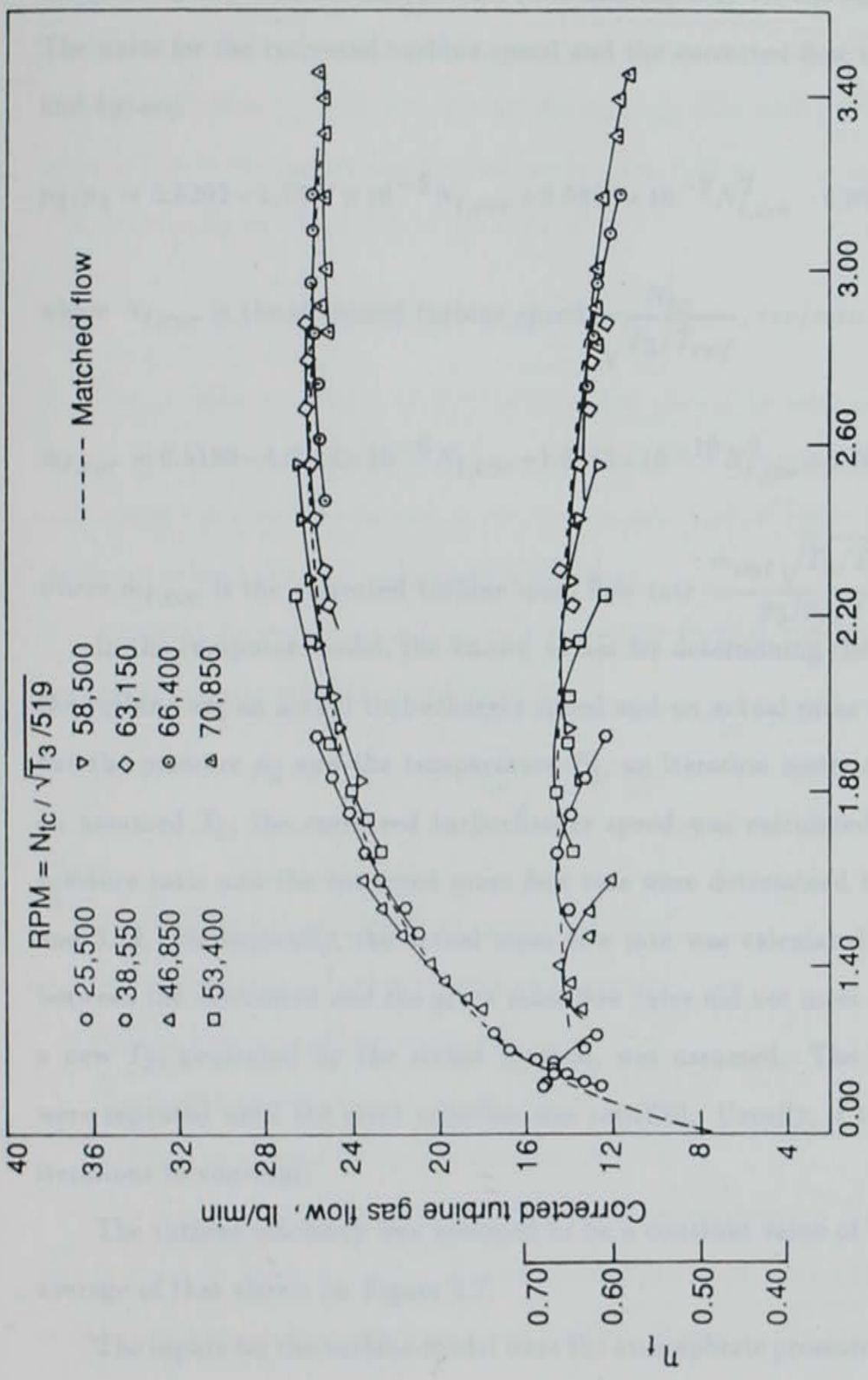

Figure 3.7: Turbine performance map from Garrett

are given by Eq. 3.21 for the pressure ratio and Eq. 3.22 for the corrected mass flow. The units for the corrected turbine speed and the corrected flow rate were rev/min and kg/sec.

$$p_3/p_4 = 5.5292 - 1.7377 \times 10^{-5} N_{t,cor} + 8.5859 \times 10^{-9} N_{t,cor}^2 - 6.0909 \times 10^{-14} N_{t,cor}^3 \tag{3.21}$$

where $N_{t,cor}$ is the corrected turbine speed $\dfrac{N_{tc}}{\sqrt{T_3/T_{ref}}}$, rev/min.

$$\dot{m}_{t,cor} = 0.5199 - 4.0918 \times 10^{-6} N_{t,cor} + 1.6783 \times 10^{-10} N_{t,cor}^2 + 0.8928 \times 10^{-16} N_{t,cor}^3 \tag{3.22}$$

where $\dot{m}_{t,cor}$ is the corrected turbine mass flow rate $\dfrac{\dot{m}_{out}\sqrt{T_3/T_{ref}}}{p_3/p_{ref}}$, kg/sec.

In the computer model, the known values for determining the characteristics of the turbine are an actual turbocharger speed and an actual mass flow rate. To find out the pressure p_3 and the temperature T_3, an iteration method was used. With an assumed T_3, the corrected turbocharger speed was calculated first. Then, the pressure ratio and the corrected mass flow rate were determined by using Eqs. 3.21 and 3.22. Consequently, the actual mass flow rate was calculated. If the difference between the calculated and the given mass flow rates did not meet an error criterion, a new T_3, generated by the secant method, was assumed. The procedures above were repeated until the error criterion was satisfied. Usually, it took less than five iterations to converge.

The turbine efficiency was assumed to be a constant value of 65%, which is the average of that shown on Figure 3.7.

The inputs for the turbine model were the atmospheric pressure p_4 which is equal

to p_1, the mass flow rate $\dot{m}_{out}$, and the angular velocity of the turbocharger ω. The outputs from the turbine model were the back pressure p_3, the exhaust temperature before the turbine T_3, and the turbine efficiency η_t. The back pressure p_3 was useed as an input to the engine combustion model. Eq. 3.20 needs η_t to calculate the gas temperature T_4 at the outlet of the turbine.

3.3.2 Dynamic turbocharger model

The moment of inertia of the turbocharger should be considered when the engine is run through a transient cycle, which has been discussed in Section 2.3.3. A differential equation was developed for the dynamic turbocharger model according to Newton's second law and conservation of energy.

Applying Newton's second law and neglecting friction, the derivative of the turbocharger angular velocity is expressed as

$$J_{tc}\frac{d\omega}{dt} = \mathcal{T}_t - \mathcal{T}_c \tag{3.23}$$

where

J_{tc}=turbocharger moment of inertia, $kg - m^2$,

ω=turbocharger angular velocity, rad/sec,

t=time over a transient cycle, sec,

$\mathcal{T}_t$=torque applied on the turbine, $N - m$, and

$\mathcal{T}_c$=torque applied on the compressor, $N - m$.

The moment of inertia was experimentally determined by Garrett Automotive and is given in Table 4.1. The $\mathcal{T}_c$ and $\mathcal{T}_t$ are calculated according to the inlet and outlet conditions of the compressor and turbine. Based on the energy balances, they

are given as follows.

$$\mathcal{T}_c\omega = \dot{m}_{in}(h_2 - h_1) \tag{3.24}$$

$$\mathcal{T}_t\omega = \dot{m}_{out}(h_3 - h_4) \tag{3.25}$$

where

$\dot{m}_{in}$=rate of mass flow entering the engine cylinder, kg/sec,

$\dot{m}_{out}$=rate of mass flow leaving the engine cylinder, kg/sec,

h_1=enthalpy of the gas in the compressor inlet, J/kg,

h_2=enthalpy of the gas in the compressor outlet, J/kg,

h_3=enthalpy of the gas in the turbine inlet, J/kg, and

h_4=enthalpy of the gas in the turbine outlet, J/kg.

The properties of h_1, h_2, h_3, and h_4 can be calculated from the subroutine PEREZ with the inputs of temperature, pressure, and equivalence ratio.

The initial value for Eq. 3.23 is the speed at which the turbocharger shaft is turning when the engine is operated at its idle condition. The reason for this is that the first point of the EPA transient cycle is the idling condition. Eq. 3.23 was integrated by using subroutine LSODE [68].

3.4 Dynamic Engine Model

The overall model also includes a dynamic engine model that accounts for the effect of the engine moment of inertia when the engine is operated over a transient cycle. Due to the moment of inertia, more power is needed for the engine to accelerate from a lower speed to a higher speed, compared with the power required for the engine to run at the steady-state condition at the final speed. The engine's moment of inertia involves the piston and connecting-rod assembly, the crankshaft, and the flywheel.

The value used, shown in Table 4.1, was given by the engine manufacturer. One question which was brought up during the model development was whether or not the moment of inertia of the electric dynamometer should be included into the model. This inertia was not included because the torque quantity of interest to the EPA is that measured at the flywheel of the engine.

A differential equation was developed for the dynamic engine model as follows. Applying Newton's second law, the derivative of the engine speed is expressed as

$$2\pi J_e \frac{dN}{dt} = \mathcal{T}_{cyl} - \mathcal{T}_{shft} \tag{3.26}$$

where

J_e=engine moment of inertia,

N=engine speed,

t=time,

$\mathcal{T}_{cyl}$=net torque produced by cylinder gas minus the friction torque, and

$\mathcal{T}_{shft}$=engine shaft torque.

When the engine is operated at steady-state, then $\frac{dN}{dt}$ is zero. Hence, $\mathcal{T}_{cyl}$ and $\mathcal{T}_{shft}$ are identical. But if the engine is in transition from one speed to another, then $\mathcal{T}_{cyl}$ will be different from $\mathcal{T}_{shft}$. For acceleration, $\mathcal{T}_{cyl}$ is greater than $\mathcal{T}_{shft}$.

The engine speed trajectory is shown in Figure 5.1 for the EPA specified transient cycle. The values of $\frac{dN}{dt}$ could be found by fitting a cubic spline to the data from the cycle. Due to the nature of the dynamometer control, it takes about 0.4 seconds for the engine to transit from one speed to another regardless of how big the change is. Also, there exists a time delay period of between 0.30 to 0.50 seconds for the engine to respond to the speed input. Figure 3.8 shows the engine response to step changes in the engine speed command. Figure 3.8 (a) is for a speed change from 1250 to 1350

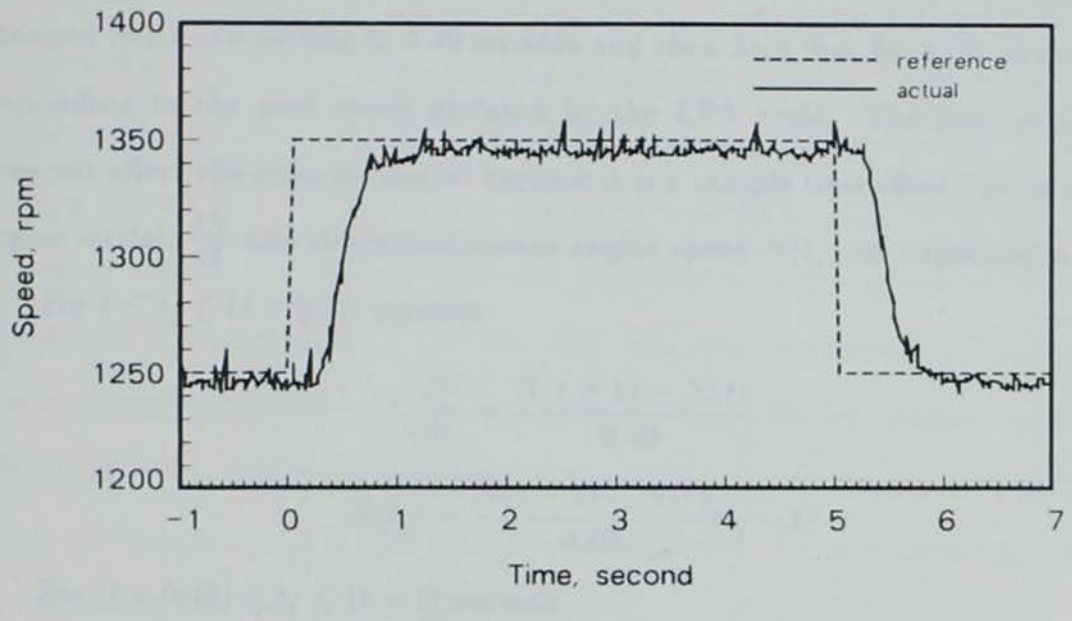

(a)

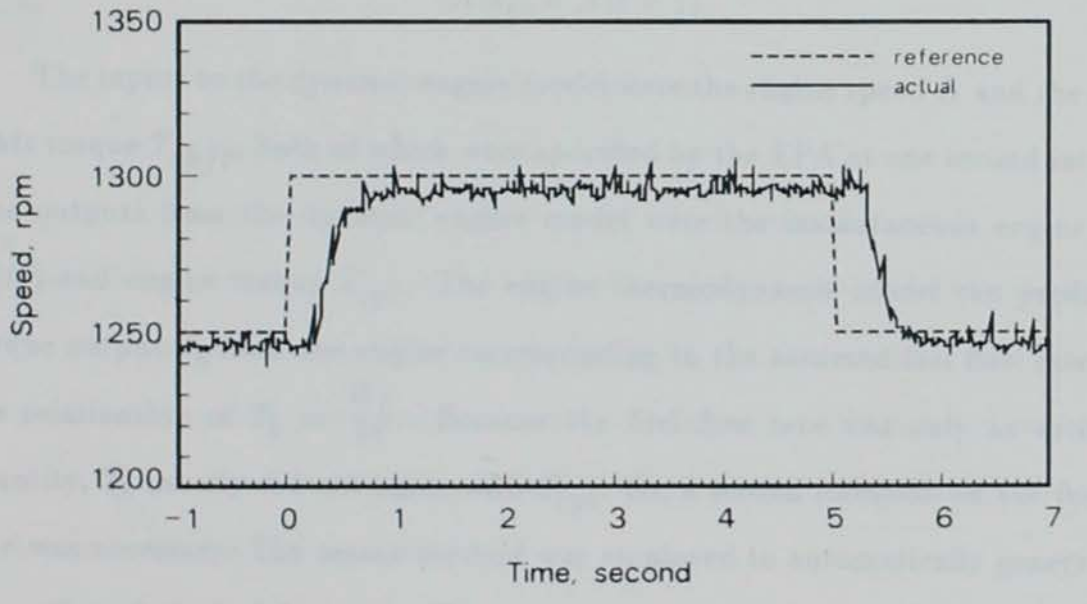

(b)

Figure 3.8: Step input to the speed reference command of dynamometer

rpm and (b) is for a speed change from 1250 to 1300 rpm.

The engine speed control operated in a manner such that the engine speed changed to its new setting in 0.40 seconds and then held that for 0.60 seconds before responding to the next speed dictated by the EPA cycle. The time delay period does not affect the dynamic model because it is a sample time offset. In the dynamic engine model, $\frac{dN}{dt}$ and the instantaneous engine speed $N(t_i)$ are expressed as follows.

For $t \leq t_i \leq (t + 0.40)$ seconds

$$\frac{dN}{dt} = \frac{N(t+1) - N(t)}{0.40} \tag{3.27}$$

$$N(t_i) = \frac{N(t+1) - N(t)}{0.40}(t_i - t) \tag{3.28}$$

For $(t + 0.40) < t_i \leq (t + 1)$ seconds

$$\frac{dN}{dt} = 0.0 \tag{3.29}$$

$$N(t_i) = N(t+1) \tag{3.30}$$

The inputs to the dynamic engine model were the engine speed N and the engine shaft torque $\mathcal{T}_{shft}$, both of which were specified by the EPA at one second intervals. The outputs from the dynamic engine model were the instantaneous engine speed $N(t_i)$ and engine torque $\mathcal{T}_{cyl}$. The engine thermodynamic model can predict the torque output $\mathcal{T}_b$ from the engine corresponding to the assumed fuel flow rate using the relationship of $\mathcal{T}_b = \frac{W_b}{4\pi}$. Because the fuel flow rate was only an estimated quantity, $\mathcal{T}_b$ usually did not agree with $\mathcal{T}_{cyl}$. So, a second iteration on the fuel flow rate was necessary. The secant method was employed to automatically generate the new value of the fuel flow rate. The iteration stopped when the difference between $\mathcal{T}_b$ and $\mathcal{T}_{cyl}$ was within the specified error tolerance for the given fuel flow rate.

3.5 Particulate Calculation

A series of steady-state tests were conducted to determine the particulate emission as a function of the engine equivalence ratio and speed. The equivalence ratio ranged from about 0.10 to 1.10. The high equivalence ratios were obtained by restricting the air flow to the engine. This restriction was accomplished by running the engine without the turbocharger and installing an orifice upstream of the intake manifold to further reduce the air flow rate. Polynomial expressions were fit to the measured particulate emissions on a rate basis for six different engine speeds, 1200, 1300, 1500, 1700, 1900, and 2100 *rpm*. Regression analysis was performed on the fit curves to determine the coefficients of determination. Eq. 3.31 is the general form for calculating the rate of particulate emission.

$$P_{rate} = a_0 + a_1\phi + a_2\phi^2 + a_3\phi^3 + a_4\phi^4 \tag{3.31}$$

where

P_{rate}=the rate of particulate emission, gm/hr,

ϕ=overall equivalence ratio in the cylinder, and

a_0, a_1, a_2, and a_4=the polynomial coefficients listed in Table 3.2.

Table 3.2 shows the polynomial coefficients and the coefficients of determination. Except for 1200 *rpm*, the equivalence ratio range for the polynomial was divided into two parts and separate polynomials were fit for each region. The point of intersection of the two polynomials was the upper limit of the lower range and the lower limit of the higher range for the equivalence ratio.

If the engine speed and the computer calculated equivalence ratio are available, the instantaneous particulate emission rate can be calculated by using Table 3.2

Table 3.2: Polynomial coefficients for particulate emission

Speed rpm	Equivalence ratio range	$a_0 \cdot 10^{-2}$ gm/hr	$a_1 \cdot 10^{-2}$ gm/hr	$a_2 \cdot 10^{-2}$ gm/hr	$a_3 \cdot 10^{-2}$ gm/hr	$a_4 \cdot 10^{-2}$ gm/hr	r^2
1200	0.044–0.715	0.1320	−0.6237	1.7855	−1.1803	0.0000	0.9970
1300	0.103–0.714	0.1962	−0.8925	1.6950	−0.6854	0.0000	0.9458
1300	0.714–0.999	0.0975	0.0913	0.2346	−3.1771	4.0334	0.9930
1500	0.105–0.580	0.2687	−1.5418	3.7302	−2.7457	0.0000	0.9927
1500	0.580–1.063	−0.0096	1.5045	−5.0030	4.6413	0.0705	0.9800
1700	0.070–0.584	0.1974	−0.5490	0.5457	0.1194	0.0000	0.9801
1700	0.584–1.019	−7.7597	32.206	−44.656	21.434	0.0000	0.9878
1900	0.104–0.601	0.3375	−1.3924	2.4350	−1.3316	0.0000	0.9952
1900	0.601–1.128	−5.9496	23.254	−30.489	14.178	0.0000	0.9983
2100	0.109–0.534	0.8397	−5.2506	11.730	−8.4514	0.0000	0.9973
2100	0.534–1.112	0.7322	−2.9224	3.2345	0.0000	0.00000	0.9297

at that time during a transient cycle. It was assumed that the engine speed and equivalence were constant over a period of one second. The particulate emission over the period is the product of the particulate emission rate times one second. The total particulate emission was obtained by integration over a whole transient cycle period, which is 1,199 seconds for the EPA transient cycle. Brake specific particulate emission was calculated by dividing the total particulate emission by the total work output from the engine during the cycle.

Obviously, the inputs for the particulate calculation subroutine were the instantaneous equivalence ratio and speed. The output from the subroutine was the particulate emission rate at a particular time.

3.6 Summary

The overall engine model consists of a model for calculations of engine thermodynamics and fluid mechanics, a model for calculations of turbocharger characteristics, a model for calculations of engine dynamics, and a model to calculate particulate emission. The basic input to the model is a transient cycle testing schedule, that is, torque and speed trajectories, and the output is the total particulate emission over the cycle. One call to the engine thermodynamic model takes 144 steps of main calculations over crank angles of 720° at an interval of 5°. So most of the computer time is spent on this kind of calculations. There are 1,199 data points for an EPA transient cycle. It took about 15 hours for the computer to complete the integration of the EPA transient cycle on a DEC 3100 work-station.

4. EXPERIMENTAL APPARATUS

The objectives of the experiments were: (1) to measure the engine's particulate emissions during steady-state tests and over transient cycles, (2) to obtain engine performance parameters such as equivalence ratio, engine torque, engine speed, air and fuel flow rates, and the turbocharger characteristics, and (3) to verify the ability of the computer model to predict engine performance parameters and diesel particulate emission during transient cycles. The equipment discussed in this chapter was essential for accomplishing these tasks.

This chapter is divided into five sections. An overview of the engine test setup is given in the first section. The second and third sections describe the dilution tunnels and the dilution air system. The particulate sampling system and weighing chamber are presented in the fourth section. Finally, the fifth section describes the data acquisition system used to record the experimental data.

4.1 Engine Test Setup

The engine used in this study was a John Deere Model 4276T four-cylinder, four stroke, turbocharged diesel engine. The combustion system was a bowl-in-piston, direct-injection, medium swirl type. The basic engine specifications are presented in Table 4.1. Although the normal idle speed for this engine was 800 rpm, the idle speed

Table 4.1: John Deere 4276T four cylinder engine specifications

Bore	106.5 mm
Stroke	127.0 mm
Connecting Rod Length	202.9 mm
Displacement	4525.2 cm^3
Compression Ratio	16.8 : 1
Valve Timing	
Intake	opens at 2° bTDC, closes at 80° aBDC
Exhaust	opens at 56° bBDC, closes at 29° aTDC
Maximum Power	58.1 kW @ 2100 rpm
Peak Torque	305.0 Nm @ 1300 rpm
Engine Inertia	1.405 $kg\text{-}m^2$
Turbocharger Inertia	1.0575×10^{-4} $kg\text{-}m^2$

for this study was redefined as 1200 rpm. This was due to a torsional resonance in the engine and dynamometer system at about 1050 rpm.

The engine was connected to a 150 HP General Electric direct current dynamometer. The engine and dynamometer were controlled by a Z-386 computer through an Analog Devices RTI-820 interface board. The computer sends speed signals to the dynamometer and gives torque commands to a microprocessor which then sends a signal to a linear actuator attached to the fuel governor lever. This controller was used to set and maintain the engine's speed and load during steady-state tests and to control the engine during transient tests [72, 73].

The volume flow rate of air into the engine was measured using a Meriam laminar flow element with a Baratron differential pressure transducer used to measure the pressure drop. The diesel fuel flow rate was measured using a stop-watch and a Toledo electronic scale.

Thermocouples were located at the air inlet to measure the inlet air dry and wet bulb temperature, at the intake manifold to measure the engine boost temperature and at a number of locations in the exhaust line for measuring the bulk exhaust temperatures before and after the turbine. Thermocouples were also used to measure the engine oil, fuel, and coolant temperatures.

The atmospheric pressure was measured with a cistern barometer. Boost pressure and exhaust back-pressure were measured both with pressure gages and pressure transducers. The calibration of the pressure transducers is provided in Appendix B. Also, a pressure gage was installed to measure engine lubricating oil pressure.

An important means for validating the engine model developed in this study was to compare predicted and measured turbocharger speed. Since this is not a routine engine measurement, a device for measuring turbocharger speed was built. The device consists of a Uniphase Model 106-1 laser, two fiber-optic light guide tubes, a light detector, and a frequency-to-voltage converter. The laser is a 20 mW, Class IIIb Helium-Neon type. One of the light guide tubes sends the laser beam to a small foil reflector which is fixed on the end of the turbocharger shaft. Then the reflected laser beam is conducted through the other fiber-optic tube to a photo-transistor which is installed inside the light detector. The voltage produced by the photo-transistor is amplified to a 5-volt output. The circuit of the light detector is presented in Appendix C. The light detector gives one five volt pulse each time the turbocharger shaft turns a revolution. Thus, the frequency of the square wave can be used to measure the turbocharger speed. In order to record the turbocharger speed on the computer, the frequency was converted to a voltage signal. For this purpose, a frequency-to-voltage converter was built to allow the computer to record the turbocharger speed

during the test. The turbocharger speed calculation is described in Appendix D.

4.2 Dilution Tunnels

A double dilution particulate measurement system was used in this study. A primary dilution tunnel was used to dilute the engine exhaust gas with compressed air. A secondary dilution tunnel was employed to mix a portion of the diluted exhaust gas with additional compressed air. The purpose of using the dilution tunnels was to simulate the diesel exhaust-air mixing process after the exhaust is emitted from the engine tail-pipe. This process is very important due to the adsorption and condensation of unburned hydrocarbons, which contribute to the soluble organic fraction of the particulates.

Figure 4.1 shows a diagram of the primary and secondary dilution tunnels. The primary dilution tunnel is 0.305 meters in diameter [39]. The distance between the introduction of the engine exhaust and the particulate sample transfer tube to the secondary dilution tunnel is 3.05 meters which corresponds to 10 tunnel diameters. Such a length ensured that there was sufficient time for the engine exhaust to mix with the air. The diameter of the primary dilution tunnel was chosen so that it would allow turbulent flow and the Reynolds Number inside the tunnel is greater than 1.0×10^5. The length of the primary dilution tunnel is sufficient to cause complete mixing of the exhaust and the dilution air.

The primary tunnel was built in 1989 [39]. It was made of standard galvanized spiral tubing. This material is not ideal since it does not have a perfectly smooth interior. Although no problems were observed during the tests conducted for this project, a rough interior increases the chances of particulate deposition and re-entrainment.

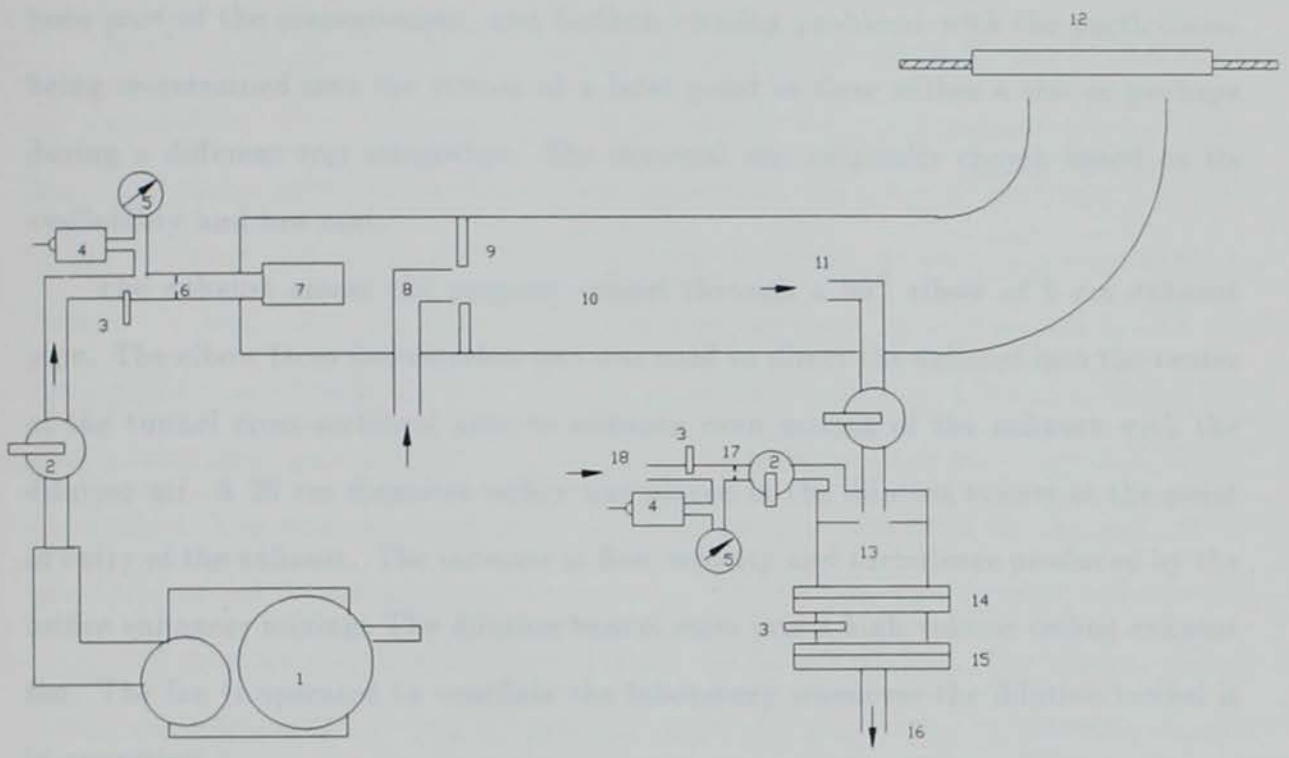

1 -- air compressor
2 -- ball valve
3 -- thermocouple
4 -- pressure transducer
5 -- pressure gage
6 -- primary air orifice
7 -- muffler
8 -- engine exhaust pipe
9 -- circular plate
10 -- primary dilution tunnel
11 -- sample transfer tube
12 -- exhaust fan
13 -- secondary dilution tunnel
14 -- primary filter holder
15 -- back-up filter holder
16 -- sampling tube
17 -- secondary air orifice
18 -- secondary dilution air

Figure 4.1: Schematic diagram of the primary and secondary dilution tunnels

There is the potential of catching some of the particulates that would otherwise have been part of the measurement, and further, causing problems with the particulates being re-entrained into the stream at a later point in time within a test or perhaps during a different test altogether. The material was originally chosen based on its availability and low cost.

The exhaust enters the primary tunnel through a 90° elbow of 6 cm exhaust pipe. The elbow faces downstream and was used to direct the exhaust into the center of the tunnel cross-sectional area to enhance even mixing of the exhaust with the dilution air. A 20 cm diameter orifice was placed in the dilution tunnel at the point of entry of the exhaust. The increase in flow velocity and turbulence produced by the orifice enhances mixing. The dilution tunnel exits into a high-volume ceiling exhaust fan. The fan is operated to ventilate the laboratory whenever the dilution tunnel is in operation.

The secondary dilution tunnel is made of standard aluminum pipe with 11.43 cm inside diameter. The particulate sample transfer tube to the secondary dilution tunnel faces upstream in the primary dilution tunnel. The tube is made from stainless-steel with 1.905 cm inside diameter. The distance from the inlet plane to the exit plane of the tube is 53 cm. The length between the exit plane of the tube and the primary particulate sampling filter is 12.70 cm, which provides an average residence time of 0.30 seconds for the double-diluted sample. The geometric design of the tunnels meets the EPA dilution method specifications [3].

4.3 Dilution Air System

The primary dilution air is provided by an Ingersoll-Rand Centac II two-stage air compressor. The compressor was set to provide an outlet gage pressure of 6.20 bar. The compressor's controller is able to maintain the pressure within $\pm$ 0.07 *bar* of the set value. A 5 cm diameter pipe line introduces the air to the primary dilution tunnel. A ball valve was installed in the line, followed by a standard in-line air filter and a smooth-edged orifice. A static pressure transducer, a Viatran model 141 with a maximum gage pressure of 22.5 bar, and a thermocouple were installed before the orifice. The pressure transducer was calibrated as described in Appendix B to provide a means for determining the pressure. The air flow rate depends only on the measured pressure and temperature because the flow is choked. The smooth-edged orifice was calibrated and Eq. E.1 given in Appendix E was used to calculate the air mass flow rate [39].

A considerable amount of noise is created by the uncontrolled expansion of the dilution air as it enters the dilution tunnel. An air-exhaust muffler was fitted to the end of the compressed air line and the noise was reduced to a tolerable level.

The dilution air ball valve shown in Figure 4.1 is fully opened during testing. The primary dilution ratio, defined as the ratio of the diluted-exhaust mass flow rate (the dilution-air mass flow rate plus the engine exhaust mass flow rate) to the engine exhaust mass flow rate, varies with the engine speed and load. The maximum dilution air flow rate achieved in the primary tunnel is approximately 0.72 kg/s. The engine exhaust flow rate varies from about 0.04 kg/s for the low-speed, light-load condition to about 0.09 kg/s for the full-speed, full-load condition. Therefore, dilution ratios can be as large as 18 and as small as 8.

As mentioned before, the Reynolds number in the primary tunnel can be as high as 1.0×10^5. The highly turbulent flow enhances the mixing process. Carbon dioxide mixing tests were conducted to determine the ability of the primary dilution tunnel to thoroughly mix the exhaust and air [39]. A stream of CO_2 was introduced at the tunnel inlet and both horizontal and vertical sampling traverses were made across the tunnel and uniform concentrations were found.

The velocity of the diluted exhaust in the tunnel ranges from 6.0 m/s to 10.0 m/s. The time for the particulates to interact with the dilution air is less than 0.5 seconds. The secondary dilution tunnel was used to increase the residence time of the diluted exhaust.

The secondary dilution air comes from the Physical Plant of Iowa State University. The compressed air goes through an in-line oil removal filter, followed by an air pressure regulator and a smooth-edged orifice before entering the tunnel. A Model 141 Viatran pressure transducer with a maximum gage pressure of 6.90 bar, and a thermocouple were installed before the orifice to measure the air pressure and temperature. The air pressure was regulated at 2.10 bar. A pressure gage was also mounted to monitor the air pressure during the tests. The pressure transducer has been calibrated with a dead-weight tester. The relationship between the pressure and the measured voltage is described in Appendix B. A Model 1.5M175 ROOTS Meter was used to calibrate the orifice and an equation was developed to calculate the secondary dilution air flow rate as described in Appendix E.

4.4 Particulate Matter Measurements

This section discusses the particulate sampling system and the particulate weighing chamber.

4.4.1 Particulate sampling system

A schematic diagram of the particulate sampling system appears in Figure 4.2. The system consists of a ball valve, a filter holder, a sample pump, an electric by-pass valve, and a gas meter with a frequency counter. The ball valve was mounted upstream of the secondary dilution tunnel. The valve is opened at the start of a test and then closed to prevent the diluted exhaust from entering the secondary dilution tunnel between two tests. Downstream of the tunnel the filter holder supports a primary filter and a backup filter. Two fritted discs were used as the supports for the filters. The back-up filter is located 8.9 cm downstream of the primary filter. Two filters are used to achieve high efficiency for collecting the particulate matter.

Accurate measurements require that the sampling system must be leak-proof. In order to check the leakage of the system, a leak test was conducted before the experiments. A discussion of the leak test is included in Appendix F.

The sampling pump has a by-pass line with an electrically actuated modulating valve to regulate the flow. The opening of the valve is automatically controlled by the computer, which provides a means for adjusting the flow rate through the particulate filters during the tests. This is necessary since the flow rate will tend to drop as the filter is gradually loaded with particulate. The system was designed so that the mass flow rate through the gas meter was constant. The mass flow rate was maintained at two times the mass flow rate through the orifice in the secondary dilution air line.

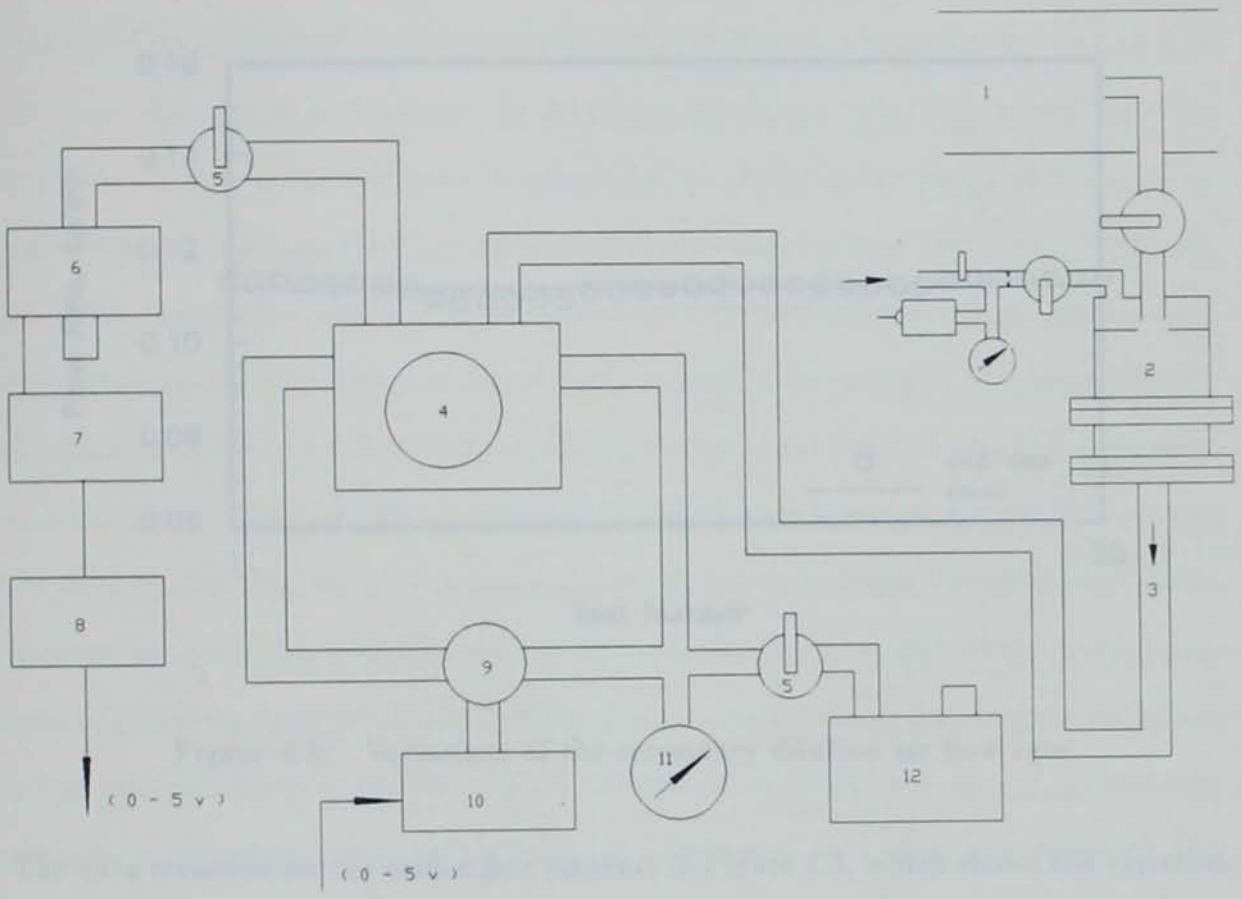

1 -- primary dilution tunnel
2 -- secondary dilution tunnel
3 -- sampling tube
4 -- sampling pump
5 -- ball valve
6 -- ROOTS meter
7 -- frequency counter
8 -- frequency-to-voltage converter
9 -- modulating valve
10 -- electrical controller
11 -- vacuum gage
12 -- vacuum pump

Figure 4.2: Schematic diagram of particulate sampling system

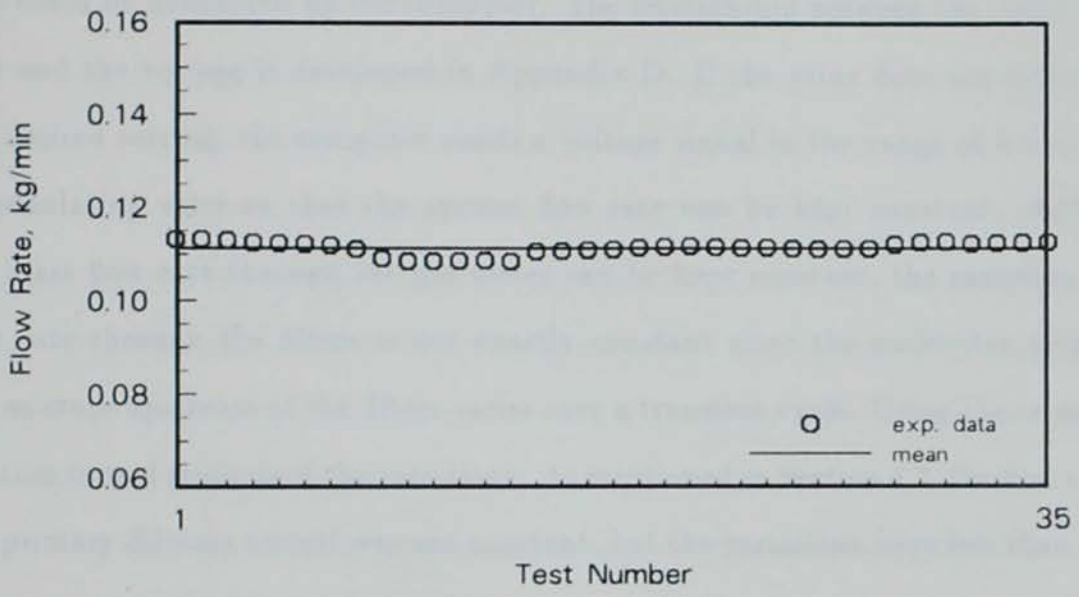

Figure 4.3: Variations of the secondary dilution air flow rate

The data recorded for the orifice flow appears in Figure 4.3, which shows the variation of the secondary dilution air flow rate for 35 different steady-state tests. The average flow rate was 0.1113 kg/min and the coefficient of variance was 2.62%. The mass flow rate through the orifice can be considered constant and the air flow rate used as a reference value.

There were two thermocouples placed in the system, one in the sample chamber, between the primary filter and back-up filter and another installed before the gas meter. The sampling mass flow rate can be calculated using an ideal gas equation with measured temperature and atmospheric pressure, assuming that the mixture upstream of the the gas meter has the same molecular weight as air. The volume

flow rate was converted to a frequency signal by the gas meter and displayed on the frequency counter. A frequency-to-voltage converter was used so that the actual flow rate could be monitored by the computer. The relationship between the volume flow rate and the voltage is developed in Appendix D. If the value does not agree with the desired setting, the computer sends a voltage signal in the range of 0-5 volts to a modulating valve so that the system flow rate can be kept constant. Although the mass flow rate through the gas meter can be kept constant, the sampling mass flow rate through the filters is not exactly constant since the molecular weight of the mixture upstream of the filters varies over a transient cycle. Using the secondary dilution tunnel minimized the variations. As mentioned in Section 4.3, the flow rate in the primary dilution tunnel was not constant, but the variations were less than 7.0%. To measure particulate matter emission accurately, the flow rate of the particulate sampling system must be a constant fraction of the total diluted exhaust flow rate in the primary dilution tunnel. Due to the nature of the system design, it was not possible to maintain the constant fraction. However, this does not diminish the repeatability of the measurements because a consistent particulate sampling method was employed during the course of the study.

For the collection of particulate, 110 mm Pallflex TX40H120WW filters were used, which had a 100 mm stain diameter after being placed on the filter holder. According to the EPA specification, the recommended minimum loading on a 70 *mm* primary filter with a 60 mm stain diameter is 5.3 milligrams over a transient cycle test. To achieve an equivalent loading (mass/stain area), the particulate sampling flow rate was chosen so that the minimum loading on the primary filter was 15.0 milligrams during the test. The minimum sampling flow rate used for the tests was

$3.3 \times 10^{-3}\ m^3/s$ through the filters.

4.4.2 Particulate weighing chamber

A weighing chamber was built for storing and weighing the filters. The chamber measures 915 × 760 × 790 mm. The filters were put in petri dishes on two shelves placed in the chamber during their conditioning. The filters were weighed in the chamber using a Mettler Model AE240 analytical balance. The balance has a precision (standard deviation) of 20 micrograms and a readability of 10 micrograms. Compressed air is passed through an oil removal filter and diffused into the weighing chamber. No swirl was created inside the chamber, hence, no air motion affected the stability of the balance. The purpose of introducing the air into the chamber was to keep the chamber at a stable temperature and humidity. During all filter conditioning and weighing, the temperature of the chamber was maintained within ± 3 K of 297 K and the relative humidity of the chamber was maintained within ± 5 percent of 30 percent. The ambient conditions of the chamber are described in Appendix G. A 60 mm thick foam pad was placed beneath the chamber to isolate the chamber from external vibration.

Two unused reference filters were always kept in the weighing chamber. They were the same size and material as the sample filters and were usually weighed at the same time as the sample filters. The reason for the reference filters was to check the balance and chamber conditions. If there was an unacceptable change of the reference filter weight, the weighing would be stopped and the problem corrected. The reference filters were changed at least once per month, which is specified by the EPA. Four sets of reference filters, a total of 8 filters, were used for covering four

months of tests. The weight changes of the reference filters between sample filter weighings were within ± 1.0 percent and these data are presented in Appendix G. The weighing procedure for the filters is also discussed in Appendix G.

4.5 Data Acquisition System

The Analog Devices RTI-820 board was used with a Zenith 386 computer to acquire data from the experimental equipment. The data were then stored on the Zenith computer for analysis. The RTI-820 board sampled the data at the rate of 21 channels per second for a steady-state test and at the rate of 21 channels every 0.2 seconds over a transient test. The data sets were averaged every 9 seconds for the steady-state test and every one second for the transient test. Only the averaged data were stored on the computer. Table 4.2 shows the measurements which the computer recorded.

The next chapter discusses the procedures used to operate the equipment described above.

Table 4.2: Computer recorded measurements

Measurements
Engine:
Speed
Torque
Rack Position
Turbocharger Speed
Pressures:
Boost Pressure
Exhaust Back Pressure
Primary Dilution Air Orifice
Secondary Dilution Air Orifice
Temperatures:
Ambient(wet bulb)
Ambient(dry bulb)
Intake Manifold
Fuel
Oil
Exhaust(before turbine)
Exhaust(after turbine)
Primary Dilution Air Orifice
Secondary Dilution Air Orifice
Filter Holder Chamber
ROOTS Meter Entry
Flow Rates:
Air Flow Rate to the Engine
Particulate Sampling Rate

5. EXPERIMENTAL PROCEDURE AND DATA ANALYSIS

This chapter describes the procedures used to collect the experimental data. In this study, particulate matter was sampled under steady-state conditions, over an EPA transient cycle, and for discrete segments of various transient cycles. The first section presents the experimental procedure and the matrix of different operating conditions for the steady state tests. The EPA transient test procedures are described in the second section. The other transient test procedures are discussed in the third section. The fourth section describes the procedure for soluble hydrocarbon extraction and the last section discusses data analysis.

5.1 Steady State Test Procedures

The purpose of the steady-state tests was to establish turbocharger performance maps and to investigate the effects of engine fuel-air ratio and speed on particulate emission. The maps were used to support the dynamic turbocharger model described in Section 3.3. The measured particulate emission at different engine fuel-air ratios and speeds was used to develop polynomial expressions which ultimately would be integrated to obtain the total particulate emission.

The tests were carried out at six different speeds (1200 rpm, 1300 rpm, 1500 rpm, 1700 rpm, 1900 rpm, and 2100 rpm) and ten different load conditions (-10%, 0%, 20%,

40%, 50%, 60%, 70%, 80%, 90%, and 100% of the maximum torque at the selected speed). The length of test time was varied according to the different engine operating conditions. The length was chosen so that the particulate filters could accumulate the maximum amount of sample without overloading the constant mass flow rate operation of the particulate sampling system.

It was found that the maximum overall equivalence ratio under steady-state conditions was no more than 0.65 if the turbocharger stayed with the engine. During the actual transient cycles, however, the overall equivalence ratio definitely exceeds 0.65 and can approach 1.0. This case usually occurs during rapid increases in load. To get the desired torque, the fuel input to the engine has to be changed quickly. However, the rapid fueling does not result in instantaneous response of the turbocharger due to its inertia and the compressibility of the exhaust gas link from the engine. The resultant lag between the rate of change of air flow and fueling leads to rapid increases in the overall equivalence ratio in the combustion chamber. To extend the equivalence ratio to higher values, the turbocharger was removed from the engine so that the air flow rate could be reduced. To obtain even higher overall equivalence ratios, beyond 1.0, a restriction was installed upstream of the intake manifold. An orifice with a diameter of 20 *mm* was used as the restriction to the air entering the engine.

The procedure for the steady-state tests started with placing the particulate filters in the weighing chamber. After 48 hours, the filters were weighed with the Mettler micro-balance. The weighing procedure is described in Appendix G.

Once the tare weights of the filters were determined, the engine tests could be conducted. Before starting the engine, the primary dilution air and the secondary

dilution air were run through the tunnels for at least 5 minutes. The purpose of this procedure was to keep the tunnel surfaces free of the deposits which could remain from previous tests. Also, the particulate sampling system was simultaneously operated to clean out the sample system. It should be noted that the primary dilution air valve was always fully open during the tests.

After the engine was started, the speed and load were set to the desired values. When the engine reached the equilibrium operating condition as indicated by stable coolant, oil, and exhaust temperatures, two filters were placed in the filter holders shown in Figure 4.2. Then the particulate sample transfer valve and the secondary dilution air valve were opened and the particulate sampling system was turned on. About 10 seconds were allowed to pass before starting the control program. The reason for this was to enable the particulate sampling system to be controlled quickly and accurately. The sampling flow rate control program needs both the reference and actual flow rate values. If the actual value is far away from the reference value, it takes a long time for the system to achieve an accurate control. Before starting the control program, the system was run at a flow rate which was close to the reference value. Hence, the difference between the actual flow rate and reference flow rate was small and the system could quickly enter its accurate control mode.

As soon as the control program started, the data acquisition system automatically recorded the data shown in Table 4.2. Other data were also manually recorded such as atmospheric pressure, pressure upstream of the compressor, coolant temperature, diesel fuel consumption, and vacuum downstream of the particulate filters. At the end of the test, the particulate sample pump was turned off, the diluted exhaust gas and the secondary dilution air were immediately shut off, and the test duration

was recorded. The used filters were removed from the filter holders shortly after the test and placed in the weighing chamber for stabilization.

The engine was then brought to another steady-state condition according to the test schedule. After placing a new pair of particulate filters into the filter holders, the next data collection was ready. It usually took about 5 minutes for this period.

After 48 hours' stabilization, the used filters were ready for weighing. They were handled using steel forceps and weighed in the weighing chamber. The difference in the final weight and the tare weight was considered to be the mass of the particulate sample. These data were then combined with the sample flow rate and total tunnel flow rates to determine the total mass of particulate matter emitted by the engine during the test period.

5.2 EPA Transient Test Procedures

In 1986 the Environmental Protection Agency (EPA) specified a new test procedure for heavy-duty diesel engine emissions measurement. The test requires the engine to be run through a twenty-minute transient operation cycle that simulates city and highway driving of a truck in both New York and Los Angeles. Figure 5.1 shows how the speed and load for the engine are expected to vary for the cycle. The test requires that the engine be connected to a dynamometer that can be controlled by a computer. The computer sends signals to the dynamometer controller to regulate the engine's speed. Then, while the speed is changing to follow the transient cycle, a rack actuator is used to vary the engine's flywheel torque to match the required torque.

The EPA transient tests conducted for this study followed as closely as possible

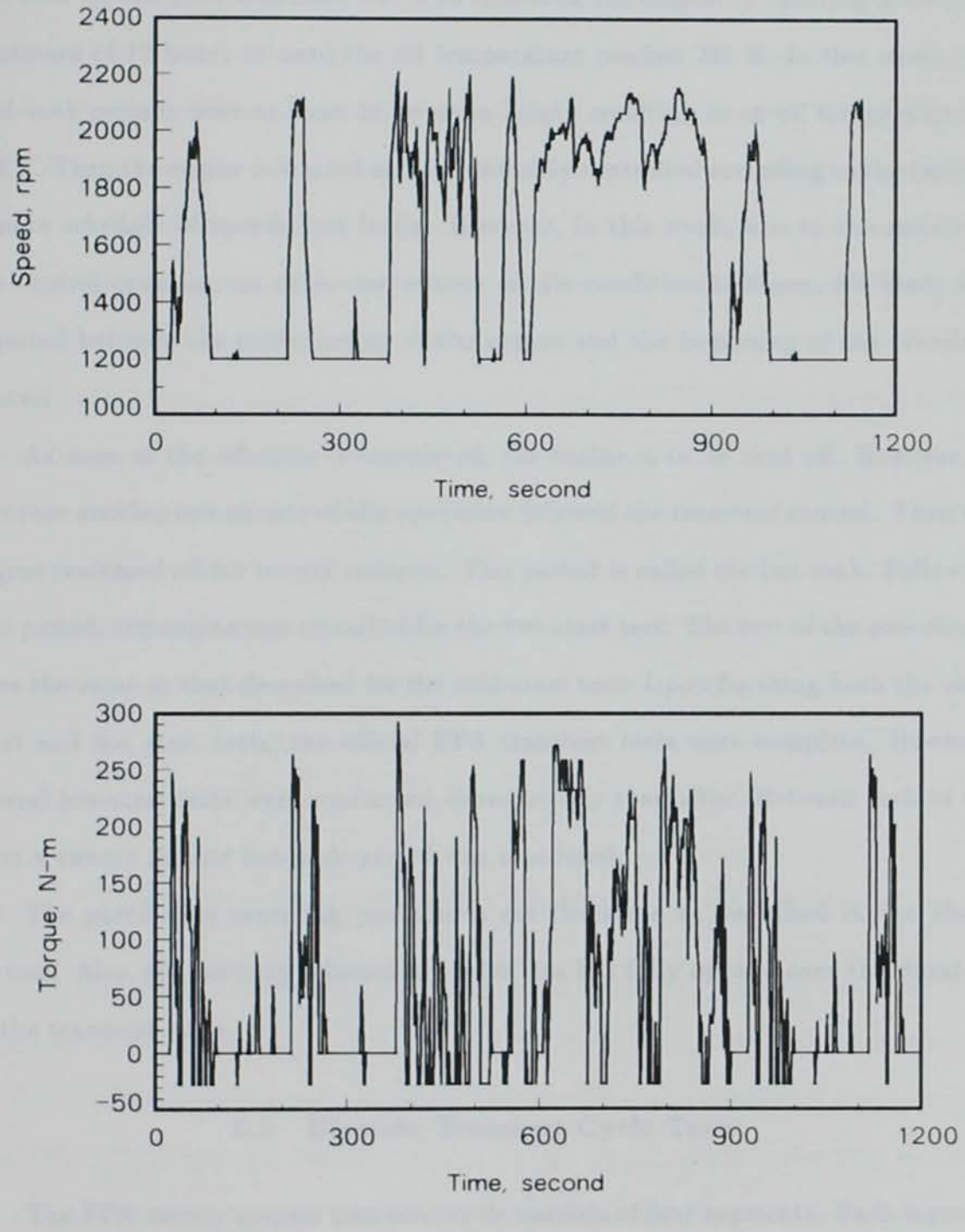

Figure 5.1: Reference speed and torque trajectories for the transient cycle

the procedure specified in the Code of Federal Regulations (CFR) [3]. The procedure specified for the EPA transient test is to cold-soak the engine by shutting it off for a minimum of 12 hours or until the oil temperature reaches 297 K. In this study, the cold-soak periods were at least 24 hours in length resulting in an oil temperature of 302 K. Then the engine is started and immediately controlled according to the twenty-minute schedule of speeds and loads. However, in this work, due to the nature of the control program, an extra one minute of idle condition(1200rpm, 0% load) was required between the cold-starting of the engine and the beginning of the transient control.

As soon as the schedule is completed, the engine is to be shut off. However, in this case another one minute of idle operation followed the transient control. Then the engine remained off for twenty minutes. This period is called the hot-soak. Following this period, the engine was restarted for the hot-start test. The rest of the procedures were the same as that described for the cold-start test. Upon finishing both the cold-start and hot start tests, the official EPA transient tests were complete. However, several hot-start tests were conducted consecutively thereafter. Between each of the tests a twenty minute hot-soak period was scheduled.

The particulate sampling procedures are the same as described in the above section. Also, the primary dilution air valve was left fully opened over the duration of the transient cycle.

5.3 Discrete Transient Cycle Tests

The EPA twenty-minute transient cycle consists of four segments. Each segment lasts five minutes. The first and the fourth segments are identical. Since it was

not possible to measure the instantaneous particulate emission from the engine, it was not possible to make a second-by-second comparison with the predictions of the computer model. However, in addition to a single comparison for the entire cycle, the particulate emission was measured for each of the four quarters of the cycle for comparison with the model predictions. The purpose of the tests were to investigate the effects of different transient cycles on the particulate emission. The tests procedures were set up so that the particulate samples for each five minute transient cycle were collected when the complete EPA transient cycle was performed.

In order to collect the samples for four segments, two identical EPA transient cycles had to be conducted. The two samples for the first and the third segments could be taken during one EPA transient cycle. The other two samples could be collected during another EPA transient cycle. Five minute intervals between the first and the third segments or between the second and the fourth segments were allowed to facilitate particulate filter changes and to complete data recording. The particulate sampling system was operated in the same manner as that presented for the procedures of the EPA transient cycle.

5.4 Procedure for Soluble Hydrocarbon Extraction

The particulate sample was collected in the secondary dilution tunnel at temperatures below 325 K as specified by the EPA. Hence, the particulates included not only solid carbon, but sulfate emissions, and adsorbed and condensed hydrocarbons called the soluble organic fraction (SOF). In this study, soxhlet extraction was conducted to determine the total mass of the SOF. The extraction was performed on the particulate samples collected during the transient cycles and for a few steady-state

conditions (-15%, 60%, 90%, and 100% of the rated load at 1200 rpm).

The procedure started with placing a soiled filter in an 80×25 mm extraction thimble. After stabilizing for 48 hours in the weighing chamber, the thimble with the filter was weighed for tare weight. At all times the filters and the thimbles were handled using steel forceps. Then, the thimble was placed in a Pyrex soxhlet extraction tube. A 125 ml flask filled with 100 ml of methylene chloride was fitted below the tube and an Allihn type condenser was attached to the top of the tube. An Electromantle oven was used to heat the flask and maintain a constant flask temperature. Chilled water was running through the condenser while the methylene chloride vapor was condensed. When the thimble was filled to the top with condensate, the soxhlet automatically drained the condensed solvent and the SOF back to the flask, and the cycle started again. Each cycle took 3 to 3.5 minutes to complete. Twenty cycles were run on each filter. Because only methylene chloride condensate entered the extractor, all of the SOF was ultimately transferred to the flask.

After the last cycle was finished, the thimble with the extracted filter were replaced into the weighing chamber for 48 hours. At the end of that period, it was weighed. The difference in the tare weight and the final weight was considered to be the mass of the SOF.

5.5 Data Analysis

5.5.1 Turbocharger performance

One of the objectives of conducting steady-state tests was to generate the performance maps of the compressor and turbine. When studying turbocharger performance characteristics, it is quite helpful if results from different inlet conditions

can be directly compared to one another. Turbocharge compressor and turbine performance can be characterized by the following four parameters: the mass flow rate $\left(\frac{\dot{m}\sqrt{T_u/T_{ref}}}{p_u/p_{ref}}\right)$, pressure rise $\left(\frac{p_h}{p_l}\right)$, efficiency (η), and speed $\left(\frac{N}{\sqrt{T_u/T_{ref}}}\right)$. Here, subscripts d, u, h, and l stand for downstream, upstream, higher pressure side, and lower pressure side. The mass flow rate and speed are corrected for changes in the inlet temperature and pressure. The reference temperature T_{ref} and pressure p_{ref} are chosen to be 298 K and 1.0 bar. Among these four variables, any two of them can be expressed as a function of the other two variables.

As mentioned in Section 4.5, data related to the turbocharger performance were collected during the tests, including the inlet and outlet temperatures and pressures of the compressor and the turbine, pressure rises across the compressor and the turbine, and the turbocharger speed. After the data analysis, the pressure rise and efficiency were expressed as a function of the mass flow rate and speed for both the compressor and the turbine.

5.5.2 Calculation of particulate emission from measurements

According to Code of Federal Regulation [3], the total mass of particulates produced by the engine in either the hot or cold start test, P_{mass}, is found from the following equation:

$$P_{mass} = (V_{mix} + V_{sf})\left(\frac{p_f}{V_{sf}}\right) \tag{5.1}$$

where

P_{mass}=the total particulate emitted,

V_{mix}=the total diluted exhaust volume through the primary dilution tunnel,

V_{sf}=the total volume of sample withdrawn from the primary dilution tunnel, and

p_f=the mass collected on filters.

This equation was developed for PDP-CVS systems. Since the system used in this study was different from the EPA specified system, Eq. 5.1 was modified. It is described as follows.

$$P_{mass} = (m_{mix} + m_{sf}) \left(\frac{p_f}{m_{sf}} \right) \tag{5.2}$$

where

P_{mass}=the total particulate emitted,

m_{mix}=the total diluted exhaust mass through the primary dilution tunnel,

m_{sf}=the total mass of sample withdrawn from the primary dilution tunnel, and

p_f=the mass collected on filters.

As discussed in Section 1.2, the purpose of this study was to predict transient particulate emissions based on steady-state particulate measurements with predicted engine overall equivalence ratio. Because the primary dilution air flow rate was constant and the ball valve was always kept fully opened, dilution ratios were consistent for both steady-state and transient tests. Also, the mass flow rate of sample was kept constant during the tests. So, the mass flows could easily be calculated. Thus, Eq. 5.2 was employed for the particulate calculation in this study.

m_{mix} was expressed as:

$$m_{mix} = m_{pda} + m_{in} + m_f \tag{5.3}$$

where

m_{pda}=the total mass of dilution air through the primary dilution tunnel, which

was calculated by integrating Eq. E.1. from Appendix E, over a period of time,

m_{in}=the total air entering the engine, which was measured by a laminar flow element, and

m_f=the total fuel consumed during the test.

It is noted that the total mass of exhaust gas is the summation of m_{in} and m_f.

m_{sf} was given as:

$$m_{sf} = m_{smp} - m_{sda} \tag{5.4}$$

where

m_{smp}=the total mass of sample through the secondary dilution tunnel, and

m_{sda}=the total mass of dilution air entering the secondary dilution tunnel, which was calculated by integrating Eq. E.2, from Appendix E, over a period of time.

Assuming that the pressure drop across the ROOTS gas meter is negligible and that the sample through the secondary dilution tunnel has the same molecule weight as air, $\dot{m}_{smp}$ was calculated as follows.

$$\dot{m}_{smp} = \frac{p_{atm} Q_{rt}}{R_{air} T_{brt}} \tag{5.5}$$

where

p_{atm}=the atmospheric pressure,

Q_{rt}=the volumetric flow rate through the ROOTS meter,

R_{air}=the gas constant for air, and

T_{brt}=the temperature before the ROOTS meter.

As mentioned in Section 5.1, steady-state tests were always performed when the engine was at fully warmed-up conditions. Hence this study emphasized comparisons

between the experimental measurements and model-predicted values only for the hot start tests, though some cold start tests were conducted.

It has been shown that diesel particulate emission is mainly dependent on engine load (equivalence ratio) and speed if the same kind of diesel fuel is used [74], [75]. Gagele [76] indicated that the effect of ambient temperature on the particulate emission was not significant. After completion of the steady-state tests discussed in Section 5.1, the particulate emission was expressed as a function of the engine overall equivalence ratio and speed. The emission was on a mass rate basis (grams/min) rather than on a brake specific basis (g/bkW-hr). The primary reason for this is that if the emission were in the unit of g/bkW-hr, the emissions at idling or motoring could not be expressed since the brake work is zero. Brake specific value is easily obtained if the work performed is known.

5.5.3 Statistical analysis

To provide a quantitative basis for comparing model-predicted values with experimental measurements, a statistical analysis was performed. The association between two variables was studied by using the method of least squares and linear regression [77]. The experimental measurement was chosen as variable x and the model-predicted value as y. The best fit equation has the form:

$$y = a + bx \tag{5.6}$$

where

a=the intercept of the regression line on y,

b=the slope of a regression line,

x=the experimental measurement, and

y=the model-predicted value.

If the model-predicted and experimental values agree perfectly, then a will equal zero and b will equal one.

Intercept a and slope b can be found by the following equations.

$$a = \frac{\sum_{i=1}^{n} x_i^2 \sum_{i=1}^{n} y_i - \sum_{i=1}^{n} x_i \sum_{i=1}^{n} x_i y_i}{n \sum_{i=1}^{n} x_i^2 - \left(\sum_{i=1}^{n} x_i \right)^2} \tag{5.7}$$

and

$$b = \frac{n \sum_{i=1}^{n} x_i y_i - \sum_{i=1}^{n} x_i \sum_{i=1}^{n} y_i}{n \sum_{i=1}^{n} x_i^2 - \left(\sum_{i=1}^{n} x_i \right)^2} \tag{5.8}$$

The coefficient of determination (r^2) can be calculated as follows.

$$r^2 = \frac{\left[\sum_{i=1}^{n} (x_i - \bar{x})(y_i - \bar{y}) \right]^2}{\sum_{i=1}^{n} (x_i - \bar{x})^2 (y_i - \bar{y})^2} \tag{5.9}$$

where

$$\bar{x} = \frac{\sum_{i=1}^{n} x_i}{n}$$

$$\bar{y} = \frac{\sum_{i=1}^{n} y_i}{n}$$

and

where n=Number of Observations

The relative error between model-predicted and measured values is defined as follows.

$$RE = \frac{X_{mdl} - X_{exp}}{X_{exp}} \times 100.0\% \tag{5.10}$$

where

X_{mdl}=the model predicted value, and

X_{exp}=the experimentally measured value.

These statistical quantities will be used in the following chapter to characterize the agreement of the predicted and measured values.

6. RESULTS AND DISCUSSION

In this chapter the predictions of the engine model are compared with the experimental data. The chapter is composed of four sections. In the first section, the model-predicted engine performance parameters which affect overall equivalence ratio are compared with experimental measurements. These parameters include boost pressure and temperature, back pressure and temperature, and turbocharger speed. The second section presents the model-predicted instantaneous equivalence ratios over the EPA transient cycle. In addition, the air and fuel flow rates predicted by the model are compared to the experimental data. In the third section the distributions of equivalence ratio and engine speed over the EPA transient cycle schedule are statistically analyzed. Finally, the fourth section presents a comparison of the model-predicted particulate emissions with experimental measurements for different transient cycles.

All the experimental data for the comparisons discussed in this chapter were obtained when the engine was run at hot starting conditions. This means the engine was started after having previously run the engine long enough to bring the engine oil and coolant to their equilibrium operating temperatures. The reason for this was that the turbocharger performance maps and the particulate emission calculations for the engine model were based on hot steady-state measurements. To be consistent,

all the comparisons are performed for the hot starting cases of the transient cycle.

Data analyses have been performed for the comparison of the model predictions on with the experimental measurements. The methods and basic equations were presented in Section 5.5.3. The terminology and the symbols are consistent with those presented in that section.

6.1 Model's Capability of Predicting Engine Performance Parameters

The engine model can predict boost pressure and temperature, back pressure and temperature, and turbocharger speed. This section presents the comparison of the measured test data for these quantities with the model predictions.

The duration of the EPA transient test is 1,199 seconds. The EPA specifies discrete engine speed and torque values for each one-second time interval. Following EPA specified criteria, the validity of the actual speed and torque trajectories was checked for each completed transient cycle test. The items to be checked are the maximum standard error SE, intercept a, slope b, and the coefficient of determination r^2 for the experimental measurements on reference values. The calculations of SE, a, b, and r^2 were discussed in Section 5.5.3. The criteria were set for engine speed, torque, and brake power. It turned out that all 12 EPA transient cycle tests conducted for this study were valid.

6.1.1 Boost pressure and temperature

The boost pressure was calculated in the computer program by using the compressor map at the current values of the corrected air flow rate and the turbocharger speed. As discussed in Sections 4.1 and 4.5, the engine boost pressure and temper-

ature were measured upstream of the intake manifold using a Viatran 141 pressure transducer and a type K thermocouple. The measured data were recorded on a Z-386 computer. The experimentally measured and model-predicted quantities are compared as follows.

The instantaneous pressure ratio of the turbocharger compressor is shown in Figure 6.1 over the EPA transient cycle. The qualitative agreement between the model-predicted and the measured boost pressure is very good. In order to make a quantitative comparison, Figure 6.2 shows the correlation between the model-predicted and the measured boost pressure for one of the transient cycle tests. The boost pressure was normalized and expressed as the ratio of the boost pressure to the atmospheric pressure. In Figure 6.2, the horizontal axis presents the measured data and the vertical axis presents the model-predicted values. The intercept of the linear regression line was -0.079, the slope 1.074, and the coefficient of determination 0.899. The ideal linear regression is also illustrated in Figure 6.2. The equations used to calculate these quantities are given in Section 5.5.3. This method of quantifying the comparison between the predicted and experimental data was chosen because it is consistent with the procedure mandated by the EPA for comparing actual engine speed and torque with their reference values. Several scattered data points far away from the linear regression line might be due to either the error measurement of the pressure or the phase offset between the measurement and the prediction. This technique for comparison may somewhat exaggerate the differences between the two sets of data since small phase shifts can give the large apparent scatter shown in Figure 6.2. However, the slope and intercept should still be useful for making comparison.

Agreement between predictions and measured values over the entire transient

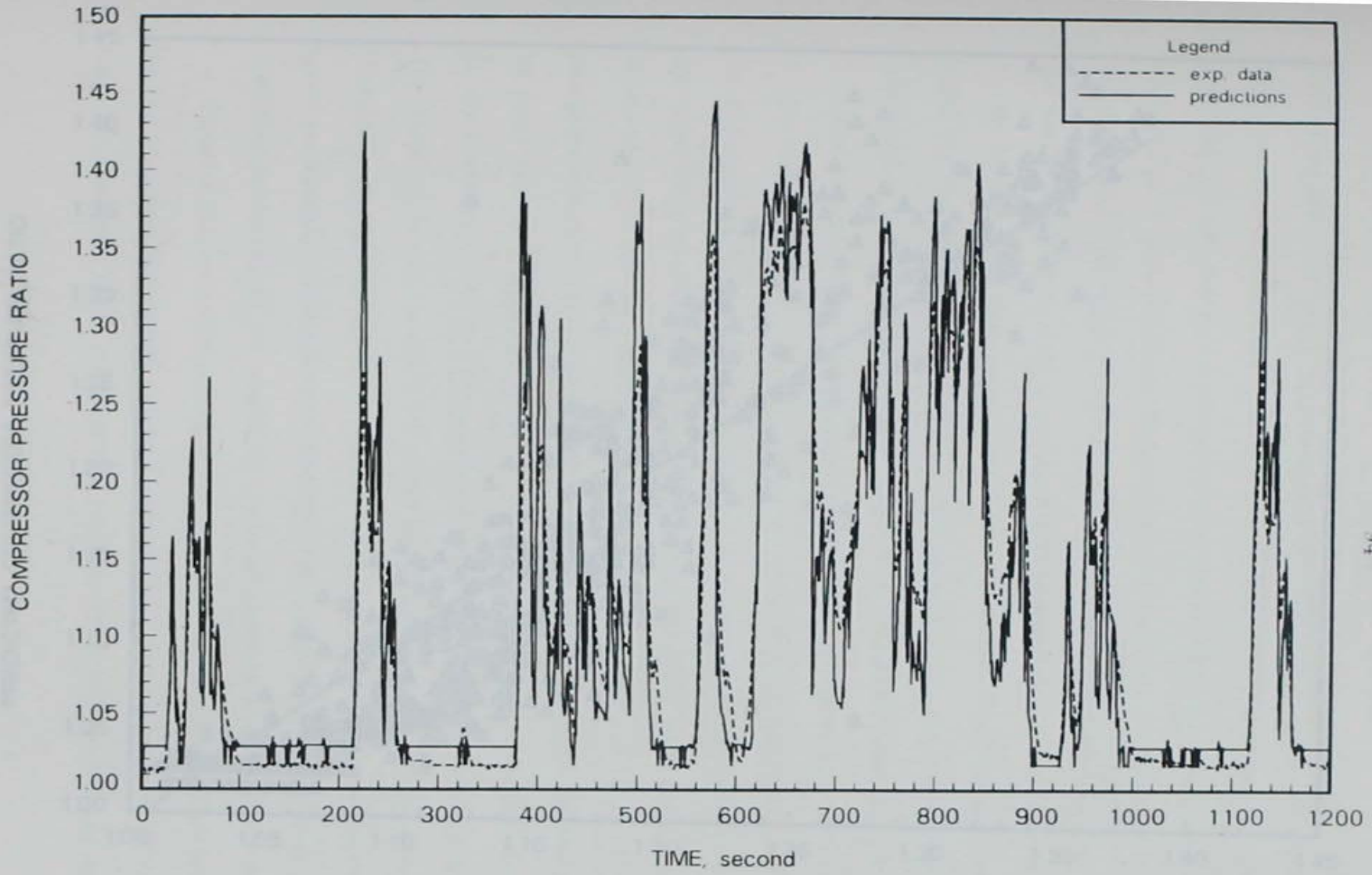

Figure 6.1: Comparison of model-predicted and measured boost pressures over the EPA transient cycle

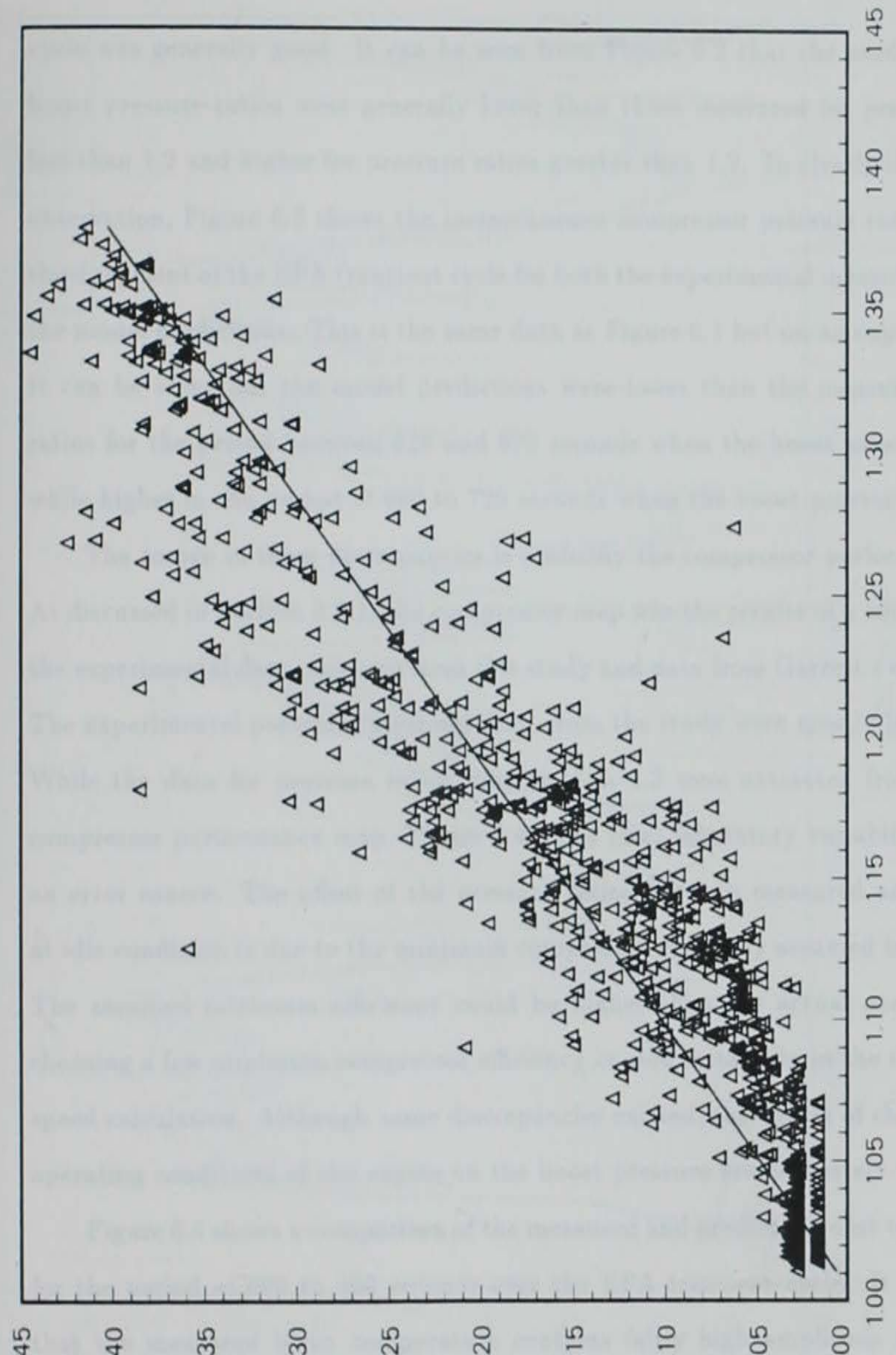

Figure 6.2: Linear regression analysis on boost pressures

cycle was generally good. It can be seen from Figure 6.2 that the model-predicted boost pressure ratios were generally lower than those measured for pressure ratios less than 1.2 and higher for pressure ratios greater than 1.2. To clearly illustrate the observation, Figure 6.3 shows the instantaneous compressor pressure ratios over the third segment of the EPA transient cycle for both the experimental measurements and the model predictions. This is the same data as Figure 6.1 but on an expanded scale. It can be seen that the model predictions were lower than the measured pressure ratios for the period between 620 and 670 seconds when the boost pressure is high, while higher in the period of 680 to 720 seconds when the boost pressure is low.

The source of these discrepancies is probably the compressor performance map. As discussed in Section 3.3.1, the compressor map was the results of a combination of the experimental data obtained from this study and data from Garrett's experiments. The experimental pressure ratios obtained from the study were mostly less than 1.2. While the data for pressure ratios greater than 1.2 were extracted from Garrett's compressor performance map, Figure 3.4. The inter-laboratory variability could be an error source. The offset of the pressure ratios between measured and predicted at idle condition is due to the minimum compressor efficiency assumed in the model. The assumed minimum efficiency could be higher than the actual one. However, choosing a low minimum compressor efficiency caused instability in the turbocharger speed calculation. Although some discrepancies existed, the effects of changes in the operating conditions of the engine on the boost pressure are accurately predicted.

Figure 6.4 shows a comparison of the measured and predicted boost temperatures for the period of 600 to 900 seconds over the EPA transient cycle. It can be seen that the measured boost temperature contains fairly high amplitude spikes. The

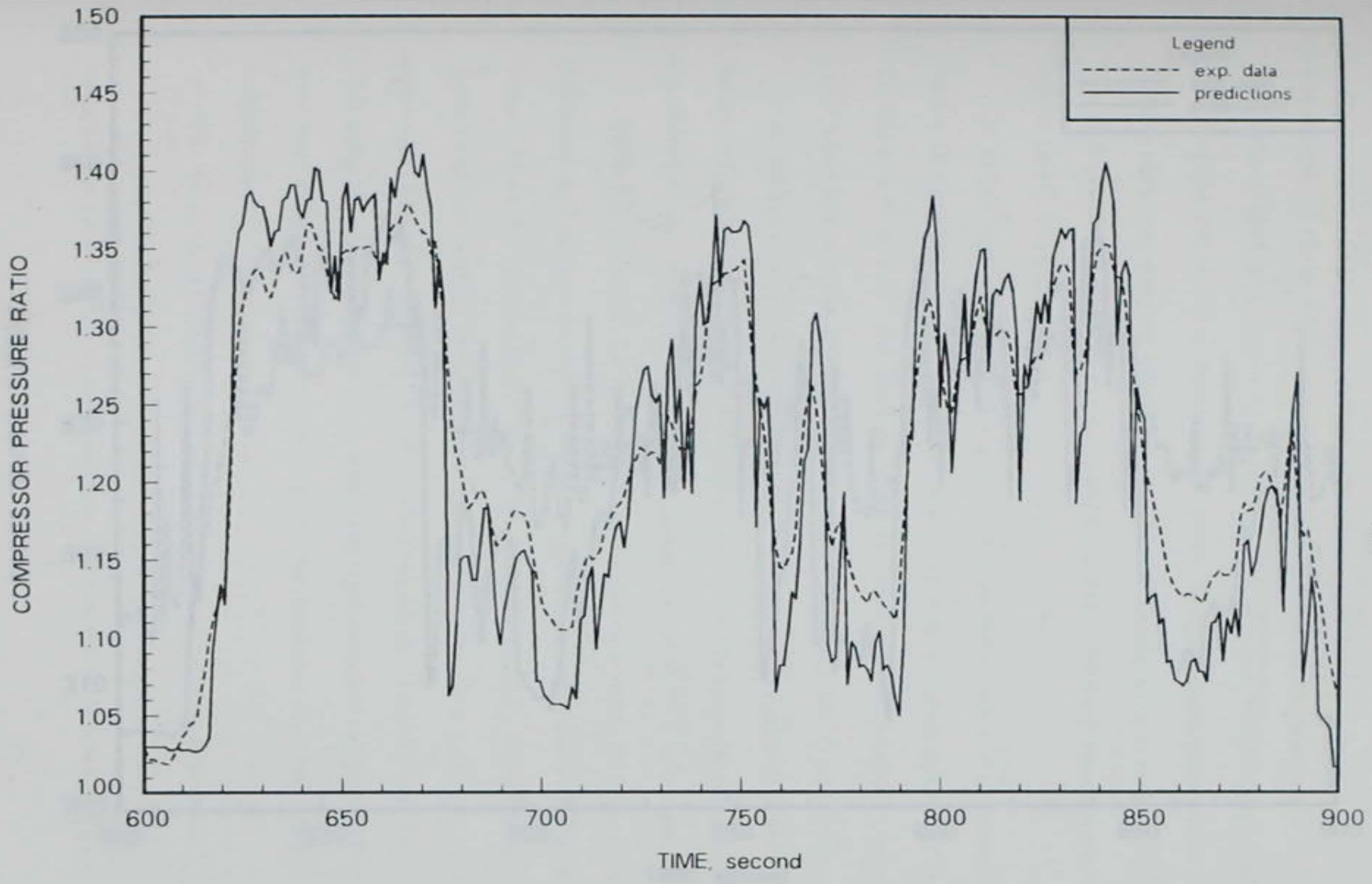

Figure 6.3: Comparison of model-predicted and measured boost pressure over the third segment of the EPA transient cycle

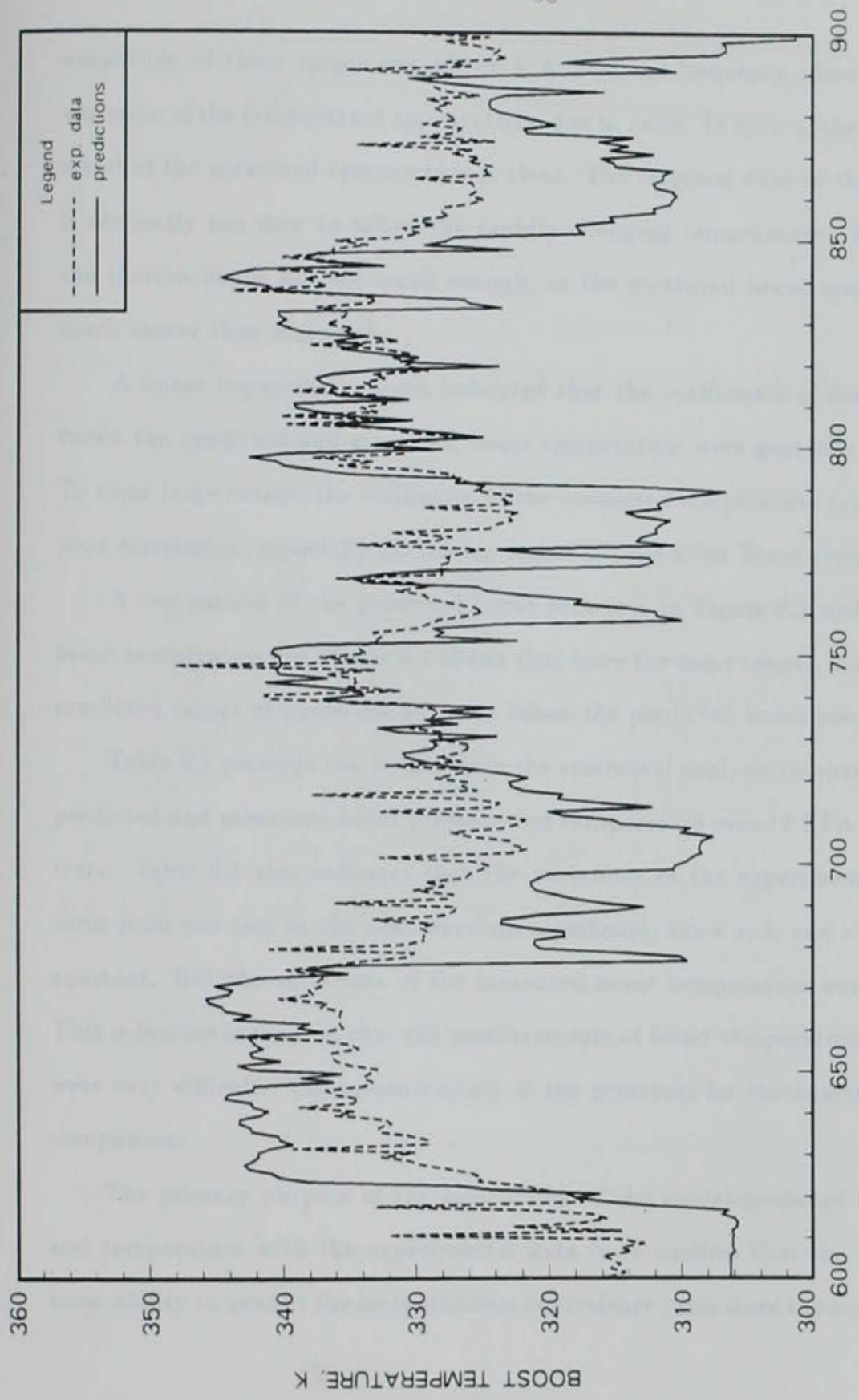

Figure 6.4: Comparison of model-predicted and measured boost temperature over the third segment of the EPA transient cycle

amplitude of these spikes was about 5 K and the frequency about 0.2 Hz. The variation of the temperature appears to be due to noise. In spite of the noise spikes the trend of the measured temperature is clear. The response time of the thermocouple is obviously too slow to follow the rapidly changing temperature. The diameter of the thermocouple was not small enough, so the measured boost temperature varies much slower than expected.

A linear regression analysis indicated that the coefficients of determination between the predicted and measured boost temperature were generally less than 0.60. To some large extent, the oscillation of the measured temperature contributes to the poor correlation, especially for the big spikes at such a low boost temperature range.

A comparison of the predicted boost pressures in Figure 6.3 with the predicted boost temperatures in Figure 6.4 shows they have the same trends, that is, the model predicted values of boost temperature follow the predicted boost pressure.

Table 6.1 presents the results from the statistical analysis comparing the model-predicted and measured boost pressure and temperature over 12 EPA transient cycle tests. Table 6.1 also indicates that the variations of the experimental boost pressures from one test to the next were not significant, since a, b, and r^2 were roughly constant. But the variations of the measured boost temperature were much larger. This is further indication that the measurements of boost temperature for the engine were very difficult. The measurements of the pressures for the engine were easy by comparison.

The primary purpose of the comparison of the model-predicted boost pressure and temperature with the experimental data is to confirm that the model has the basic ability to predict the instantaneous equivalence ratio since the equivalence ratio

Table 6.1: Comparison of model-predicted and measured boost pressures and temperatures

Case	Pressure ratio, p_2/p_1			Boost temperature, T_2		
	a	b	r^2	a K	b	r^2
1	-0.079	1.074	0.899	-38.31	1.105	0.561
2	-0.056	1.056	0.904	41.87	0.869	0.464
3	-0.073	1.069	0.904	-45.27	1.134	0.561
4	-0.085	1.080	0.904	-32.63	1.090	0.544
5	-0.078	1.074	0.896	-12.23	1.026	0.509
6	-0.049	1.049	0.897	-3.400	1.012	0.519
7	-0.0637	1.059	0.905	-25.18	1.075	0.532
8	-0.0679	1.063	0.904	-45.89	1.142	0.569
9	-0.0572	1.052	0.906	-35.50	1.111	0.538
10	-0.054	1.049	0.903	-24.65	1.076	0.528
11	-0.059	1.053	0.900	-36.53	1.114	0.535
12	-0.056	1.050	0.905	-32.29	1.102	0.552

a — Intercept
b — Slope
r^2 — Coefficient of determination

is strongly affected by the boost pressure and temperature. It should be apparent from the above discussion that the model can accurately predict the instantaneous engine boost pressures during the EPA transient cycle, but it is not possible to say this for boost temperature since the measured data is not reliable. It will be shown later that the turbocharger performance is predicted well and this provides implicit validation of the predicted boost temperature.

6.1.2 Back pressure and temperature

The exhaust pressure and temperature before the turbocharger turbine were measured during the tests. Figure 6.5 shows the trajectory of the back pressure both measured and predicted over the EPA transient cycle. To more clearly illustrate the trends of the curves, the second segment of the EPA transient cycle is shown in Figure 6.6.

Figure 6.7 illustrates the linear regression analysis for the two curves shown in Figure 6.5. The intercept, slope, and coefficient of determination for the linear regression line were 0.093, 0.924, and 0.937. It can be seen from Figure 6.5– 6.6 that the model predictions consistently match the measured back pressures over the entire transient cycle test, except at very low back pressures. The source of the low level oscilations is probably noise from the pressure transducer. The difference in the baseline levels at idle is probably due to slight error in the turbocharger maps.

Good agreement between the simulation results and the measurements lead to a conclusion that that the model can accurately predict the back pressure. This also implies that the turbine performance map was properly constructed because the back pressure is one of the outputs from the turbine performance map. In general,

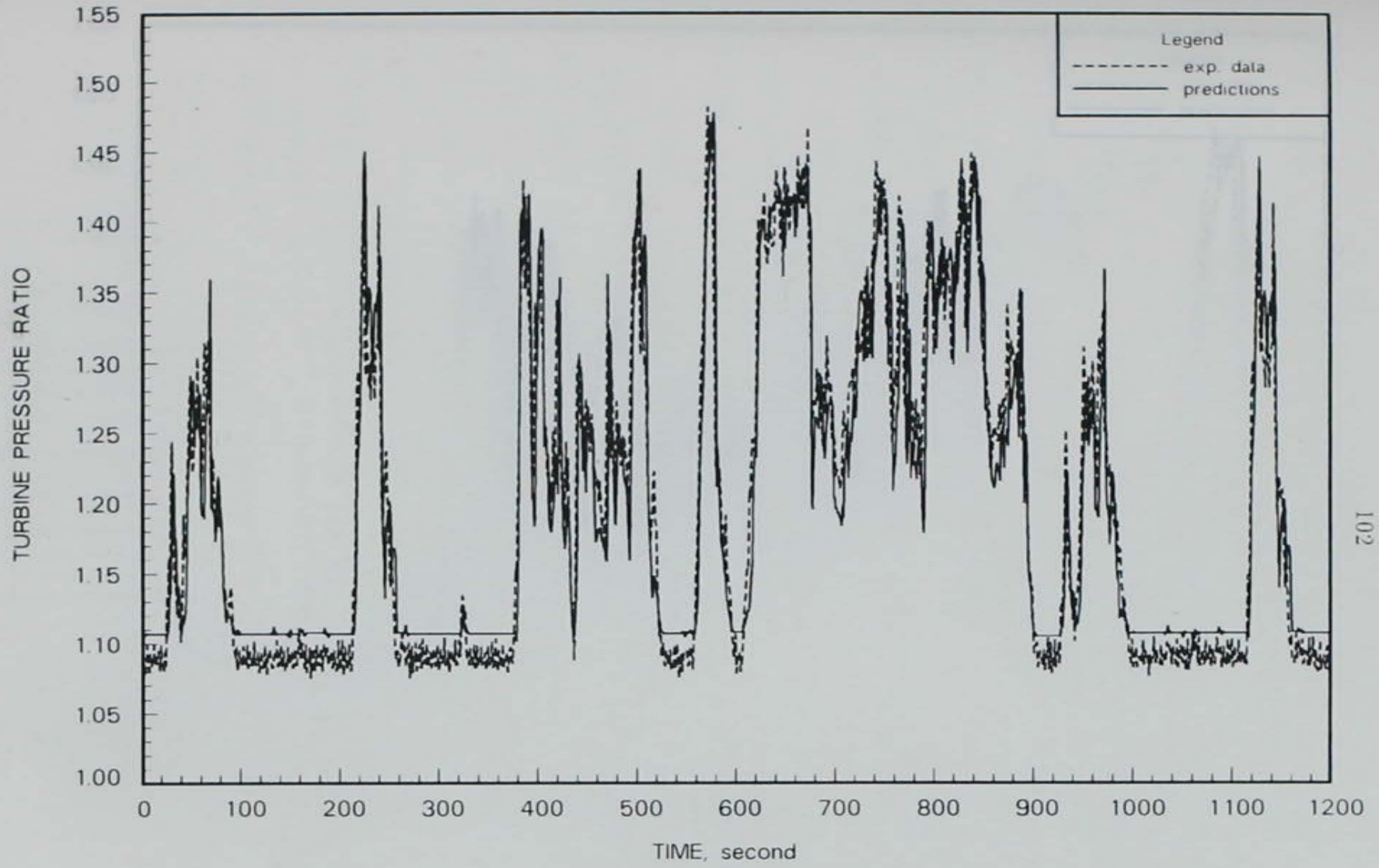

Figure 6.5: Comparison of model-predicted and measured back pressures

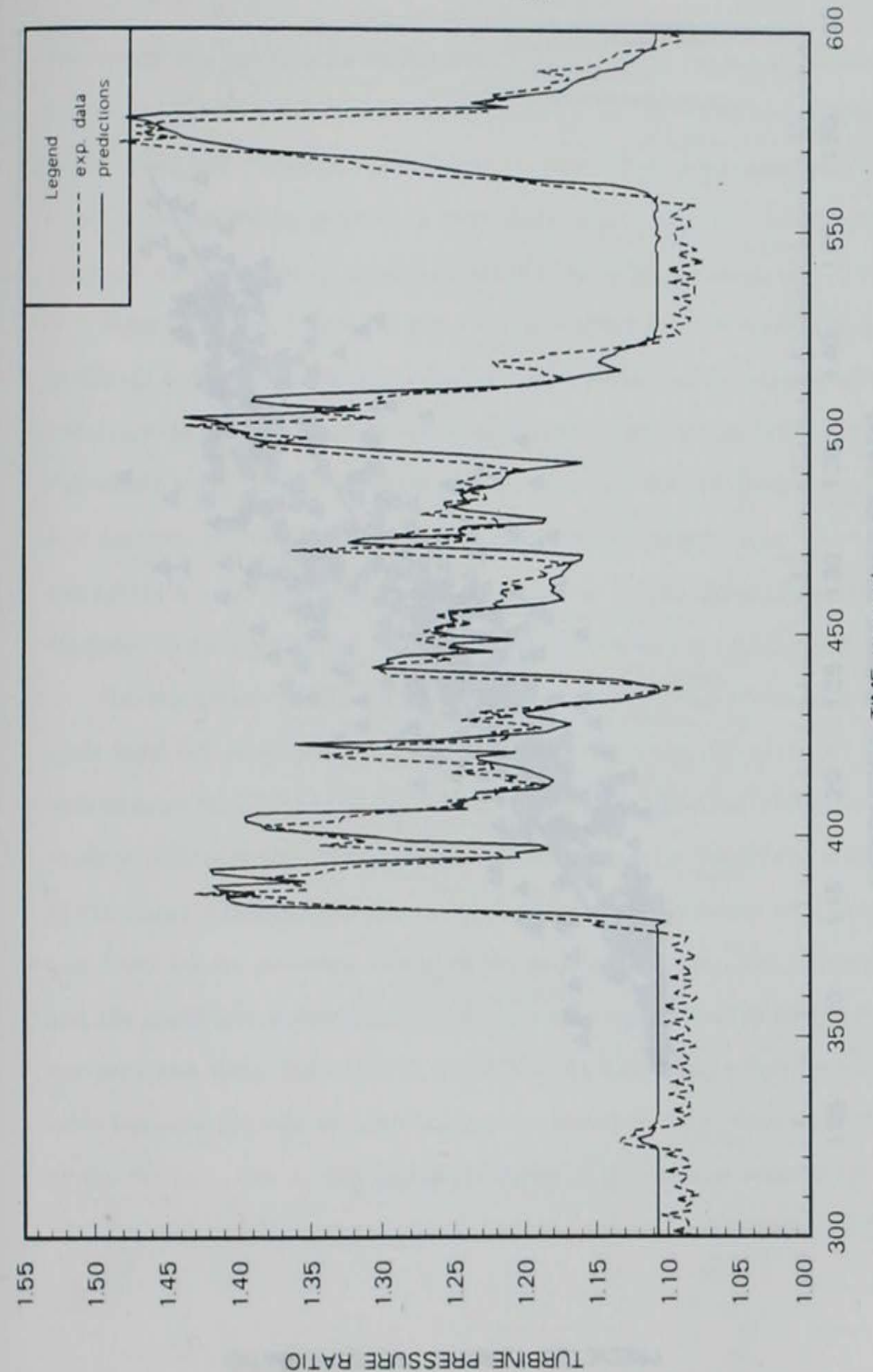

Figure 6.6: Comparison of model-predicted and measured back pressure over the second segment of the EPA transient cycle

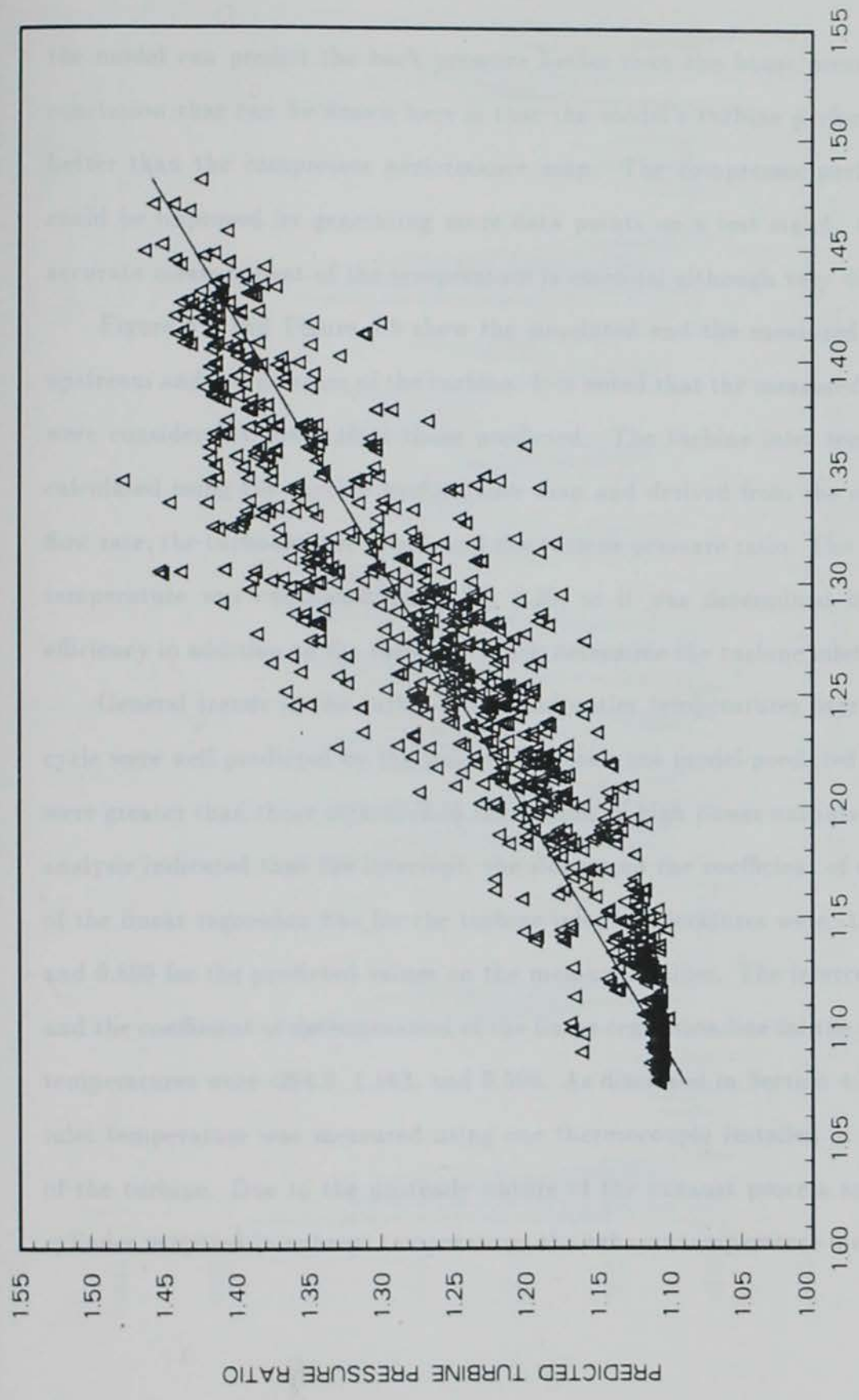

Figure 6.7: Linear regression analysis on back pressures

the model can predict the back pressure better than the boost pressure. Another conclusion that can be drawn here is that the model's turbine performance map is better than the compressor performance map. The compressor performance map could be improved by generating more data points on a test stand. Of course, the accurate measurement of the temperature is essential although very difficult.

Figure 6.8 and Figure 6.9 show the simulated and the measured temperatures upstream and downstream of the turbine. It is noted that the measured temperatures were considerably lower than those predicted. The turbine inlet temperature was calculated using the turbine performance map and derived from the corrected mass flow rate, the turbocharger speed, and the turbine pressure ratio. The turbine outlet temperature was calculated using Eq. 3.20, so it was determined by the turbine efficiency in addition to the variables which determine the turbine inlet temperature.

General trends in the turbine inlet and outlet temperatures over the transient cycle were well predicted by the model. However, the model-predicted temperatures were greater than those measured in the regions of high power outputs. A statistical analysis indicated that the intercept, the slope, and the coefficient of determination of the linear regression line for the turbine inlet temperatures were -134.0 K, 1.342 and 0.809 for the predicted-values on the measured-values. The intercept, the slope, and the coefficient of determination of the linear regression line for the turbine outlet temperatures were -264.0, 1.563, and 0.596. As discussed in Section 4.1, the turbine inlet temperature was measured using one thermocouple installed in the upstream of the turbine. Due to the unsteady nature of the exhaust process and cylinder to cylinder variation in exhaust temperature, the exhaust temperature measured by the

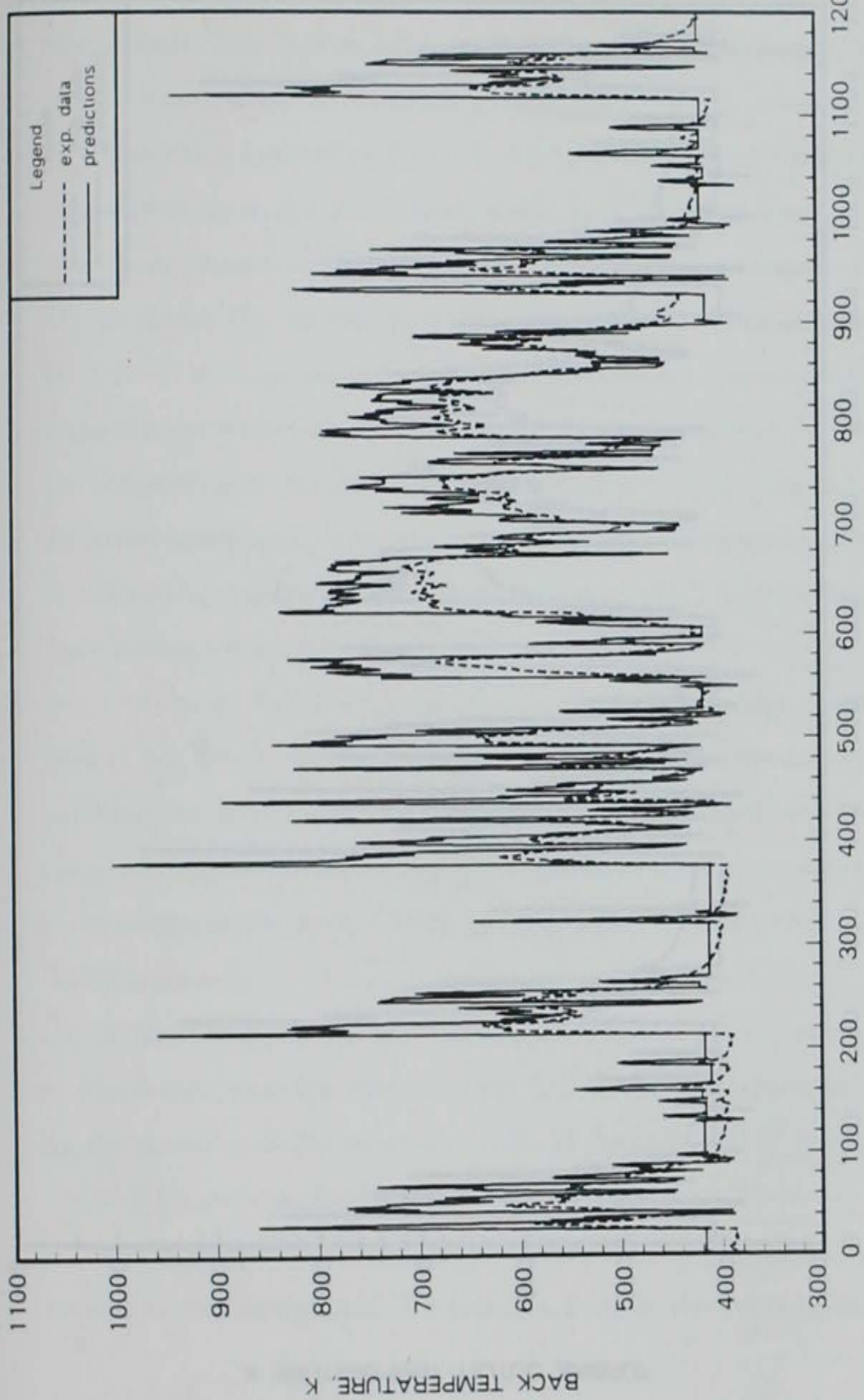

Figure 6.8: Comparison of model-predicted and measured turbine inlet temperatures

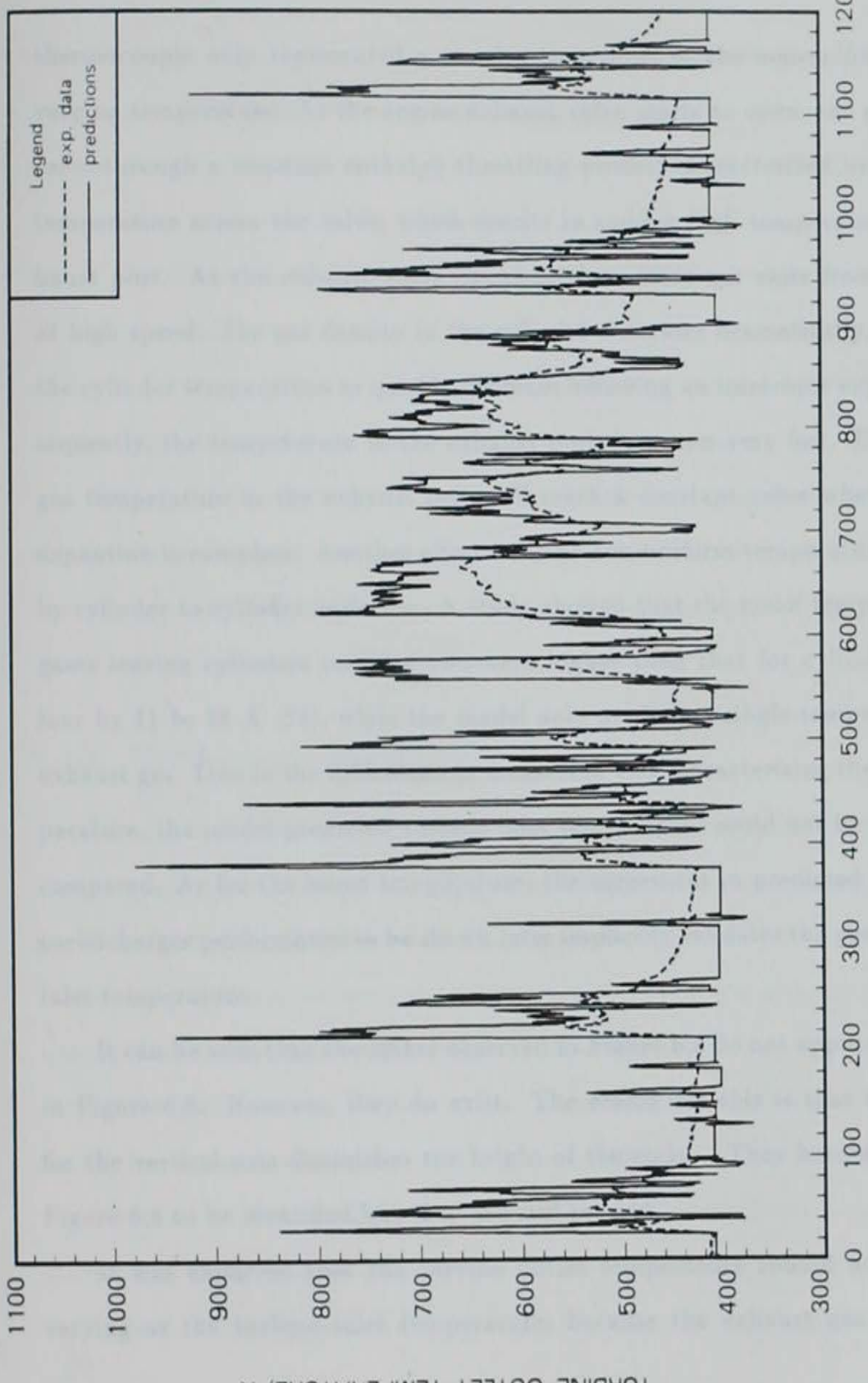

Figure 6.9: Comparison of model-predicted and measured turbine outlet temperatures

thermocouple only represented a rough mean value of the non-uniform and time-varying temperature. As the engine exhaust valve starts to open, the gas passes the valve through a constant enthalpy throttling process characterized by the constant temperature across the valve, which results in sudden high temperatures in the exhaust port. As the exhaust valve opens further, more gas exits from the cylinder at high speed. The gas density in the cylinder decreases dramatically, which causes the cylinder temperature to quickly decrease following an isentropic expansion. Consequently, the temperature in the exhaust port decreases very fast. Eventually, the gas temperature in the exhaust port will reach a constant value when the exhaust expansion is complete. Another effect was the non-uniform temperature contributed by cylinder to cylinder variation. A study showed that the mean temperature of the gases leaving cylinders one and two were higher than that for cylinders three and four by 11 to 28 K [78], while the model only predicts a single temperature for the exhaust gas. Due to the difficulties in measuring and characterizing the exhaust temperature, the model-predicted turbine inlet temperature could not be quantitatively compared. As for the boost temperature, the agreement in predicted and measured turbocharger performance to be shown later implicitly validates the predicted turbine inlet temperature.

It can be seen that the spikes observed in Figure 6.4 do not appear to be present in Figure 6.8. However, they do exist. The reason for this is that the large scale for the vertical axis diminishes the height of the spikes. They become too small in Figure 6.8 to be identified but they are still present.

It was expected that the turbine outlet temperature should not be as time-varying as the turbine inlet temperature, because the exhaust gas is well mixed

after it passes the turbine. Unfortunately, the results were in conflict with this expectation. The coefficient of determination for the model-predicted turbine outlet temperature on the measured values was lower than that for the model-predicted turbine inlet temperature. The difficulty in measuring the temperature was still the major contributor to the discrepancy. Also, the assumption of the constant turbine efficiency could decrease the accuracy of predicting the outlet temperatures. The capability of the model in predicting the turbine outlet temperature will be discussed further after presenting the results of the turbocharger speed.

Table 6.2 lists all the statistical results by the linear regression analysis for the predicted and the measured back pressures and temperatures. It should be mentioned that the primary reason for the lack of agreement between the predicted and measured data is the error in the measured data.

6.1.3 Turbocharger speed

The turbocharger speed was measured over a transient cycle using the laser detector described in Section 4.1. The model-predicted and measured turbocharger speed are compared in Figure 6.10 for one of the transient cycle tests. Figure 6.11 shows the correlation between the model prediction and the measured turbocharger speeds. The horizontal axis represents the measured speeds and the vertical axis represents the predicted ones. The intercept, slope, and the coefficient of determination for the linear regression line were -233.2 rpm, 1.007, and 0.895 respectively.

The turbocharger speed was a particularly difficult quantity to predict since it was derived from both the compressor and the turbine performance maps as well as the dynamic turbocharger model. As Eq. 3.23, 3.24, and 3.25 indicated, the turbine

Table 6.2: Comparison of model-predicted and measured back pressures and turbine inlet temperatures

Case	Pressure ratio, p_3/p_4			Back temperature, T_3		
	a	b	r^2	a	b	r^2
				K		
1	0.093	0.924	0.937	-134.0	1.342	0.809
2	0.107	0.908	0.946	-158.7	1.382	0.835
3	0.097	0.920	0.937	-132.4	1.339	0.824
4	0.092	0.925	0.940	-130.1	1.339	0.810
5	0.096	0.922	0.938	-118.5	1.319	0.793
6	0.122	0.898	0.937	-132.0	1.350	0.801
7	0.104	0.912	0.942	-132.3	1.353	0.804
8	0.112	0.905	0.938	-139.0	1.367	0.799
9	0.124	0.894	0.940	-135.1	1.362	0.805
10	0.117	0.899	0.941	-135.6	1.361	0.800
11	0.118	0.899	0.939	-133.7	1.362	0.793
12	0.113	0.902	0.940	-132.8	1.369	0.814

a — Intercept

b — Slope

r^2 — Coefficient of determination

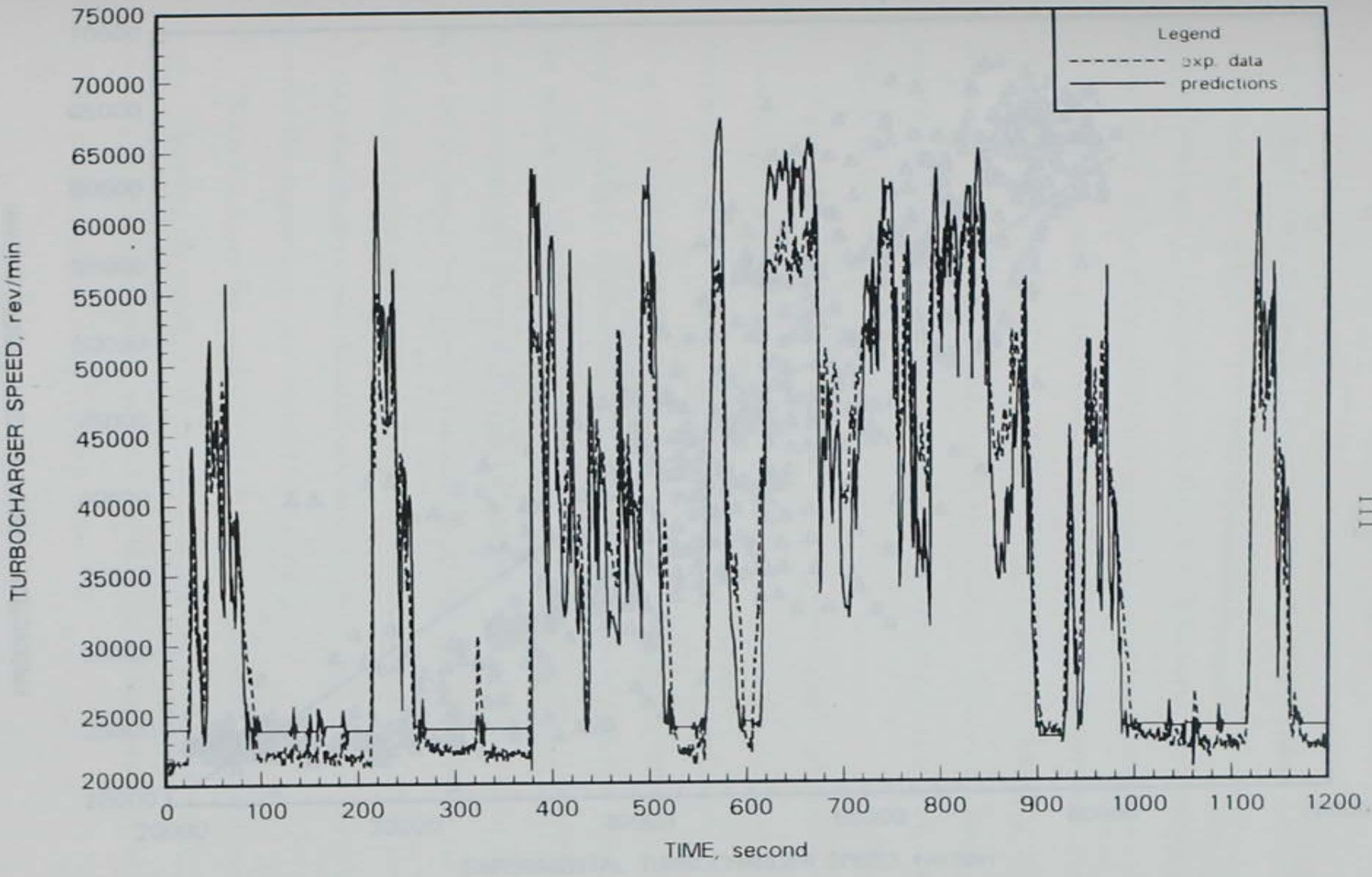

Figure 6.10: Comparison of model-predicted and measured turbocharger speeds over the EPA transient cycle

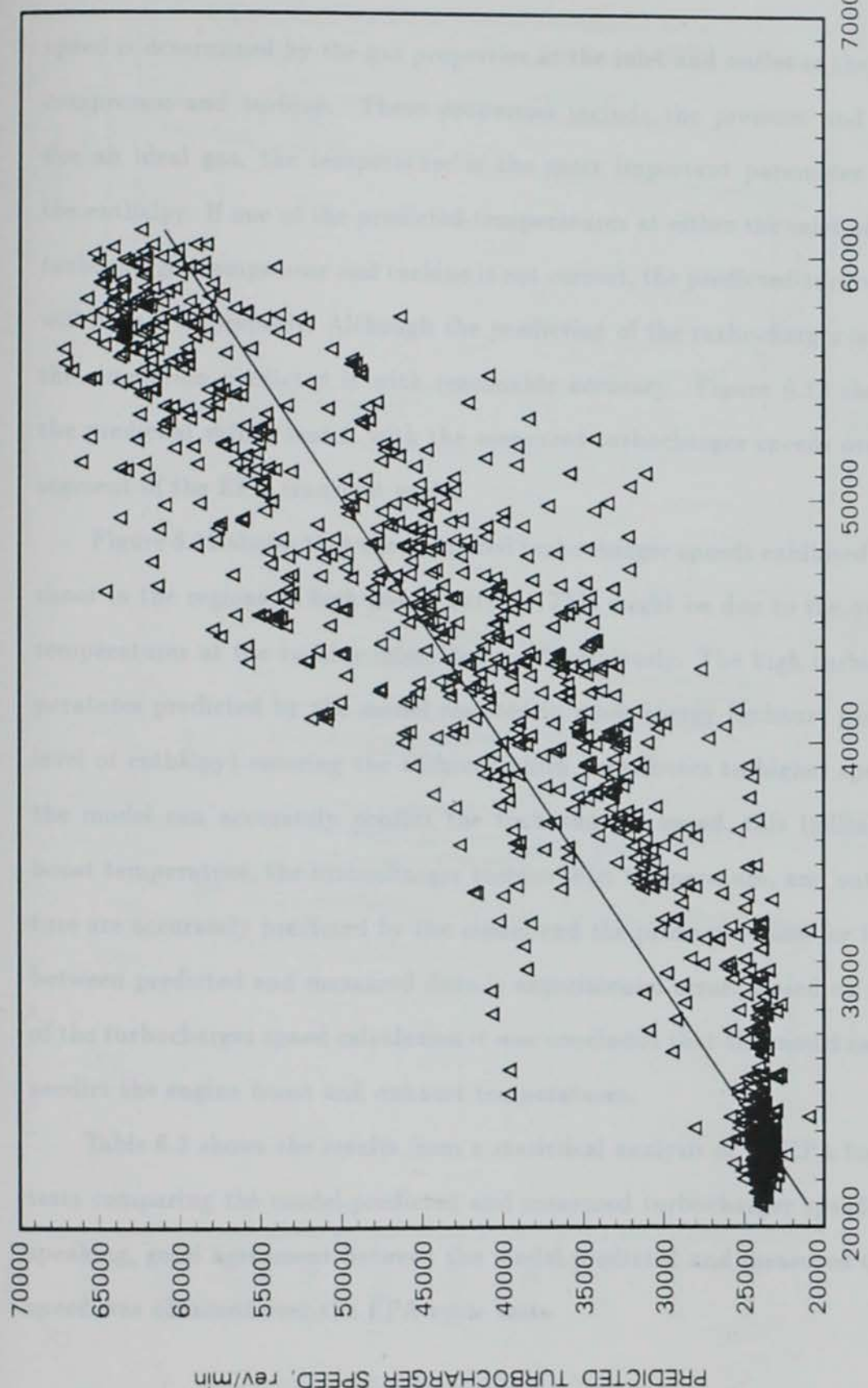

Figure 6.11: Linear regression analysis on turbocharger speeds

speed is determined by the gas properties at the inlet and outlet of the turbocharger compressor and turbine. These properties include the pressure and temperature. For an ideal gas, the temperature is the most important parameter to determine the enthalpy. If one of the predicted-temperatures at either the inlet or outlet of the turbocharger compressor and turbine is not correct, the predicted-turbocharger speed will behave improperly. Although the prediction of the turbocharger is complicated, the simulation predicted it with reasonable accuracy. Figure 6.12 shows how well the predicted values match with the measured turbocharger speeds over the second segment of the EPA transient cycle.

Figure 6.12 shows that the predicted turbocharger speeds exhibited a small overshoot in the regions of high power output. This might be due to the over-estimated temperatures at the turbine inlet, discussed previously. The high turbine inlet temperatures predicted by the model resulted in more energy (exhaust gas with higher level of enthalpy) entering the turbine, which contributes to higher speed. Because the model can accurately predict the turbocharger speed, this indicated that the boost temperature, the turbocharger turbine inlet temperature, and outlet temperature are accurately predicted by the model and the primary reason for the difference between predicted and measured data is experimental error. Based on the accuracy of the turbocharger speed calculation it was concluded that the model can accurately predict the engine boost and exhaust temperatures.

Table 6.3 shows the results from a statistical analysis of 12 EPA transient cycle tests comparing the model-predicted and measured turbocharger speeds. Generally speaking, good agreement between the model-predicted and measured turbocharger speed was obtained over the EPA cycle tests.

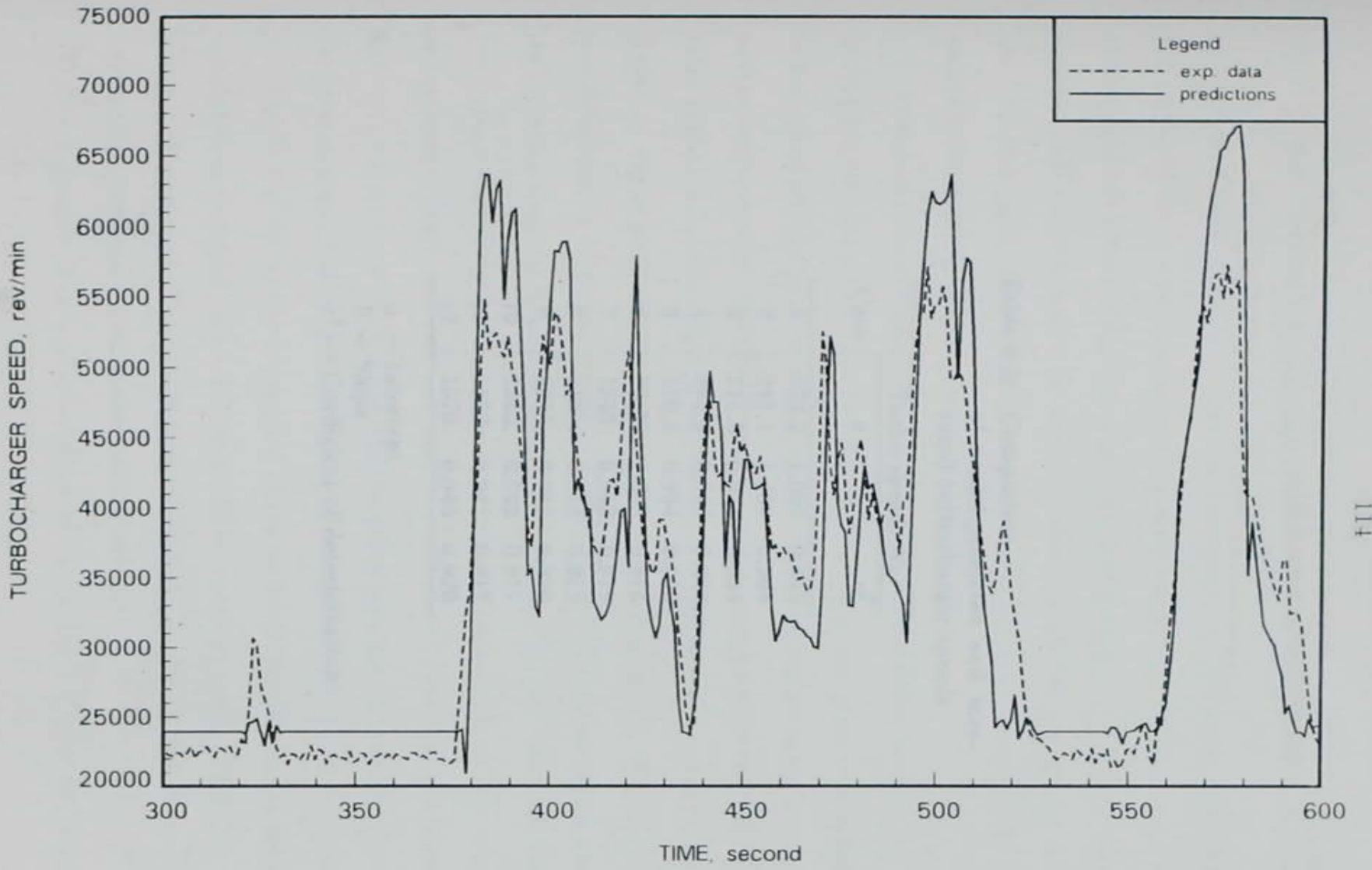

Figure 6.12: Comparison of model-predicted and measured turbocharger speeds over the second segment of the EPA transient cycle

Table 6.3: Comparison of model-predicted and measured turbocharger speeds

Case	Turbo speed, N_{tc}		
	a	b	r^2
	rpm		
1	-233.2	1.007	0.895
2	-241.1	1.008	0.908
3	714.5	0.972	0.908
4	320.9	0.986	0.908
5	170.8	0.994	0.900
6	79.75	1.028	0.876
7	1343.	0.943	0.919
8	1161.	0.948	0.919
9	1295.	0.942	0.920
10	1245.	0.942	0.917
11	1162.	0.947	0.917
12	1070.	0.945	0.920

a — Intercept
b — Slope
r^2 — Coefficient of determination

6.2 Model's Capability of Predicting Equivalence Ratio

As mentioned in Section 2.3.3, instantaneous experimental equivalence ratios are very difficult to measure during a transient cycle. The equipment set up for this study could not measure the equivalence ratios directly due to a lack of instantaneous fuel flow rate measurements. To verify the model-predicted equivalence ratios during the transient cycle, indirect fuel flow rate calculations were conducted by correlating steady-state fuel flow measurements to transient data.

To estimate the instantaneous equivalence ratio, the diesel fuel flow was measured during a steady-state test. The fuel flow rate at the steady-state only depends on the engine speed and the position of an actuator that was attached to the governor lever to control engine torque. A series of steady-state tests were conducted and the fuel flow rates were measured for different combinations of engine speed and actuator position. Based on the experimental results, a polynomial equation, Eq. H.1 in Appendix H, was developed to calculate the diesel fuel flow rate. The independent variables for the equation were the engine speed and the actuator, or rack, position. Because the two independent variables were recorded over a transient cycle by the computer, the instantaneous diesel fuel flow rate could be calculated using Eq. H.1. Since the air flow rate was measured by a laminar flow element and also recorded by the computer, the instantaneous fuel-to-air ratio during the transient cycle could be estimated.

Figure 6.13 shows the comparison of the model-predicted and the experimental-calculated equivalence ratios during an EPA transient cycle. Their correlation is shown in Figure 6.14. The comparison between the predicted and the experimental-calculated equivalence ratios shows good agreement.

The regression line was determined by using Eq. 5.6 with the x axis as the

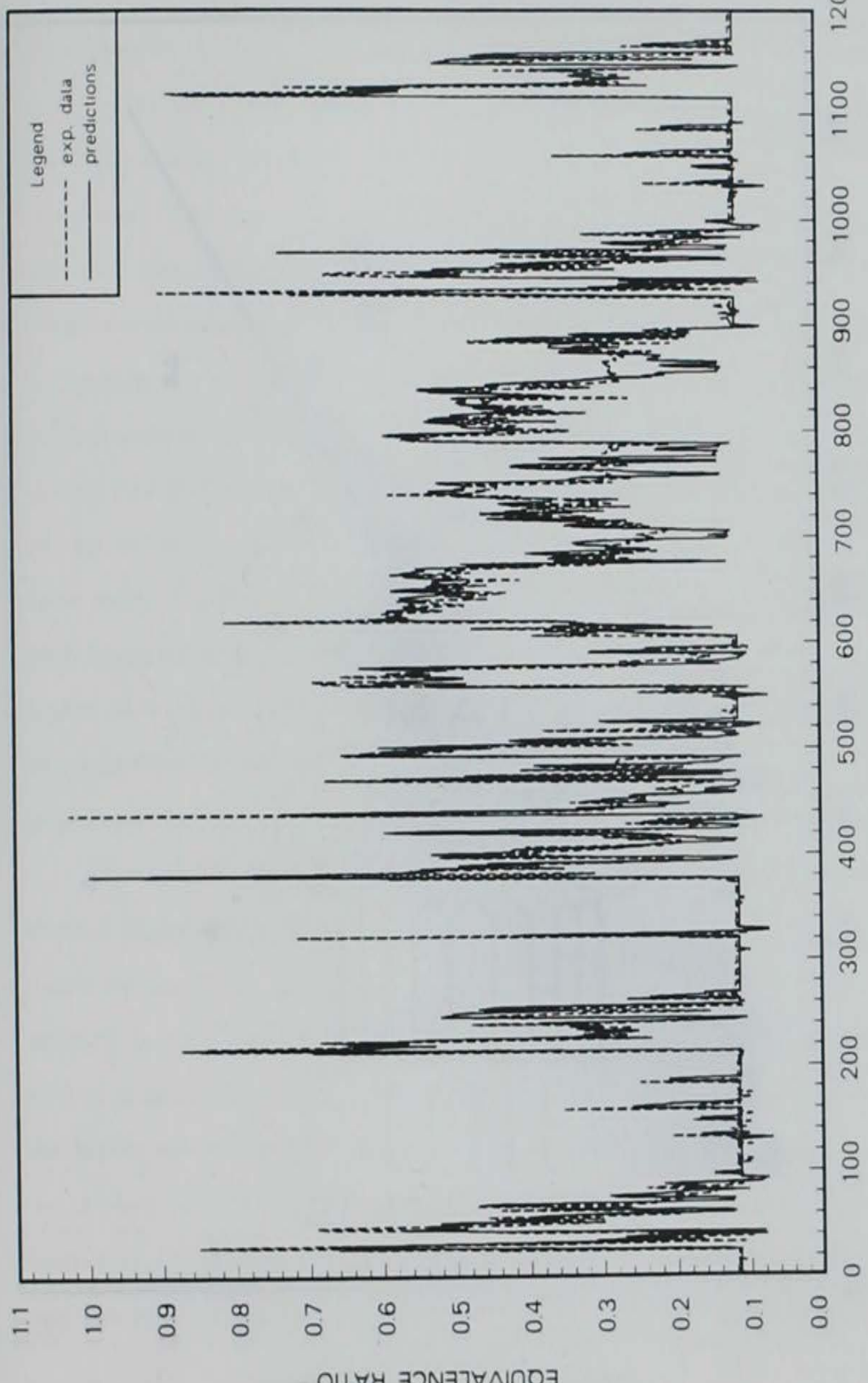

Figure 6.13: Comparison of model-predicted and experimental-calculated equivalence ratios

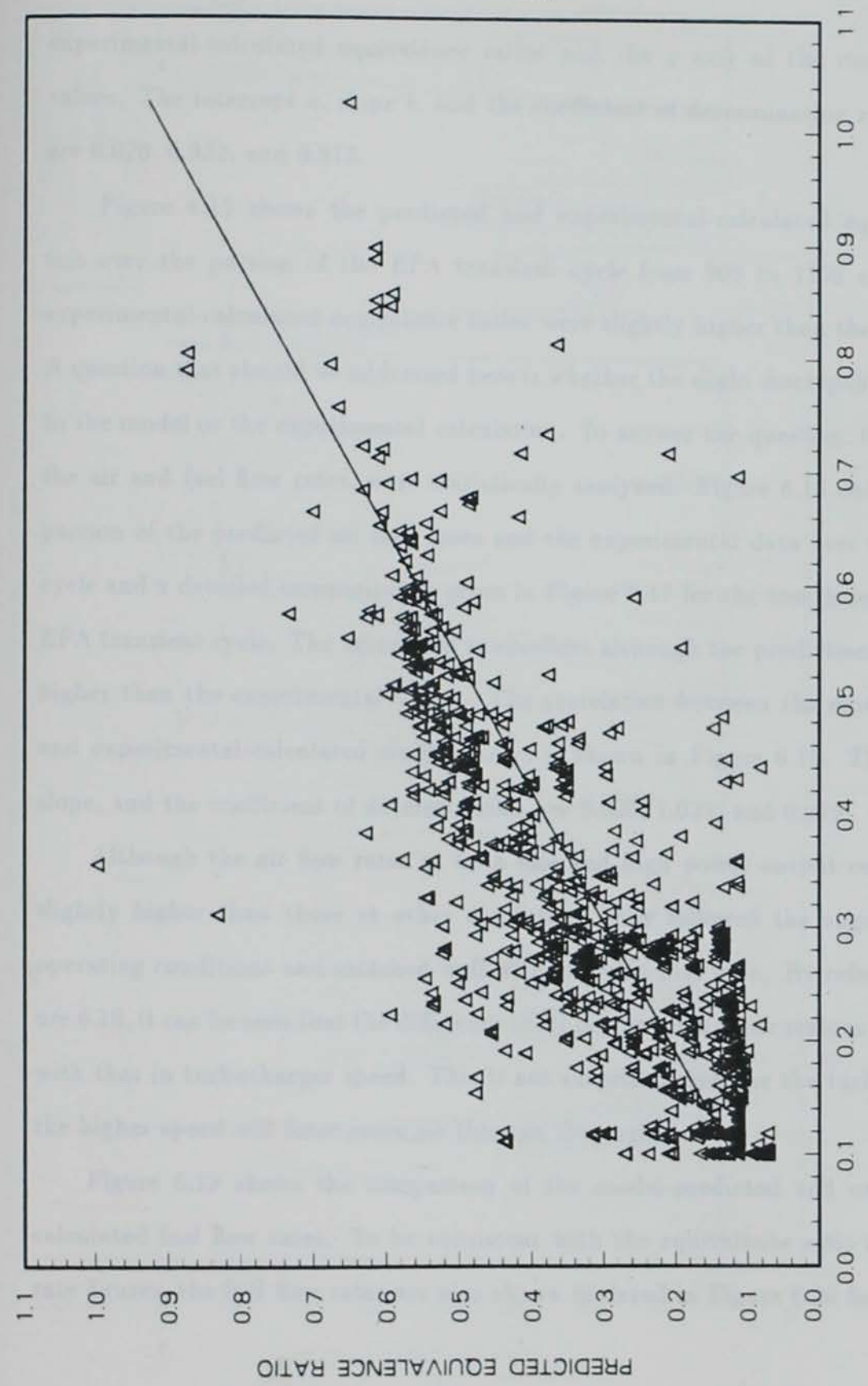

Figure 6.14: Linear regression analysis on equivalence ratios

experimental-calculated equivalence ratios and the y axis as the model-predicted values. The intercept a, slope b, and the coefficient of determination r^2 for the line are 0.020, 0.932, and 0.813.

Figure 6.15 shows the predicted and experimental-calculated equivalence ratios over the portion of the EPA transient cycle from 900 to 1200 seconds. The experimental-calculated equivalence ratios were slightly higher than those predicted. A question that should be addressed here is whether the slight discrepancies were due to the model or the experimental calculation. To answer the question, two variables, the air and fuel flow rates, were statistically analyzed. Figure 6.16 shows the comparison of the predicted air flow rates and the experimental data over the transient cycle and a detailed comparison is given in Figure 6.17 for the fourth segment of the EPA transient cycle. The agreement is excellent although the predictions are slightly higher than the experimental values. The correlation between the model-predicted and experimental-calculated air flow rates is shown in Figure 6.18. The intercept, slope, and the coefficient of determination are 0.000, 1.022, and 0.979.

Although the air flow rates at both idle and high power output conditions are slightly higher than those at other conditions, they followed the engine transient operating conditions and matched well with experimental data. By referring to Figure 6.10, it can be seen that the difference in air flow rates in those regions is consistent with that in turbocharger speed. This is not surprising because the turbocharger at the higher speed will force more air through the engine.

Figure 6.19 shows the comparison of the model-predicted and experimental-calculated fuel flow rates. To be consistent with the equivalence ratio and air flow rate figures, the fuel flow rates are also shown in detail in Figure 6.20 for the period

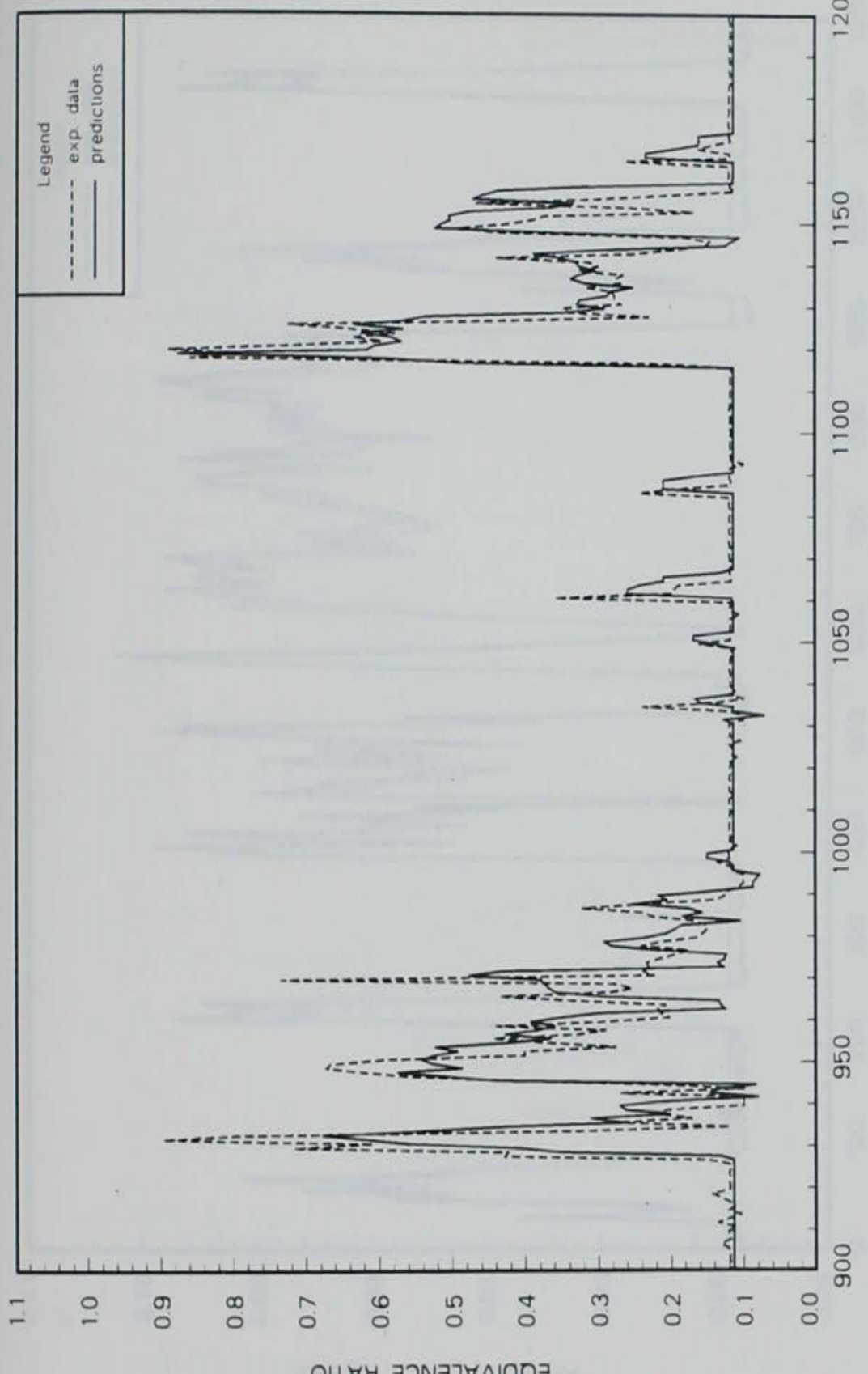

Figure 6.15: Comparison of model-predicted and experimental- calculated equivalence ratios over the fourth segment of the EPA transient cycle

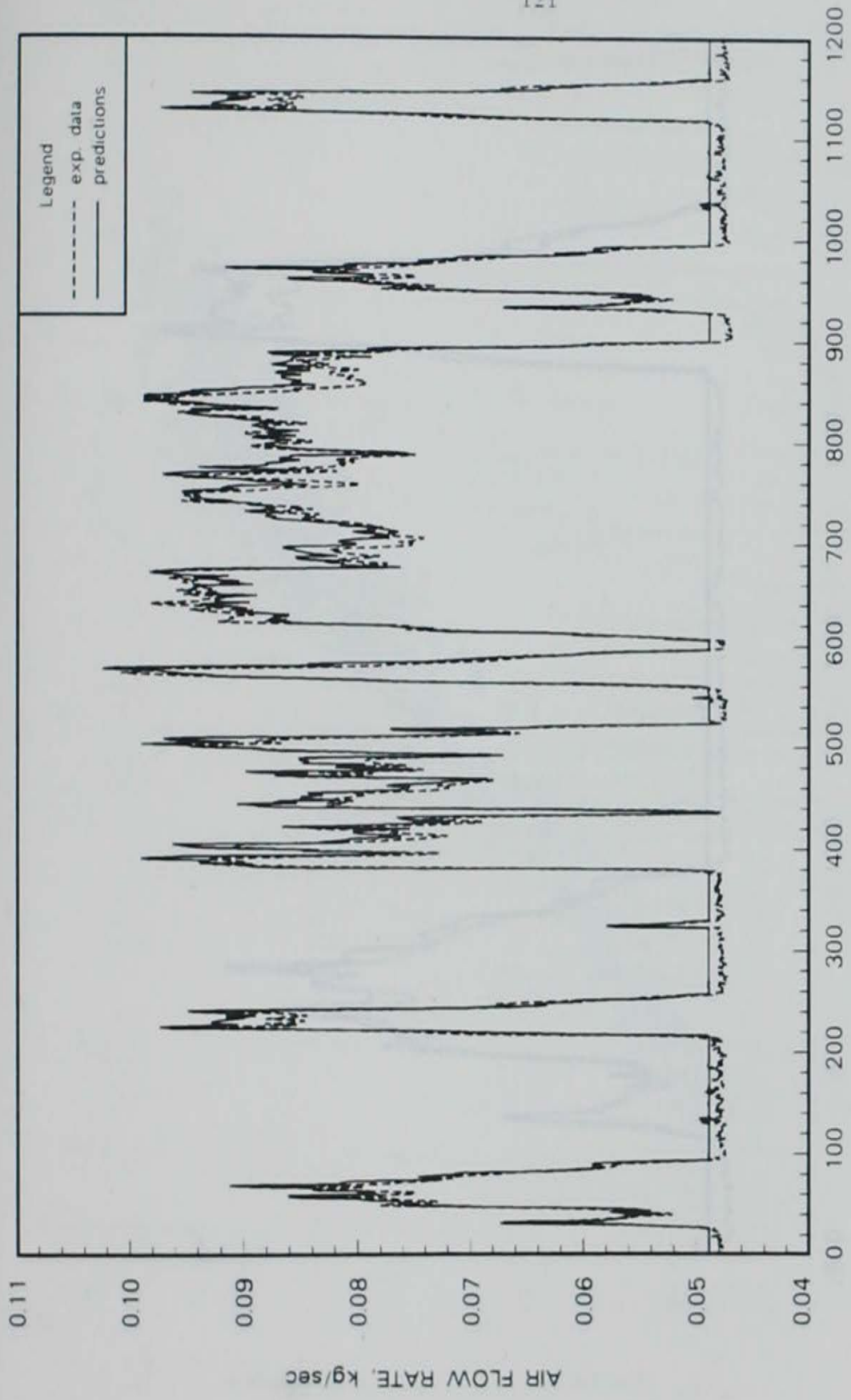

Figure 6.16: Comparison of model-predicted and measured air flow rates over the EPA transient cycle

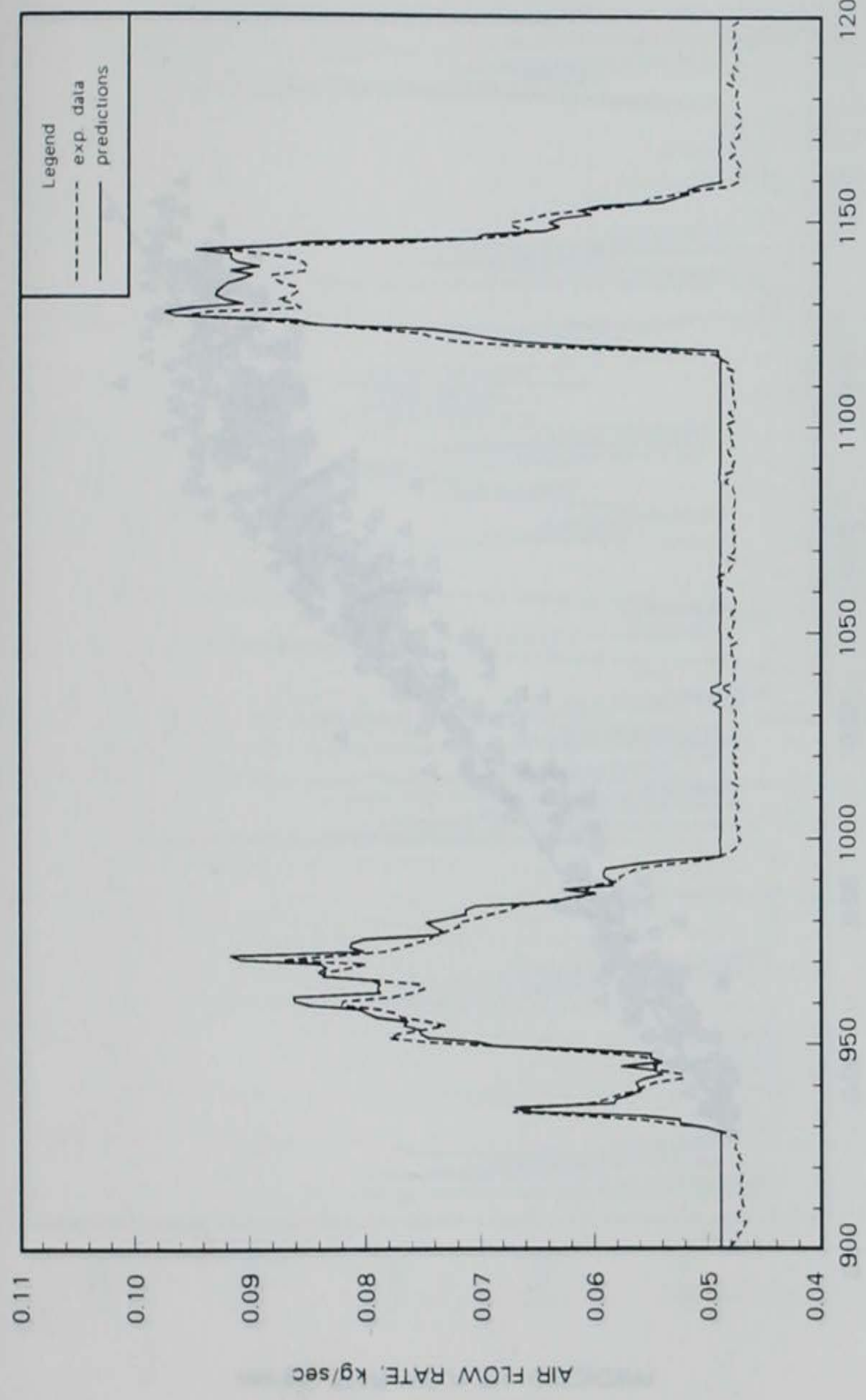

Figure 6.17: Comparison of model-predicted and measured air flow rates over the fourth segment of the EPA transient cycle

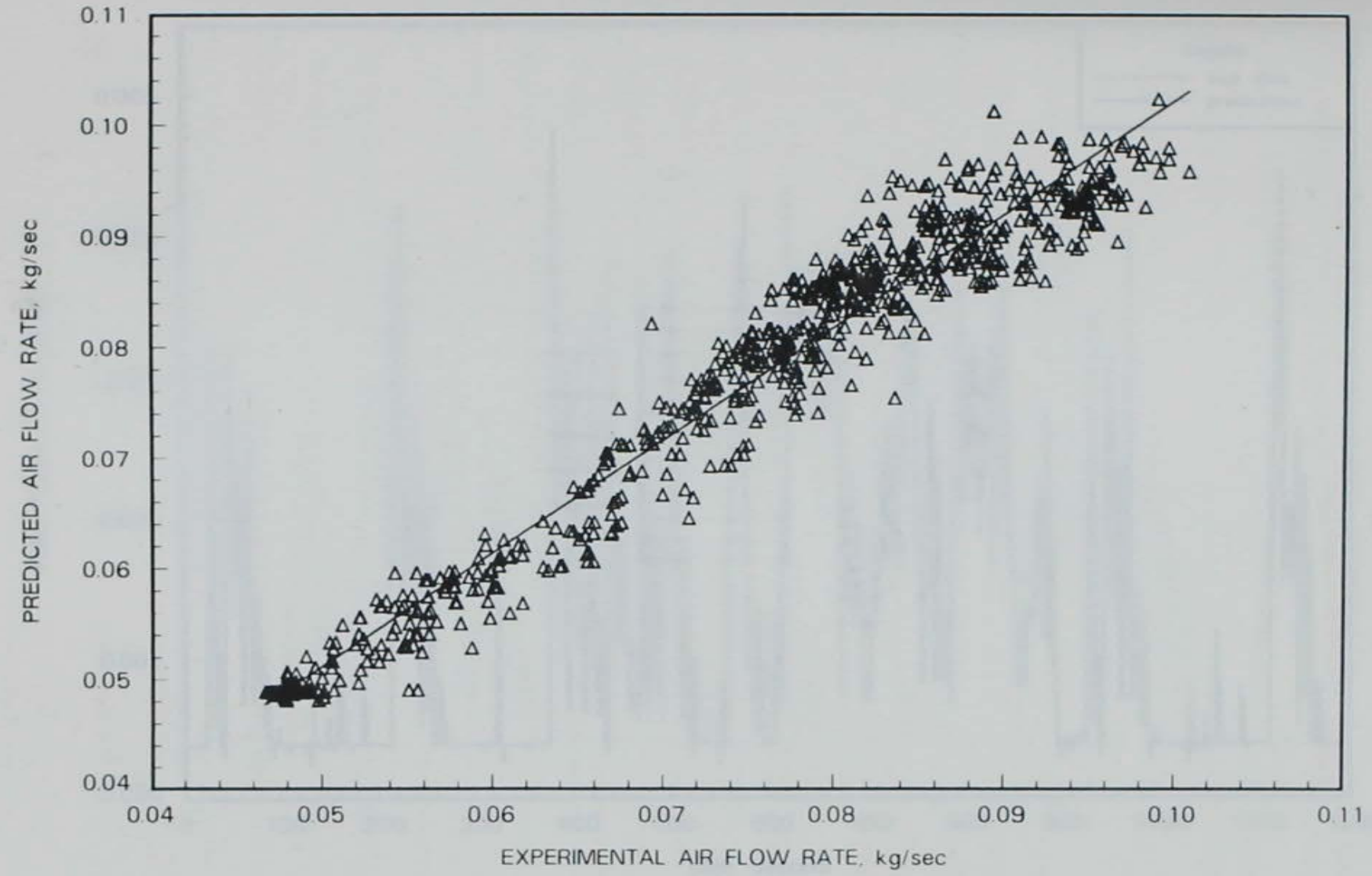

Figure 6.18: Linear regression analysis on air flow rates

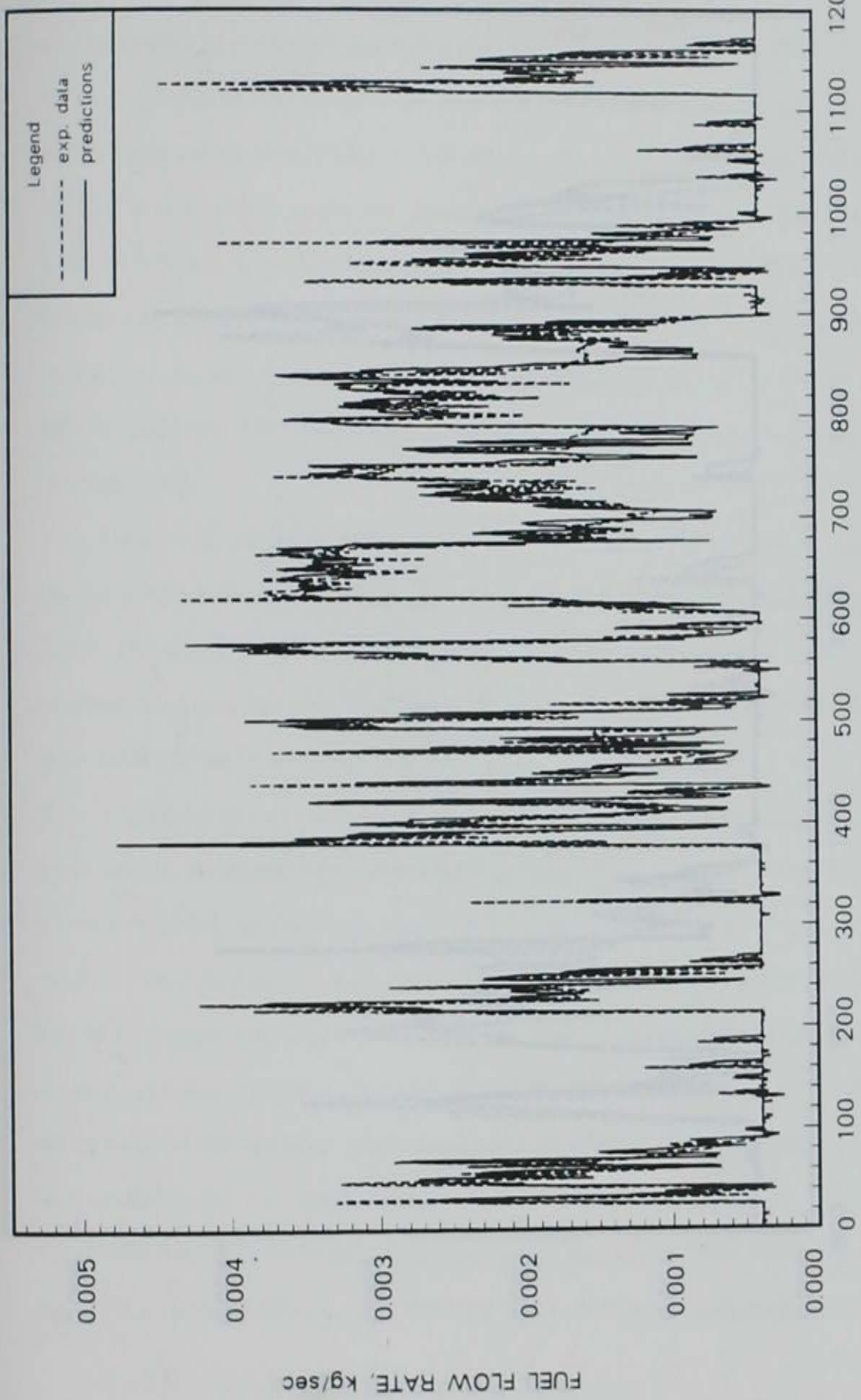

Figure 6.19: Comparison of model-predicted and measured fuel flow rates over the EPA transient cycle

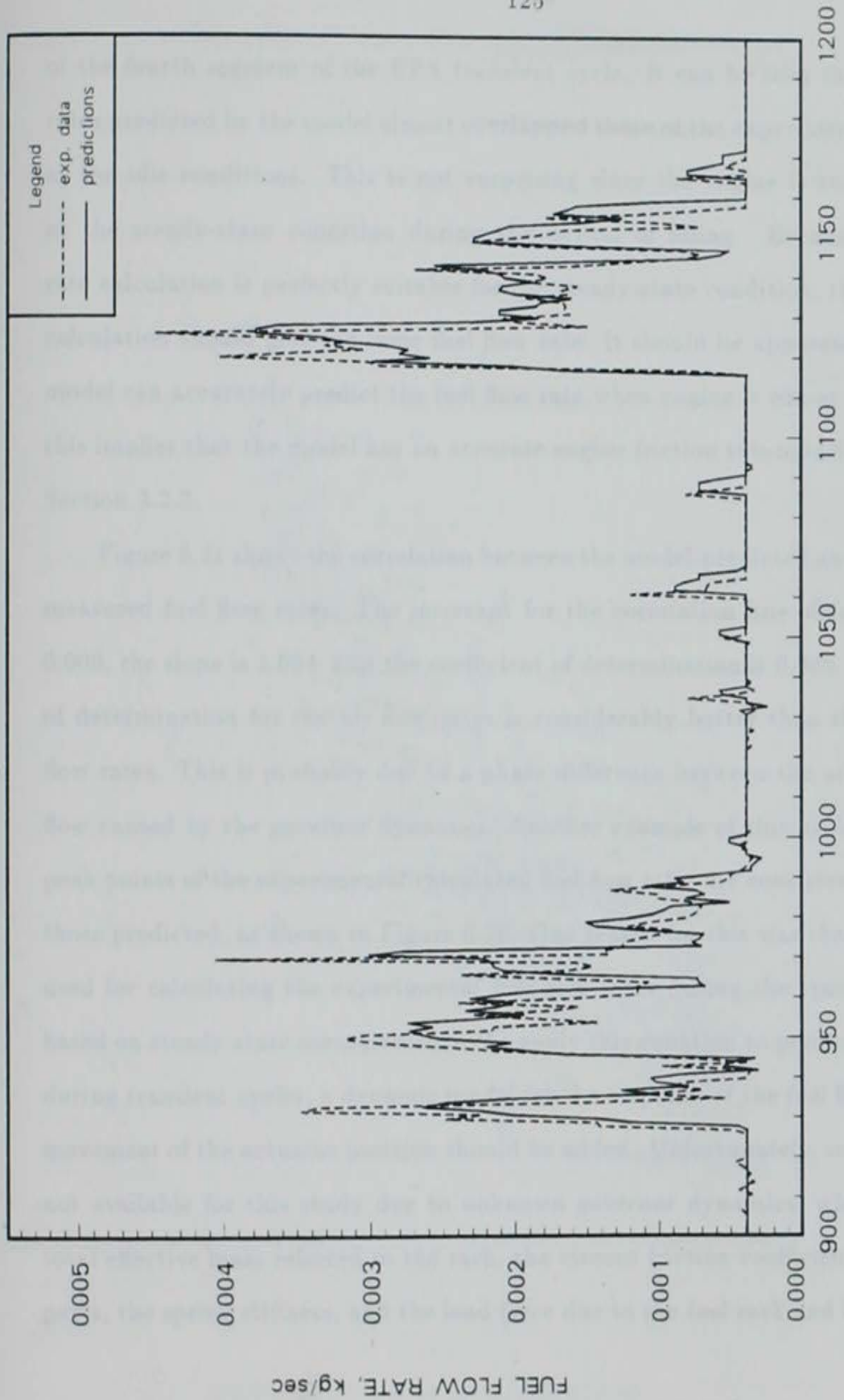

Figure 6.20: Comparison of model-predicted and measured fuel flow rates over the fourth segment of the EPA transient cycle

of the fourth segment of the EPA transient cycle. It can be seen that the fuel flow rates predicted by the model almost overlapped those of the experimental calculations at the idle conditions. This is not surprising since the engine is considered to run at the steady-state condition during the period of idling. Because the fuel flow rate calculation is perfectly suitable for the steady-state condition, the experimental calculation should give the same fuel flow rate. It should be apparent that since the model can accurately predict the fuel flow rate when engine is run at idle conditions, this implies that the model has an accurate engine friction sub-model as described in Section 3.2.3.

Figure 6.21 shows the correlation between the model-predicted and experimental-measured fuel flow rates. The intercept for the correlation line of fuel flow rates is 0.000, the slope is 1.004, and the coefficient of determination is 0.885. The coefficient of determination for the air flow rates is considerably better than that for the fuel flow rates. This is probably due to a phase difference between the actuator and fuel flow caused by the governor dynamics. Another example of this problem is that the peak points of the experimental-calculated fuel flow rates are consistently higher than those predicted, as shown in Figure 6.20. One reason for this was that the algorithm used for calculating the experimental fuel flow rates during the transient cycle was based on steady-state measurements. To apply this equation to predict fuel flow rates during transient cycles, a dynamic model for the response of the fuel flow to a sudden movement of the actuator position should be added. Unfortunately, such a model was not available for this study due to unknown governor dynamics, which include the total effective mass referred to the rack, the viscous friction coefficient of the moving parts, the spring stiffness, and the load force due to the fuel rack and linkage friction.

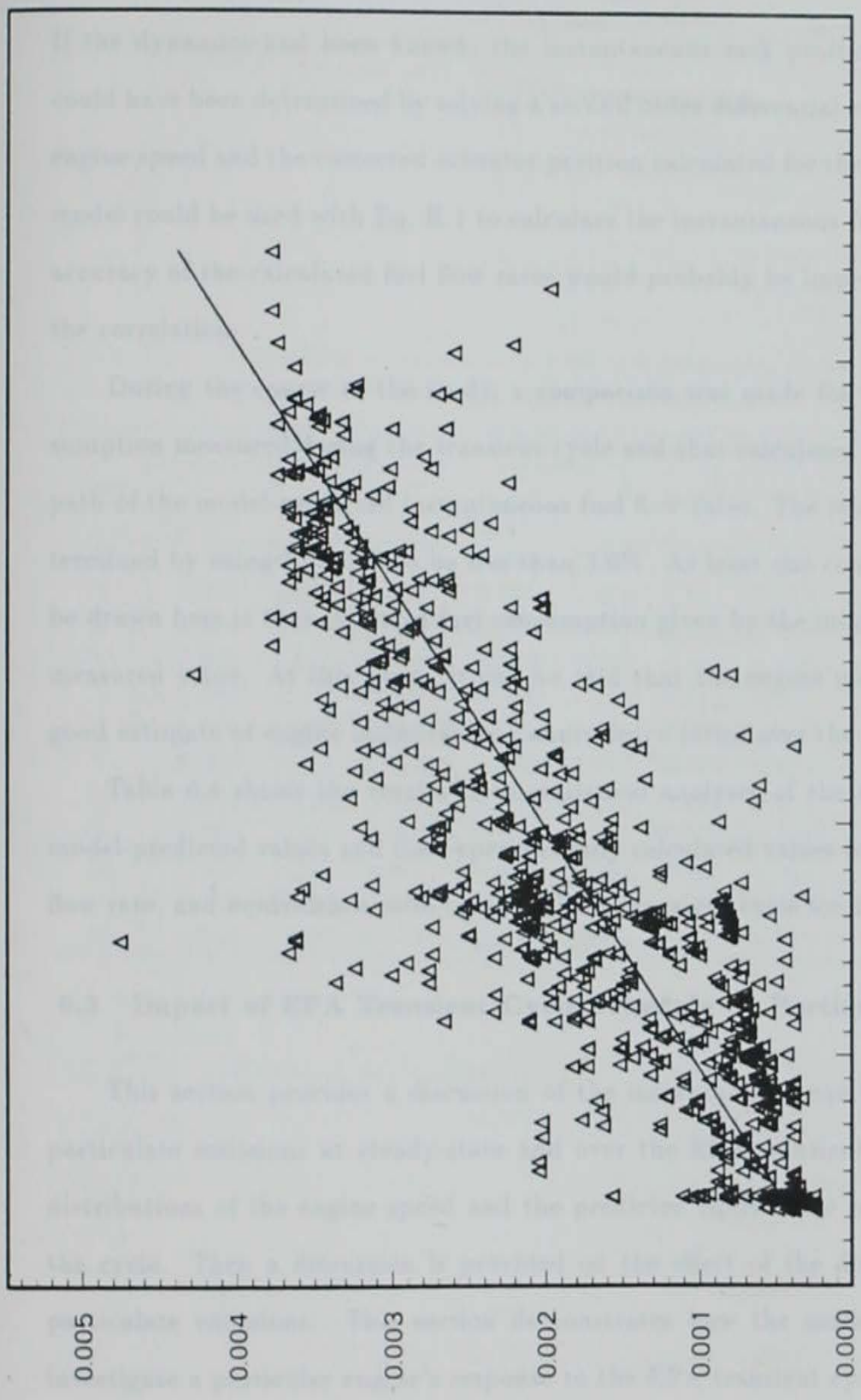

Figure 6.21: Linear regression analysis on fuel flow rates

If the dynamics had been known, the instantaneous rack position of the governor could have been determined by solving a second order differential equation [79]. Then engine speed and the corrected actuator position calculated for the dynamic governor model could be used with Eq. H.1 to calculate the instantaneous fuel flow rates. The accuracy of the calculated fuel flow rates would probably be improved and so would the correlation.

During the course of the study, a comparison was made for the total fuel consumption measured during the transient cycle and that calculated by integrating the path of the model-predicted instantaneous fuel flow rates. The relative error was determined by using Eq. 5.10 to be less than 3.0%. At least one conclusion that could be drawn here is that the total fuel consumption given by the model agrees with the measured value. At this point, it can be said that the engine model did provide a good estimate of engine instantaneous equivalence ratios over the transient cycle.

Table 6.4 shows the results from statistical analyses of the correlations of the model-predicted values and the experimentally calculated values of air flow rate, fuel flow rate, and equivalence ratio over the EPA transient cycle for 12 tests.

6.3 Impact of EPA Transient Cycle Schedule on Particulate Emissions

This section provides a discussion of the instantaneous equivalence ratios and particulate emissions at steady-state and over the EPA transient cycle. First, the distributions of the engine speed and the predicted equivalence ratios are given for the cycle. Then a discussion is provided on the effect of the distributions on the particulate emissions. This section demonstrates how the model can be used to investigate a particular engine's response to the EPA transient cycle and how it can

Table 6.4: Comparison of model-predicted and measured air and fuel flow rates and experimental-calculated equivalence ratios

Case	Air flow rate			Fuel flow rate			Equivalence ratio		
	a	b	r^2	a	b	r^2	a	b	r^2
	kg/sec			kg/sec					
1	0.000	1.022	0.979	0.000	1.004	0.885	0.020	0.932	0.813
2	0.000	1.013	0.977	0.000	1.008	0.881	0.020	0.950	0.810
3	0.000	1.020	0.979	0.000	0.995	0.872	0.024	0.925	0.803
4	0.000	1.025	0.979	0.000	1.012	0.808	0.022	0.930	0.808
5	0.000	1.025	0.978	0.000	1.018	0.877	0.020	0.945	0.799
6	0.000	1.025	0.977	0.000	1.008	0.873	0.023	0.938	0.797
7	0.000	1.023	0.978	0.000	0.987	0.876	0.026	0.913	0.806
8	0.000	1.023	0.978	0.000	1.021	0.884	0.019	0.945	0.808
9	0.000	1.021	0.978	0.000	1.009	0.889	0.020	0.930	0.814
10	0.000	1.020	0.977	0.000	1.003	0.885	0.021	0.927	0.811
11	0.000	1.022	0.978	0.000	1.004	0.880	0.021	0.929	0.805
12	0.000	1.023	0.977	0.000	1.003	0.891	0.017	0.931	0.826

a — Intercept
b — Slope
r^2 — Coefficient of determination

Table 6.5: Distributions of speed and equivalence ratio over an EPA transient cycle

Distribution		Frequency, %
Speed *rpm*	≤1200	41.54
	1200–1300	3.00
	1300–1500	6.17
	1500–1700	4.59
	1700–1900	12.01
	1900–2100	28.02
	>2100	4.67
Equivalence ratio ϕ	≤0.25	59.88
	0.25–0.35	11.01
	0.35–0.45	10.01
	0.45–0.55	11.84
	0.55–0.65	6.42
	>0.65	0.83

lead to a better understanding of the engine.

6.3.1 Distributions of engine speed and equivalence ratio over an EPA transient cycle schedule

To better understand the EPA transient cycle, the distributions of engine speed and equivalence ratio over the EPA transient cycle were investigated. The equivalence ratio was predicted by the engine model at each of the 1,199 data points of the EPA transient cycle. The purpose of investigating the distributions was to provide information for studying the distribution of the particulate emission over the transient cycle. Table 6.5 shows the distributions of speed and equivalence ratio over the EPA transient cycle. ϕ in the table denotes the equivalence ratio.

Table 6.5 shows that about 42% of the data points the engine was run at idle or below idle speed. It is obvious that the behavior of the engine at idle speed is very

important for the particulate emission. Also, for about 28% of the total time the engine was run at high speeds between 1900 and 2100 *rpm*. Hence, the level of the particulate matter produced by the engine running at high speed is also important for the total particulate emission over the transient cycle. The distribution of the predicted equivalence ratios shows that about 60% of the 1,199 equivalence ratios were less than or equal to 0.25. This implies that the particulate emission at light loads would make a large contribution to the total particulate emitted from the engine, if the level of the particulate emissions at the low load was high. The discussion here provides information that engine manufacturers could use in identifying the engine operating conditions that contribute most to emissions. In other words, in order to meet the EPA specified particulate emission, the manufacturers must reduce the emissions at those specific engine operating conditions during the EPA transient cycle.

It is also interesting to know that the minimum equivalence ratio was found to be 0.072 and the maximum equivalence ratio was 0.997. The minimum equivalence ratio is due to the very low load condition at which the engine is operated. The maximum equivalence ratio is due to the sudden acceleration of the engine during the EPA transient cycle. To correctly predict the particulate emission at high equivalence ratio conditions, it is essential for the computer model to have the information about the particulate emission data at these conditions. This explains why the turbocharger was removed from the engine to reduce the air flow rate and to extend the equivalence ratio to high values.

The EPA transient cycle consists of four segments, each lasting 300 seconds. The first and the fourth segments of the cycle are identical, and simulate New York non-

Table 6.6: Distributions of speed and equivalence ratio over three different segments of an EPA transient cycle

Distribution		Frequency, %		
Item	Range	1st or 4th Segment	2nd Segment	3rd Segment
Speed *rpm*	≤1200	63.33	37.67	2.00
	1200–1300	3.67	3.67	1.00
	1300–1500	9.33	4.00	2.33
	1500–1700	5.67	5.33	1.33
	1700–1900	6.33	18.00	17.33
	1900–2100	10.67	26.33	64.33
	>2100	1.00	5.00	11.67
ϕ	≤0.25	73.67	67.67	25.00
	0.25–0.35	8.67	8.67	17.67
	0.35–0.45	7.00	5.67	20.33
	0.45–0.55	6.33	9.33	25.67
	0.55–0.65	3.67	6.67	11.33
	>0.65	0.67	2.00	0.00

freeway driving conditions. The second and the third segments of the cycle simulate Los Angeles non-freeway and Los Angeles freeway driving conditions. The complete EPA transient cycle was broken down into these four segments for statistical analyses.

Table 6.6 show the distributions of speed and equivalence ratio over the three different segments of the EPA transient cycle. Table 6.6 shows that low speed and load dominate the first and fourth segments of the transient cycle. While low load dominates the second segment of the transient cycle, the engine is run at both low and high speeds. The third segment demonstrates the pattern of highway driving. The engine is run mostly at high speed, while the load is fairly even distributed in the range of equivalence ratios between 0.25 to 0.55. It appears that more acceleration happens in the second segment of the transient cycle than in the others. The reason for this is that during the second segment the engine is run at an equivalence ratio

greater than 0.65 for 6 seconds, while it is greater than 0.65 for only 2 seconds during the first or the fourth segment and no time during the third segment. It should be pointed out that the only possibility for the engine to reach the equivalence ratio greater than 0.65 is that the engine experiences rapid acceleration.

It is clear from this analysis of the distribution of the equivalence ratio and its possible effect on the particulate emission that the model, based on engine characteristics close to the emission-producing combustion process, provides a high degree of flexibility in identifying the important facts affecting particulate emission.

6.3.2 Discussion of trends of particulate emission

Figure 6.22 shows the experimental steady-state particulate emission data and the polynomial curves which were fit to the data for six different engine speeds. To clearly illustrate the trends of the curves, Figure 6.22 is separated into two figures. One is shown in Figure 6.23 with the equivalence ratio ranging from 0.0 to 0.60, and the other is shown in Figure 6.24 with the equivalence ratio from 0.60 to 1.10.

It was found that the rate of particulate emission is a minimum for an equivalence ratio of about 0.50. The reason for this is that at this point the engine experienced a complete combustion with very low hydrocarbon emission, which contributes to the soluble organic fraction (SOF) of particulates. This was accompanied by more soot oxidation in the cylinder, which resulted in less soot production.

When the engine was run either lean or rich of this minimum point, more particulates were emitted from the engine. At lean conditions, more unburned fuel and lubricant oil contributed to SOF which in turn increased total particulate emission. At lean conditions, the temperature may be too low to completely burn these un-

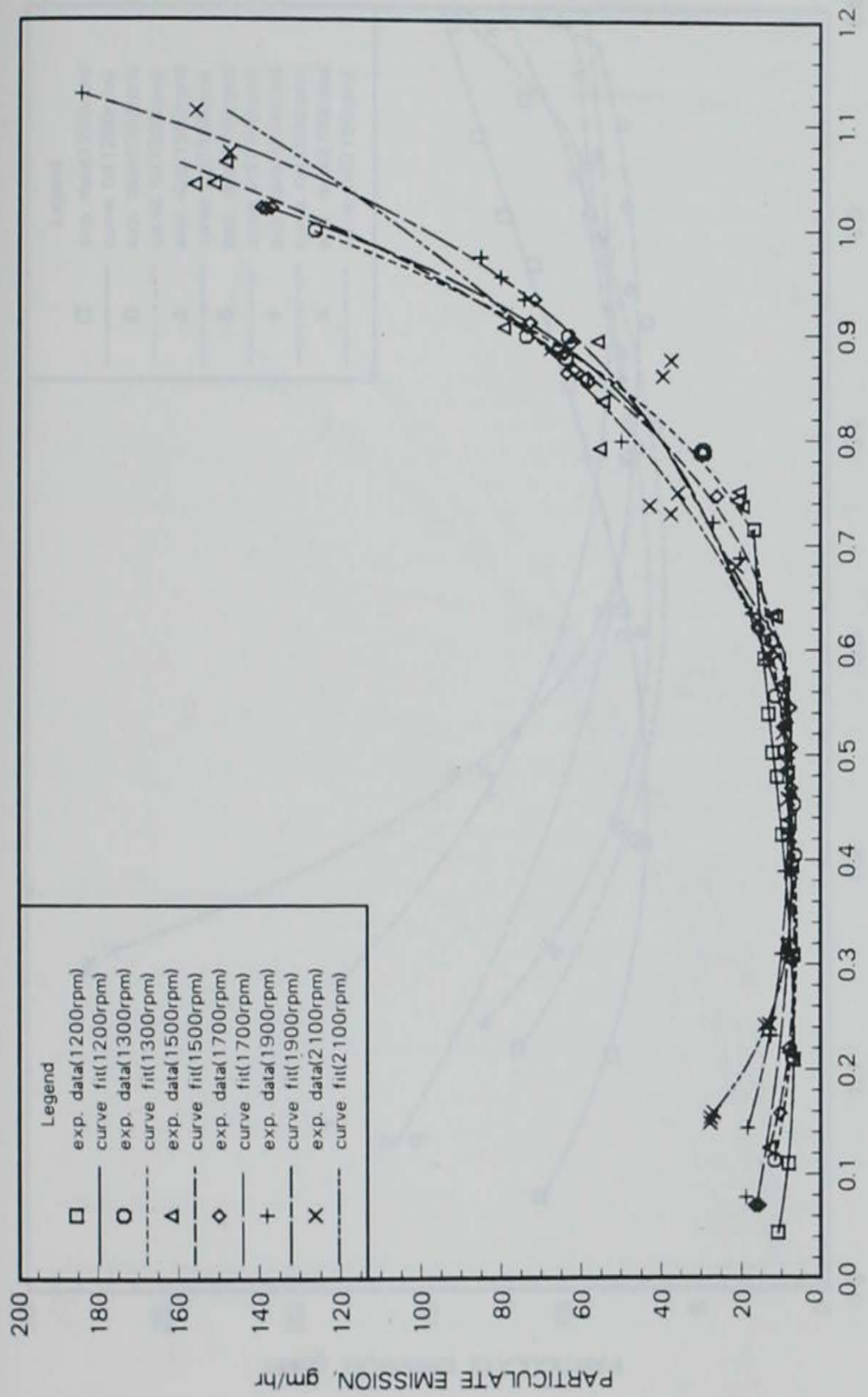

Figure 6.22: Particulate emissions vs. equivalence ratio ranging from 0.05 to 1.10

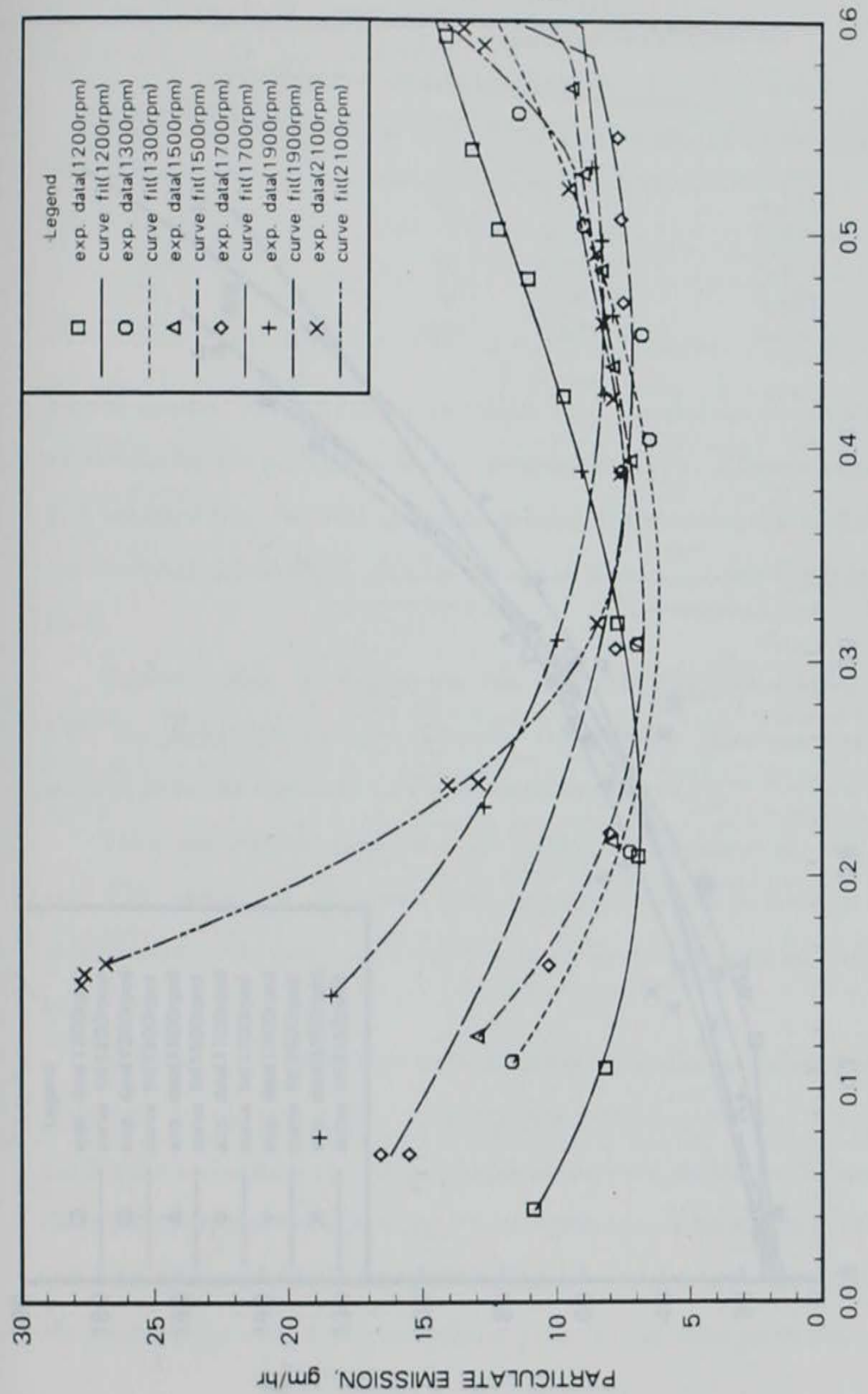

Figure 6.23: Particulate emissions vs. equivalence ratio ranging from 0.05 to 0.60

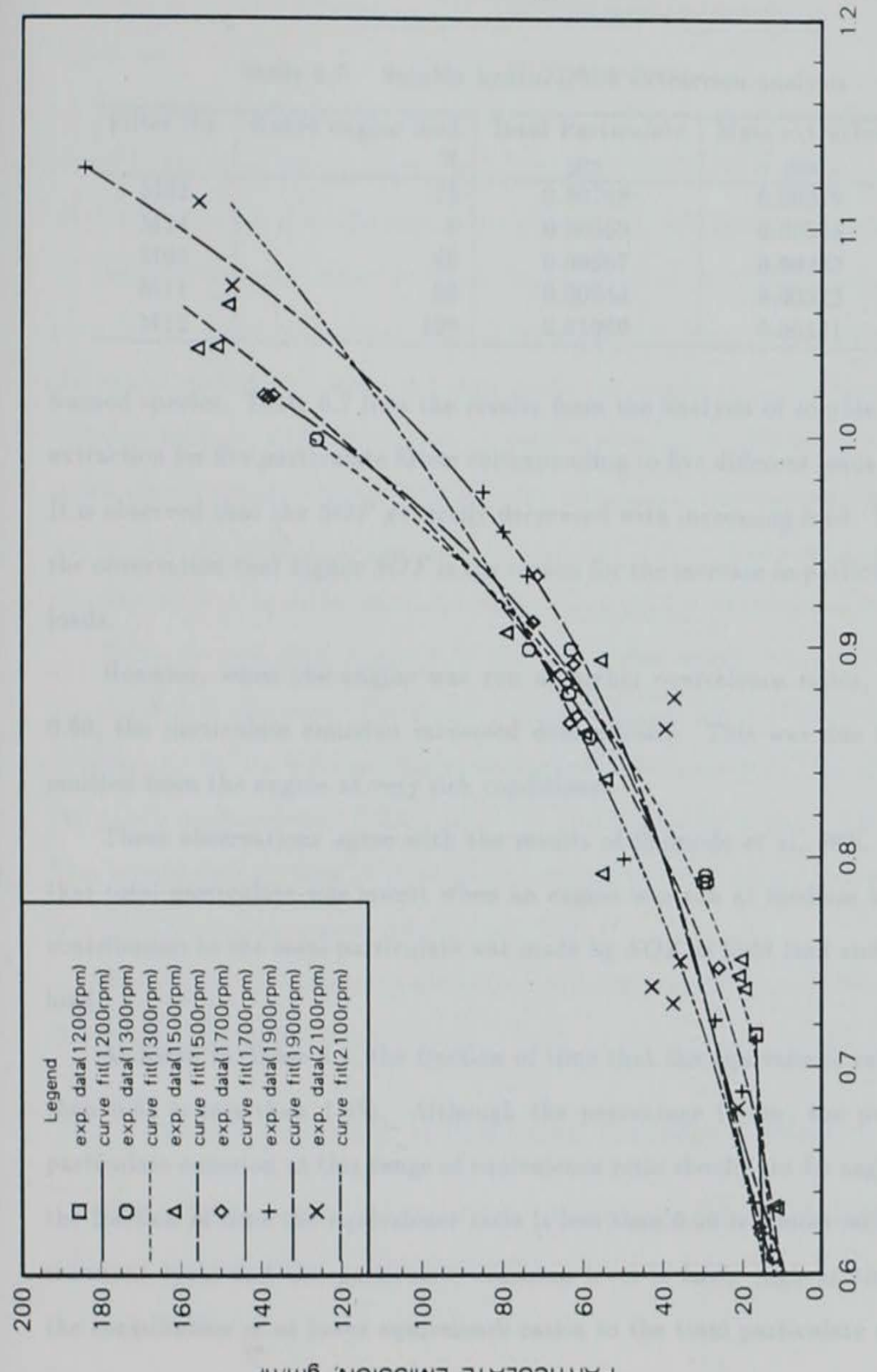

Figure 6.24: Particulate emissions vs. equivalence ratio ranging from 0.60 to 1.10

Table 6.7: Soluble hydrocarbon extraction analysis

Filter No.	Rated engine load %	Total Particulate gm	Mass extracted gm	SOF %
M02	-15	0.00748	0.00379	50.67
M14	0	0.00569	0.00318	55.89
M05	60	0.00667	0.00233	34.93
M11	90	0.00944	0.00312	33.05
M12	100	0.01069	0.00171	16.00

burned species. Table 6.7 lists the results from the analysis of soluble hydrocarbon extraction for five particulate filters corresponding to five different loads at 1200 rpm. It is observed that the SOF generally decreased with increasing load. This supports the observation that higher SOF is the reason for the increase in particulates at light loads.

However, when the engine was run at higher equivalence ratios, greater than 0.60, the particulate emission increased dramatically. This was due to more soot emitted from the engine at very rich conditions.

These observations agree with the results of Shimode et al. [80]. They stated that total particulate was lowest when an engine was run at medium load. A great contribution to the total particulate was made by SOF at light load and soot at high load.

As listed in Table 6.5, the fraction of time that the equivalence ratio is greater than 0.65 is less than 1.0%. Although the percentage is low, the portion of the particulate emission at this range of equivalence ratio should not be neglected. Since the fraction of time the equivalence ratio is less than 0.20 is almost 60% if the EPA transient cycle and the particulate emission level is fairly high at this condition, the contribution of at lower equivalence ratios to the total particulate emission was

significant.

Generally speaking, the effect of engine speed on particulate emission was not as strong as the effect of equivalence ratio. But it did appear that there was a significant effect of engine speed on the particulate emission for equivalence ratios less than 0.40. At higher speeds, the engine produced higher levels of particulate emission on a rate basis for the same equivalence ratio. This is not surprising because the frequency of the engine combustion event is higher when the engine is run at higher speed and the time for soot oxidation is less. To further investigate whether or not the engine speed affects the particulate emission, the particulate emission was expressed on a per cycle basis, that is, in the units of $mg/cycle$. Figure 6.25 shows the particulate emission on a cycle basis versus the equivalence ratio in the range of 0.00–0.60.

It can be seen from Figure 6.25 that the engine speed does have an impact on the particulate emission. The engine produced higher levels of particulate emission at higher speeds for low equivalence ratio except for the speed of 1700 rpm. However, the trends were reversed shortly after the equivalence ratio was greater than 0.40. This meant that the engine produced lower levels of particulate emission at higher speed for equivalence ratios greater than 0.40.

The trends of the particulate emission during the EPA transient cycle will be discussed in the nest section.

6.4 Model's Capability of Predicting Transient Particulate Emission

This section describes the particulate emission data obtained from transient cycle tests and corresponding model predictions.

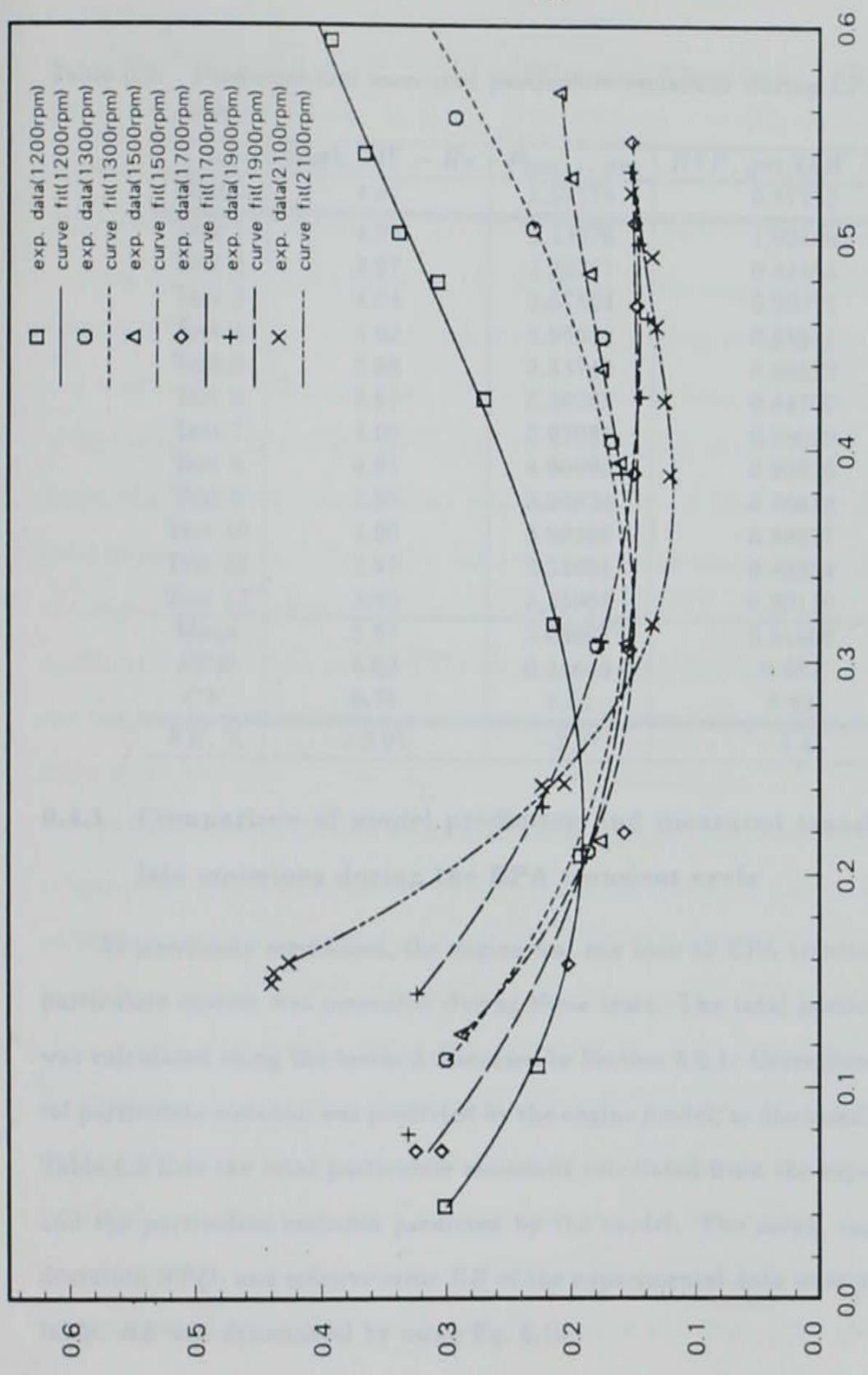

Figure 6.25: Cyclic particulate emission vs. equivalence ratio

Table 6.8: Predicted and measured particulate emissions during EPA transient cycles

Case	Work, $kW-Hr$	P_{mass}, gm	BSP, $gm/bkW-Hr$
Model	4.07	3.57178	0.87752
Test 1	4.04	4.13976	1.02469
Test 2	3.97	3.23771	0.81554
Test 3	4.04	3.67524	0.90971
Test 4	4.02	3.96658	0.98671
Test 5	3.98	3.53740	0.88879
Test 6	3.97	3.36285	0.84707
Test 7	4.00	3.92081	0.98020
Test 8	4.01	4.00905	0.99976
Test 9	3.95	3.03824	0.76918
Test 10	4.00	3.99906	0.99977
Test 11	3.97	3.54654	0.89334
Test 12	3.95	3.55969	0.90119
Mean	3.99	3.66607	0.91800
STD	0.03	0.34640	0.081
CV	0.75	9.45	8.82
RE, %	+2.01	−2.57	−4.41

6.4.1 Comparison of model prediction and measured transient particulate emissions during the EPA transient cycle

As previously mentioned, the engine was run over 12 EPA transient cycles. The particulate matter was measured during these tests. The total particulate emission was calculated using the method discussed in Section 5.5.1. Correspondingly, the total particulate emission was predicted by the engine model, as discussed in Section 3.5. Table 6.8 lists the total particulate emissions calculated from the experimental data and the particulate emission predicted by the model. The mean, sample standard deviation STD, and relative error RE of the experimental data were provided in the table. RE was determined by using Eq. 5.10.

The model-predicted particulate emission was compared with the averaged particulate emission from the 12 tests. It is apparent that the transient particulate emission was well predicted by the model with the relative error of 2.57% for the total particulate mass and of 4.41% for the specific particulate emission.

For the purpose of evaluating the variation in the experimental data, the coefficients of variation (CV's) were calculated for the total work, particulate emission, and specific particulate emission. CV is defined as the ratio of the standard deviation to the mean. It expresses the dispersion of the experimental data on a percentage basis, that is, relative rather than absolute. Table 6.8 shows that the variation in total work output from the engine from one test to the next is small. This means the the engine was well controlled and followed the EPA transient test procedure. The coefficients of variation for both the total particulate emission and specific emission are lower than 10%. The value is considerably better than 15% value reported by Stein et al. [81].

Table 6.9 shows the distribution of the particulate emission over the 6 different ranges of the equivalence ratios. The third column shows the percentage of the total particulates emitted from the engine for the different ranges of the equivalence ratios. It can be seen that 66.06% of the total particulates was emitted when the engine was run at low load conditions. The amount of the particulate produced in the engine was fairly evenly distributed for the equivalence ratios between 0.25 and 0.55. Although only 0.83% of the total time the engine was run at equivalence ratios greater than 0.25, 2.66% of the total particulates were emitted for these loads. Table 6.9 implies that to reduce the particulate emission during the EPA transient cycle, the key problem to solve is the high level of particulate emissions at low load. Once again, the model

Table 6.9: Distribution of the particulate emission over the predicted equivalence ratios

Equivalence Ratio	Frequency, %	% of Total Particulate
$\leq$0.25	59.88	66.06
0.25–0.35	11.01	9.32
0.35–0.45	10.01	7.10
0.45–0.55	11.84	10.50
0.55–0.65	6.42	4.36
$>$0.65	0.83	2.66

provides directional information about where the manufacturers should work on the engine to reduce the particulate emission.

6.4.2 Comparison of model predictions and measured particulate emissions during four segments of the EPA transient cycle

The particulates were also collected separately over the four segments of the EPA transient cycles. The calculated experimental data for three independent tests were compared with the model predictions and the results are listed in Table 6.10.

It can be seen that the model predicted specific particulate emissions were within 7% of the averaged experimental data for all the segments. The experimental data showed that the averaged specific particulate emission during the fourth segment was 9.4% less than that during the first segment. The reason for this might be due to the temperature difference of the cylinder between two the two segments. Although the engine was started at hot-start conditions, the cylinder temperature for the fourth segment would be higher than that for the first segment. The reason for this is that the fourth segment follows the third segment that is a high power output period, while the first segment starts after the 20-minute "hot-soak" period

Table 6.10: Predicted and measured particulate emissions over four segments of EPA transient cycles

Segment	Case	Work, $kW-Hr$	P_{mass}, gm	BSP, $gm/bkW-Hr$
First Segment	Model	0.57	0.806	1.414
	Test 1	0.56	0.795	1.419
	Test 2	0.55	0.848	1.542
	Test 3	0.56	0.844	1.507
	Mean	0.56	0.829	1.489
	RE, %	+1.75	−2.77	−5.03
Second Segment	Model	0.81	1.020	1.265
	Test 1	0.77	1.057	1.373
	Test 2	0.80	0.940	1.175
	Test 3	0.78	1.196	1.533
	Mean	0.78	1.064	1.360
	RE, %	+3.85	−4.14	−6.99
Third Segment	Model	2.13	1.002	0.470
	Test 1	2.10	0.991	0.472
	Test 2	2.10	1.144	0.545
	Test 3	2.11	0.964	0.457
	Mean	2.10	1.033	0.491
	RE, %	+1.43	−3.00	−4.28
Fourth Segment	Model	0.57	0.806	1.422
	Test 1	0.55	0.777	1.416
	Test 2	0.56	0.731	1.312
	Test 3	0.53	0.697	1.319
	Mean	0.55	0.735	1.349
	RE, %	+3.64	+9.66	+5.41

specified by the EPA. The engine is expected to produce more particulates at the lower test temperature than at a higher test temperature [82]. This is due primarily to adsorption of uncombusted diesel fuel and lubrication oil. The same trends were reported from Detroit Diesel, Navistar, and Cummins [83]. Results from these three engine manufacturers show that the specific particulate emissions during the fourth segment are consistently lower than those during the first segment with the amount of 2%, 6%, and 24% respectively. It can be concluded that the particulate emission data from the discrete transient tests were consistent with this findings.

Table 6.10 also shows that the model-predicted total amount of the particulate was within 2–4% less than the averaged experimental data for the first, second and third segments, while about 10% higher than the averaged experimental data for the fourth segment.

Because the model applied the same method to calculate the particulate emission for the fourth segment as for the first segment, the model over-estimated the particulate emission for the fourth segment by 9.66% for the total amount of the particulate emission and 5.41% for the specific particulate emission.

To summarize the above discussion, the model is able to predict the specific particulate emission for each segment of the transient cycle with an accuracy of 7% of the experimental measurements. This conclusion is based on the number of the tests available. More experimental data is needed to give more accurate reference values. It is more difficult to measure the particulate for the segments of the transient cycle than for the entire EPA transient cycle. There are two primary reasons for this. One is that the length of time for sampling the particulate emission for each segment is not long enough, only 5 minutes. Less particulate would be collected on

the particulate filter, which creates problems for the filter weighing. Another reason is that the technique used to collect the individual particulate samples is not precise enough. As discussed in Section 5.3, two particulate samples were collected during a completed EPA transient cycle, either for the first and third segments or for the second and fourth segments. The timing for starting the particulate sampling system was controlled manually. Ideally the system should be turned on at the precise starting point of that segment. Due to the nature of the sampling system discussed in Section 5.1, the system had to be started before the segment begins in order to achieve accurate control. At the end of the segment, the system was manually turned off. It is possible that the variation of the test length was ± 2 seconds. It is known for the EPA test procedure that the engine is operated at idle conditions between any two segments. The equivalence ratio at this condition is about 0.1 and by using Eq. 3.31, there would be 4 μg of particulate emitted in one second. The variation of the testing length could contribute to an error of about 2% of the total particulate emission in that segment. The error in the measurements could increase the percentage error between predicted and experimental particulates. One thing that might be done without modifying the system is to run more tests to generate more particulate emission data. In this way, the averaged data will be more accurate than those given in Table 6.10.

To make the model accurately predict the particulate emission for different starting conditions of the engine, some kind of correlation should be investigated. For instance, the correlation between the changes in the particulate emission and the engine test temperature. This correlation surely will depend on experimental data.

7. CONCLUSIONS

The objectives of this research were to develop a model to predict the instantaneous engine equivalence ratios over a transient cycle, to predict the particulate emission during transient cycles, and to compare the model predictions with experimental data to validate the model. The purpose of this chapter is to summarize the model results as they related to the objectives and then to propose recommendations for future research.

7.1 Summary

Comparison of the model-predicted data with experimental measurements were carried out under hot-start EPA transient cycle tests. The parameters discussed included engine intake manifold pressure and temperature, turbocharger turbine inlet pressure and temperature and turbine outlet temperature, turbocharger speed, air flow rate, fuel flow rate, equivalence ratio, and particulate emission. A discussion was provided on the impact of the distributions of the engine speed and equivalence ratio over the EPA transient cycle on the particulate emission. The results are summarized below:

1. Good agreement was obtained between the model-predicted turbocharger compressor and turbine pressure ratios and the experimental data. The

coefficient of determination was generally about 0.90 and the slope was about $\pm 7\%$ of unity.

2. Although good agreement was not established between the model-predicted boost temperature and turbocharger turbine inlet and outlet temperatures and the experimental measurements, the model did correctly predict trends in the temperature with changes in the engine operation conditions.

3. The model accurately predicted the turbocharger speed. The slope, and coefficient of determination from the regression analysis were generally greater than 0.90 for the predicted turbocharger speed on the experimental data.

4. The model accurately predicted the instantaneous air flow rates with a slope of 1.02 and the coefficient of determination of 0.98, compared with the experimental measurements.

5. The model provided good predictions of the instantaneous fuel flow rates with a slope of 1.00 and a coefficient of determination of 0.87, compared with the experimental calculations based on the steady-state fuel flow rate model.

6. The model provided a good estimation of instantaneous equivalence ratios over the transient cycle. A linear regression analysis showed that the slope and coefficient of determination for the instantaneous equivalence ratios were 0.93 and 0.81. Part of the difference between the model-predicted and the measured equivalence ratios is believed to be due to imposing the steady-state fuel flow rate on the actual transient fuel flow rate.

7. The steady-state particulate emission data indicated that both the equivalence ratio and the engine speed affected the particulate emission. The particulate emission produced by the engine was higher at both low and high equivalence ratios than at medium equivalence ratio. The particulate emission increased with the increasing of the engine speed at lower ranges of the equivalence ratio, while decreased at higher ranges of the equivalence ratio.

8. The model provided a way to analyze the instantaneous particulate emission during the transient cycle. This is greatly superior to the experimental measurement by dilution method, because the experimental measurement can only give final total particulate emission.

9. The model accurately predicted the diesel particulate emission during the EPA transient cycle and the four individual segments of the EPA transient cycle. The relative error between the model-predicted particulate emission and the average measurement was 2.6% for the total particulate emission and 4.4% for the specific brake specific particulate emission over the EPA transient cycle. For the four segments of the transient cycle, the model generally predicted the particulate emission in the same accuracy as for the EPA transient cycle. The model was validated by the experimental measurements.

10. The distribution of the particulate emission over the transient cycle provided useful information for reducing transient particulate emission.

7.2 Recommendations for Future Work

Several changes to the model are suggested in this section. These suggestions are based on the experience gained during the development and verification of the model. The changes suggested here are expected to improve the capability of the model to better predict equivalence ratio and particulate emissions. Potential new applications of the model will also be provided in the section. Some suggestions related to the experimental work are also discussed.

1. The compressor map needs to be improved. The compressor map used for this study was based on both the laboratory measurements and the turbocharger manufacturer's data. The inter-laboratory variability could contribute to errors in the compressor performance map. The compressor could be removed from the engine and placed on a test stand so that a completed compressor map could be constructed. An improved compressor map could also reduce the computer time.

2. In order to predict the particulate emission for different starting conditions, the model should include a correlation between the particulate emission and the engine test temperature. The correlation could be developed from experiments.

3. The model could be applied to predict NO_x emission during transient cycles. The reason for this is that the NO_x emission is also primarily dependent on the equivalence ratio.

4. The temperature measurements on the engine need to be improved. The work needing to be done includes relocating some of the thermocouples

and changing all the thermocouples on the engine to fast response versions.

5. The correlation on fuel flow rates did provide a way to compare the model-predicted and measured fuel flow rate. The another way suggested here is to measure the instantaneous concentrations of CO_2 in the engine exhaust gas, which could provide a second estimation of the engine equivalence ratio.

6. The time constant for controlling the particulate sampling flow rate could be reduced. The present time constant is one second. If it is too fast, the modulating valve cannot respond. Using the secondary dilution tunnel, the rate of deposition of the particulate on the filter is lowered, the sampling flow rate is not going to change significantly in one second. Five seconds would be a reasonable value for a period of control.

7. Automatic solenoid control valves could be installed in the particulate sampling system to achieve good timing control and improve the accuracy of the particulate measurements.

REFERENCES

[1] Heywood, J.B. *Internal Combustion Engine Fundamentals.* New York: McGraw-Hill, 1988.

[2] Osenga, Mike. "Emissions Update: The Clean Air Act Plus CARB." *Diesel Progress, Engines and Drives* (February 1991): 6–7.

[3] The Federal Register. *Code of Federal Regulations.* Title 40, Chapter I, Subpart N, 1988.

[4] MacDonald, J. S., Plee, Steven L., D'Arcy, James B., and Schreck, Richard M. "Experimental Measurements of the Independent Effects of Dilution Ratio and Filter Temperature on Diesel Exhaust Particulate Samples." *Society of Automotive Engineers* Technical Paper No. 800185, 1980.

[5] Harrington, J.A. and Yetter, R.A. "Application of a Mini-dilution Tube in the Study of Fuel Effects on Stratified Charge Engine Emissions and Combustion." *Society of Automotive Engineers* Technical Paper No. 811198, 1981.

[6] Susuki, J., Yamazaki, H., Toshida, Y., and Hor, M. "Development of Dilution Mini-Tunnel and Its Availability for Measuring Diesel Exhaust Particulate Matter." *Society of Automotive Engineers* Technical Paper No. 851547, 1985.

[7] Cornetti, Giorgio M., Klein, K., Fränkle, Gerhard J., and Stein, Hans J. " US Transient Cycle Versus ECE R.49 13-Mode Cycle." *Society of Automotive Engineers* Technical Paper No. 880715, 1988.

[8] Hiroyasu, H. and Arai, M. "Structures of Fuel Spray in Diesel Engines." *Society of Automotive Engineers* Technical Paper No. 900475, 1990.

[9] Wong, C. L. and Steere, D. E. "The Effects of Diesel Fuel Properties and Engine Operating Conditions on Ignition Delay." *Society of Automotive Engineers* Technical Paper No. 821231, 1982.

[10] Rife, J. and Heywood, J. B. "Photographic and Performance Studies of Diesel Combustion with a Rapid Compression Machine." *Society of Automotive Engineers* Technical Paper No. 740948, 1974.

[11] Chiu, W. S., Shahed, S. M., and Lyn, W. T. "A Transient Spray Mixing Model for Diesel Combustion." *Society of Automotive Engineers* Technical Paper No. 760128, 1976.

[12] Shahed, S. M, Flynn, P. F., and Lyn, W. T. "A Model for the Formation of Emissions in a Direct-Injection Diesel Engine." In *Combustion Modeling in Reciprocating Engines*, ed. J. N. Mattavi and C. A. Amann. New York: Plenum Press, 1980.

[13] Minami, T., Suzuki, T., Tsujimura, K., Shintani, M., and Yamaguchi, I. "Analysis of Fuel Spray Characteristics and Combustion Phenomena Under High Pressure Fuel Injection." *Society of Automotive Engineers* Technical Paper No. 900438, 1990.

[14] Hunter, C. E., Cikanek, H. A., and Gardner, T. P. "Evaluation of Some Factors Controlling DI Diesel Combustion and Exhaust Emissions." *Journal of Engineering for Gas Turbines and Power* 111 (July 1989): 355–360.

[15] Needham, J. R., Doyle, D. M., Faulkner, S. A., and Freeman, H. D. "Technology for 1994." *Society of Automotive Engineers* Technical Paper No. 891949, 1989.

[16] Haynes, B. S. and Wagner, H. G. "Soot Formation." *Progress of Energy and Combustion Science* 7 (1981): 229–273.

[17] Amann, C. A. and Siegla, D. C. "Diesel Particulates—What They Are and Why." *Aerosol Science and Technology* 1 (1982): 73–101.

[18] National Research Council. *Diesel Technology, Impacts of Diesel-Powered Light-Duty Vehicles. Report of the Technology Panel of the Diesel Impacts Study Committee.* Washington, D.C.: National Academy Press, 1982.

[19] Kamimoto, T. and Yagita, M. "Particulate Formation and Flame Structure in Diesel Engines." *Society of Automotive Engineers* Technical Paper No. 890436, 1989.

[20] Luo, L., Pipho, M. J., Ambs, J. L., and Kittelson, D. B. "Particle Growth and Oxidation in a Direct-Injection Diesel Engine." *Society of Automotive Engineers* Technical Paper No. 890580, 1989.

[21] Du, C. J. and Kittelson, D. B. "Total Cylinder Sampling from a Diesel Engine: Part III—Particle Measurements." *Society of Automotive Engineers* Technical Paper No. 830243, 1983.

[22] Graham, S. C., Homer, J. B., and Rosenfeld, J. L. J. "The Formation and Coagulation of Soot Aerosols Generated by the Pyrolysis of Aromatic Hydrocarbons." *Proc. Roy. Soc. Lond.* A344 (1975): 259–285.

[23] Smith, O. I. "Fundamentals of Soot Formation in Flames with Application to Diesel Engine Particulate Emissions." *Progress of Energy and Combustion Science* 7 (1981): 275–291.

[24] Abbass, M. K., Andrews, G. E., and Williams, P. T. "Diesel Particulate Composition Changes Along an Air Cooled Exhaust Pipe and Dilution Tunnel." *Society of Automotive Engineers* Technical Paper No. 890789, 1989.

[25] Mayer, W. J., Lechman, D. C., and Hilden, D. L. "The Contribution of Engine Oil to Diesel Exhaust Particulate Emissions." *Society of Automotive Engineers* Technical Paper No. 800256, 1980.

[26] Hedding, G. H., Kittelson, D. B., Scherrer, X., and Dolan, D. F. "Total Cylinder Sampling from a Diesel Engine." *Society of Automotive Engineers* Technical Paper No. 810257, 1981.

[27] Liu, X. and Kittelson, D. B. "Total Cylinder Sampling from a Diesel Engine: Part II." *Society of Automotive Engineers* Technical Paper No. 810360, 1981.

[28] Pipho, M. J., Ambs, J. L., and Kittelson, D. B. "In-Cylinder Measurements of Particulate Formation in an Indirect Injection Diesel Engine." *Society of Automotive Engineers* Technical Paper No. 860024, 1986.

[29] Kittelson, D. B., Ambs, J. L., and Siegla, D. C. "Particle Concentrations in a Diesel Cylinder: Comparison of Theory and Experiment." *Society of Automotive Engineers* Technical Paper No. 861569, 1986.

[30] Kittelson, D. B., Pipho, M. J., Ambs, J. L., and Luo, L. "In-Cylinder Measurements of Soot Production in a Direct-Injection Diesel Engine." *Society of Automotive Engineers* Technical Paper No. 880344, 1988.

[31] Norris-Jones, S. R., Hollis, T., and Waterhouse, C. N. F. "A Study of the Formation of Particulates in the Cylinder of a Direct Injetion Diesel Engine." *Society of Automotive Engineers* Technical Paper No. 840419, 1984.

[32] Lida, N. and Sato, G. T. "Study on Characteristics of Particulate Emissions from a Direct Injection Diesel Engine Using a Freezing Method in Sampling Process." *Society of Automotive Engineers* Technical Paper No. 841077, 1984.

[33] Matsui, Y., Kamimoto, T, and Matsuoka, S. "A Study on the Application of the Two-Color Method to the Measurement of Flame Temperature and Soot Concentration in Diesel Engines." *Society of Automotive Engineers* Technical Paper No. 800970, 1980.

[34] Matsui, Y., Kamimoto, T, and Matsuoka, S. "Formation and Oxidation Processes of Soot Particulates in a D. I. Diesel Engine—An Experimental Study via the Two-Color method." *Society of Automotive Engineers* Technical Paper No. 820464, 1982.

[35] Yan, J. and Borman G. L. "Analysis and In-Cylinder Measurement of Particulate Radiant Emissions and Temperature in a Direct Injection Diesel Engine." *Society of Automotive Engineers* Technical Paper No. 881315, 1988.

[36] Wersborg, B. L., Fox, L. K., and Howard, J. B. "Soot Concentration and Absorption Coefficient in a Low-Pressure Flame." *Combustion and Flame* 24 (Feburary 1975): 1–10.

[37] Haynes, B. S., Jander, H., and Wagner, H. G. "The Effect of Metal Additives on the Formation of Soot in Premixed Flames." *17th Symposium on Combustion* (1978).

[38] Nishida, O. and Mukōhara, S. "Optical Measurement on Soot Particle in a Non-Steady Diffusion Flame." *Society of Automotive Engineers* Technical Paper No. 841079, 1984.

[39] Murray, Bennett C. "Development of a Transient Diesel Exhaust Emissions Measurement System." M.S. Thesis, Department of Mechanical Engineering, Iowa State University, 1989.

[40] Gross, G. P., MacDonald, J. S., and Shahed, S. M. "Informational Report on the Measurement of Diesel Particulate Emissions." In *Coordinating Research Council Report No. 522*, 1982.

[41] Perez, J. M., Jass, R. E., and Leddy, D. G. "Chemical Methods for the Measurement of Unregulated Diesel Emissions." In *Coordinating Research Council Report No. 551*, 1987.

[42] Hirakouchi, N., Fukano, I., and Shoji, T. "Measurement of Diesel Exhaust Emissions with Mini-Dilution Tunnel." *Society of Automotive Engineers* Technical Paper No. 890181, 1989.

[43] Khan, I. M. and Greeves, G. "Factors Affecting Smoke and Gaseous Emissions from Direct Injection Engines and a Method of Calculation." *Society of Automotive Engineers* Technical Paper No. 730169, 1973.

[44] Khan, I. M. and Greeves G. *Heat Transfer in Flames.* New York: John Wiley and Sons, 1975.

[45] Green, H. L. and Lane, W. R. *Particulate Clouds: Dusts, Smokes and Mists.* New Jersey: D. VanNostrand Co., 1957.

[46] Park, C. and Appleton, J. P. "Shock-Tube Measurements of Soot Oxidation Rates." *Combustion Flame* 20 (1973): 369–379.

[47] Mahta, P. S., Gupta, A. K., and Gupta, C. P. "Model for Prediction of Incylinder and Exhaust Soot Emissions from Direct Injection Diesel Engines." *Society of Automotive Engineers* Technical Paper No. 881251, 1988.

[48] Callahan, T. J., Ryan III, T. W., Dietzmann, H., and Waytulonis, R. "The Effects of Discrete Transients in Speed and Load on Diesel Engine Exhaust Emissions." *Society of Automotive Engineers* Technical Paper No. 850109, 1985.

[49] Callahan, T. J., Ryan III, T. W., Martin, S. F., and Waytulonis, R. "Comparison of Predicted and Measured Diesel Exhaust Emission levels During Transient Operation." *Society of Automotive Engineers* Technical Paper No. 872140, 1987.

[50] Abe, T., Sato, T, and Hayashida, M. "Particulate Matter Emission Characteristics under Transient Pattern Driving." *Society of Automotive Engineers* Technical Paper No. 890468, 1989.

[51] Bowns, D. E. "The Dynamic Characteristics of Reciprocating Engines." *Proc. E. Mech. E.* 185 (1971).

[52] Hazell, P. A. and Flowers, J. O. "Sampled-Data Theory Applied to the Modeling and Control Analysis of Compression Ignition Engines." *International Journal of Control* 13 (1971): 549–562.

[53] Benson, R. S., Ledger, J. D., Whitehouse, N. D., and Walmsley, N. D. "Comparison of Experimental and Simulated Transient Responses of a Turbocharged Diesel Engine." *Society of Automotive Engineers* Technical Paper No. 730666, 1973.

[54] Watson, N. and Marzouk, M. "A Non-Linear Digital Simulation of Turbocharged Diesel Engines Under Transient Conditions." *Society of Automotive Engineers* Technical Paper No. 770123, 1977.

[55] Tsai, S. and Goyal, M. R. "Dynamic Turbocharged Diesel Engine Model for Control Analysis and Design." *Society of Automotive Engineers* Technical Paper No. 860455, 1986.

[56] Borman, G. L. "Mathematical Simulation of Internal Combustion Engine Processes and Performance Including Comparison with Experiment." Ph. D. Thesis, University of Wisconsin, 1964.

[57] McAulay, K. J., Wu, T., Chen, S. K., Borman, G. L., Meyers, P. S., and Uyehara, O. A. "Development and Evaluation of the Simulation of the Compression Ignition Engine." *Society of Automotive Engineers* Technical Paper 650451, 1965.

[58] Srivastava, J. P. "Transient Response Characteristics of an Exhaust Gas Turbocharger." *Institution of Mechanical Engineers, Journal of Automotive Engineering* (April 1974): 13–20.

[59] Krieger, R. B. and Borman, G. L. "The Computation of Apparent Heat Release for Internal Combustion Engines." *American Society of Mechanical Engineering* Technical Paper 66-WA/DGP-4, 1966.

[60] Van Gerpen, J. H. "Simulation of a Combined-Cycle Engine." *U.S. Army Propulsion Directorate* (1990).

[61] Ferguson, C. R. *Internal Combustion Engines–Applied Thermodynamics*. New York: John Wiley, 1986.

[62] Annand, W. J. D. "Heat Transfer in the Cylinder of Reciprocating Internal Combustion Engines." *Proceedings of Institution of Mechanical Engineers* 177 (1963): 973–990.

[63] Van Gerpen, J. H. "A Two-Stroke Diesel Engine Simulation Program." *NASA Technical Memorandum* (January 1989).

[64] Jiang, Q., Ottikkutti, P., Van Gerpen, J. H., and Van Meter, D. B. "The Effect of Alcohol Fumigation on Flame Temperature and Emissions in a Diesel Engine." *Society of Automotive Engineers* Technique Paper No. 900386, 1990.

[65] Watson, N., Pilley, A. D., and Marzouk, M. "A Combustion Correlation for Diesel Engine Simulation." *Society of Automotive Engineers* Technical Paper No. 800029, 1980.

[66] Van Gerpen, J. H., and Shapiro, H. N. "Second Law Analysis of Diesel Engine Combustion." *ASME Winter Annual Meeting* (1987).

[67] Olikara, C. and Borman, G. L. "A Computer Program for Calculating Properties of Equilibrium Combustion Products with some Applications to I.C. Engines." *Society of Automotive Engineers* Technical Paper No. 750468, 1975.

[68] Hindmarsh, A. C. "LSODE and LSODI, Two New Initial Value Ordinary Differential Equation Solvers." *ACM-Signum Newsletter* 15 (1980): 10–11.

[69] Wahba, G. and Wold S. "A Completely Automatic French Curve: Fitting Spline Functions by Cross Validation." *Communications in Statistics* 4 (1975): 1–17.

[70] Craven, P. and Wahba, G. "Smoothing Noisy Data with Spline Functions." *Numerical Mathematics* 31 (1979): 377–403.

[71] IMSL, Inc. *MATH/LIBRARY, Version 10.0.* Houston, Texas, April 1987.

[72] Tuken, T., Fullmer, R. Rees, and Van Gerpen, Jon H. "Modeling, Identification, and Torque Control of a Diesel Engine for Transient Cycles." *Society of Automotive Engineers* Technical Paper No. 900235, 1990.

[73] Tuken, T. "Adaptive Torque Control of a Diesel Engine for Transient Cycles." Ph. D. Dissertation, Department of Mechanical Engineering, Iowa State University, 1991.

[74] Simpson II, H. R. D., Andon, B. M., and Rife, J. M. "Effect of Operating Conditions on the Particulates from a Single Cylinder Diesel Engine." *Society of Automotive Engineers* Technical Paper No. 830646, 1983.

[75] Alkidas, A. C. and Cole, R. M. "Gaseous and Particulate Emissions from a Single-Cylinder Divided-Chamber Diesel Engine." *Society of Automotive Engineers* Technical Paper No. 831288, 1983.

[76] Gabele, P., Karches, W., Ray, W., and Perry, N. "Emissions from a Light-duty Diesel: Ambient Temperature and Fuel Effects." *Society of Automotive Engineers* Technical Paper No. 860618, 1986.

[77] Kennedy, John B. and Neville, Adam M. *Basic Statistical Methods for Engineers and Scientists.* 2nd ed., New York: Dun-Donnelley, Harper & Row, Publishers, 1976.

[78] Ottikkutti, P. "Multizone Modeling of a Fumigated Diesel Engine." Ph. D. Dissertation, Department of Mechanical Engineering, Iowa State University, 1989.

[79] Haddad, S. D. and Watson, N. *Principles and Performance in Diesel Engineering.* England: Ellis Horwood Limited, 1984.

[80] Shimoda, M., Suzuki, T., and Shigemori, M. "Observation of the Particulate Formation Process in the Cylinder of a Direct Injection Diesel Engine." *Society of Automotive Engineers* Technical Paper No. 870268, 1987.

[81] Stein, H. J., Ekermo A. I., and Treiber P. J. H. "Emission Correlation of Heavy-Duty Transient Test Facilities." *Society of Automotive Engineers* Technical Paper No. 892492, 1989.

[82] Braddock, J. N. "Impact of Low Ambient Temperature on Diesel Passenger Car Emissions." *Society of Automotive Engineers* Technical Paper No. 820278, 1982.

[83] Kittelson, D. B. and Johnson, J. H. "Variability in Particle Emission Measurements in the Heavy Duty Transient Test." *Society of Automotive Engineers* Technical Paper No. 910738, 1991.

APPENDIX A. DIFFERENTIAL EQUATIONS OF COMBUSTION MODEL

Six differential equations were derived from the energy and mass balances discussed in Section 3.2.1. The thermodynamic quasi-steady-state engine combustion model is basically constructed by these equations. The six equations are presented as follows.

The mass balance gives the following expression:

$$\frac{dm}{d\theta} = m'_{in} + m'_f - m'_{out} \tag{A.1}$$

The apparent fuel mass burning rate was based on the model proposed by Watson et al. [65]. It is used to calculate the rate of energy input to the engine.

$$m'_f = m_f \left[C_1 PR(\theta) + (1 - C_1) DI(\theta) \right] \tag{A.2}$$

The Annand correlation [62] is used to determine the rate of heat transfer between the combustion gas and the cylinder walls.

$$Q' = \left(\frac{A}{6N} \right) \left[0.49 \frac{k}{B} (R_e)^{0.7} (T - T_w) + b(T^4 - {T_w}^4) \right] \tag{A.3}$$

Based on the mass balance and the definition of the equivalence ratio, the rate of change in the equivalence ratio is defined as follows.

$$\frac{d\phi}{d\theta} = \frac{1 + f_s \phi}{m} \left(m'_{in} \frac{\phi_{in} - \phi}{1 + f_s \phi_{in}} - m'_{out} \frac{\phi_{out} - \phi}{1 + f_s \phi_{out}} + \frac{m'_f}{f_s} \right) \tag{A.4}$$

From the first law of thermodynamics, the rate of change in the cylinder gas pressure was solved to be:

$$\frac{dp}{d\theta} = \frac{EE + FF\frac{d\phi}{d\theta}}{DD} \tag{A.5}$$

The rate of the change in the cylinder gas temperature is derived from the ideal gas law equation and expressed as follows.

$$\frac{dT}{d\theta} = \frac{GG + \left(V - mT\frac{d\phi}{d\theta}\frac{\partial R}{\partial p}\right)\frac{dp}{d\theta}}{m\left(R + T\frac{\partial R}{\partial T}\right)} \tag{A.6}$$

The Five intermediate terms in the differential equations A.5 and A.6 are given as follows.

$$CC = \frac{\frac{\partial u}{\partial T}}{R + T\frac{\partial R}{\partial T}}$$

$$DD = (CC)V - m\left[(CC)T\frac{\partial R}{\partial p} - \frac{\partial u}{\partial p}\right]$$

$$EE = Q' - (CC + 1)p\frac{dV}{d\theta} + m'_{in}h_{in} + m'_f h_f - m'_{out}h_{out} + [RT(CC) - u]\frac{dm}{d\theta}$$

$$FF = m[(CC)T\frac{\partial R}{\partial \phi} - \frac{\partial u}{\partial \phi}]$$

$$GG = p\frac{dV}{d\theta} - mT\phi'\frac{\partial R}{\partial \phi} - m'RT$$

Other variables have been defined in Section 3.2.

These six equations plus the sub-models for simulating the engine intake and exhaust processes described in Section 3.2.2, are integrated simultaneously by using the differential equation solver LSODE [68]. The integrated results will identify the thermal properties of the cylinder gas and determine the work output from the engine. In this way, the thermodynamic quasi-steady-state engine model can interact with the models for the other system components.

APPENDIX B. CALIBRATION OF PRESSURE TRANSDUCERS

Four pressure transducers were calibrated. Three of them were Viatran Model 141 pressure transducers, which were calibrated with a dead-weight tester. The other was a differential pressure transducer, which was calibrated with regulated compressed air and a mercury manometer. The output signals from the Viatran Model 141 pressure transducers are in the millivolt range, and are connected to the low-level voltage panel of the Z-386 RTI-820 board. The high-level voltage panel of the Z-386 RTI-820 board receives the voltage signal from the differential pressure transducer. The calibration procedures and the validity of the calibration curves are discussed in this appendix.

The three Viatran Model 141 pressure transducers were individually installed upstream of the orifice in the primary dilution-air line, upstream of the orifice in the secondary dilution-air line, and upstream of the turbine inlet.

Before mounting the transducers, they were calibrated on a dead-weight tester. Calibration data were obtained by loading and unloading the weights on the tester. The voltage was recorded for each pressure setting. After taking the measurements, a linear regression analysis was carried out to fit a straight line to the experimental data.

The differential pressure transducer was installed after the engine compressor to

Table B.1: Data for pressure transducers

Type	Range	Usage	a_0	a_1	r^2
Via. 141	0.0–21.0 bar	1st Dilution	0.5486 bar	0.7469 bar/mV	1.000
Via. 141	0.0–6.9 bar	2nd Dilution	-0.0339 bar	0.1488 bar/mV	0.9992
Via. 141	0.0–2.1 bar	Back Pressure	0.0047 bar	0.0888 bar/mV	1.000
Diff.	2.17–90.46 kPa	Boost Pressure	-0.1366 kPa	20.847 kPa/V	1.000

measure the intake manifold pressure. For calibration, air pressure was applied to the pressure transducer and a mercury manometer was used to measure the pressure. After the calibration, a linear regression analysis was also performed to check the validity of the linear equation.

Table B.1 shows the pressure ranges, the coefficients of the linear equations, and the coefficients of determination for these four pressure transducers. The general form for calculating the pressure is described as follows.

$$P = a_0 + a_1 V \tag{B.1}$$

where

P=pressure applied to the transducer

V=voltage output from the transducer, and

a_0 and a_1=coefficients.

APPENDIX C. CIRCUIT FOR THE LIGHT DETECTOR

Figure C.1 shows the circuit for the light detector which was designed for measuring the turbocharger speed as discussed in Section 4.1.

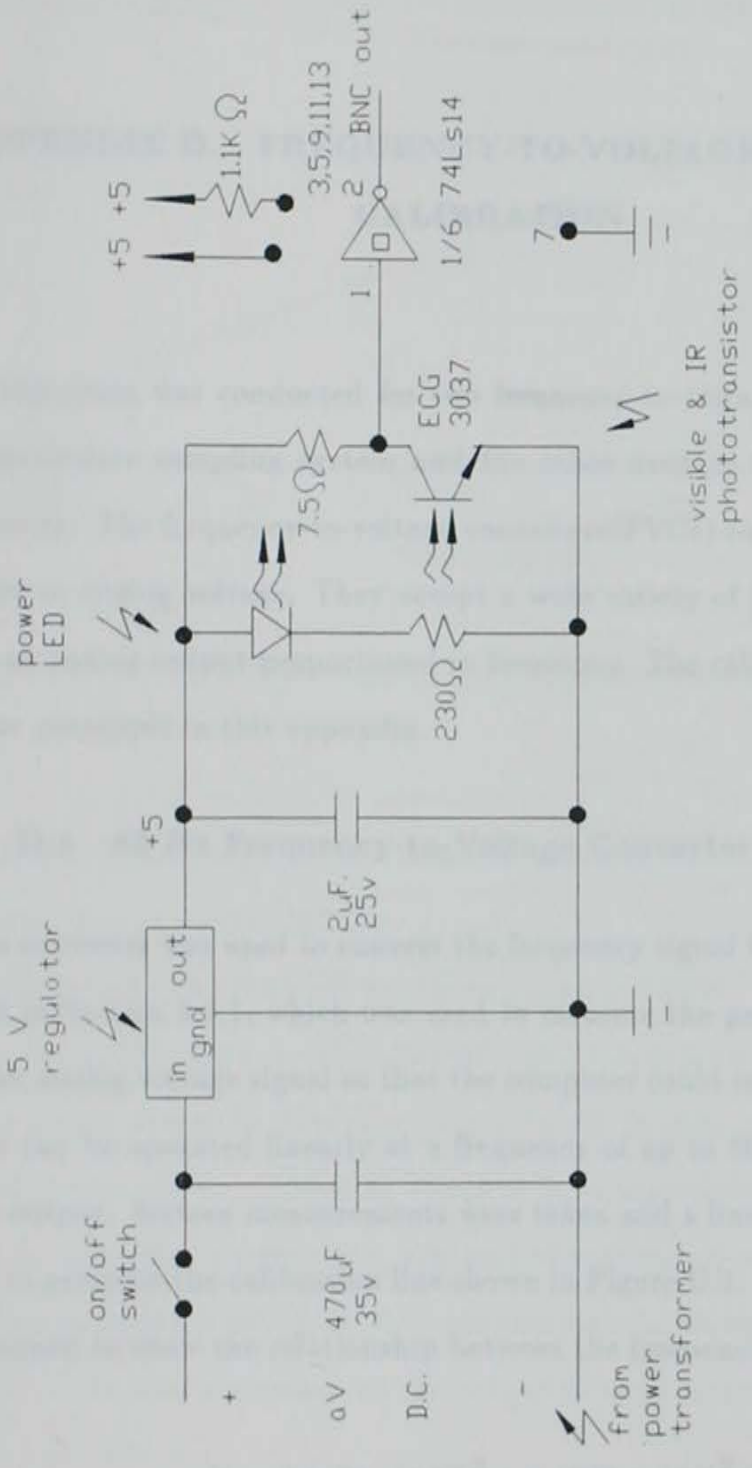

Figure C.1: Circuit diagram for the light detector

APPENDIX D. FREQUENCY-TO-VOLTAGE CONVERTER CALIBRATION

A calibration was conducted for two frequency-to-voltage converters, one used in the particulate sampling system and the other used in the turbocharger speed measurement. The frequency-to-voltage converters(FVC's) convert square waves in a TTL form to analog voltage. They accept a wide variety of periodic waveforms and produce an analog output proportional to frequency. The calibration procedures and curves are presented in this appendix.

D.1 60 Hz Frequency-to-Voltage Converter Calibration

This converter was used to convert the frequency signal from the ROOTS meter discussed in Section 4.4.1, which was used to measure the particulate sampling flow rate, to an analog voltage signal so that the computer could record the flow rate. The converter can be operated linearly at a frequency of up to 60 Hz which corresponds to 5 Vdc output. Sixteen measurements were taken and a linear expression was fit to the data to generate the calibration line shown in Figure D.1. The following equation was developed to show the relationship between the frequency input and the voltage output.

$$V = 2.4472 \times 10^{-2} + 8.4737 \times 10^{-2} f \qquad \text{(D.1)}$$

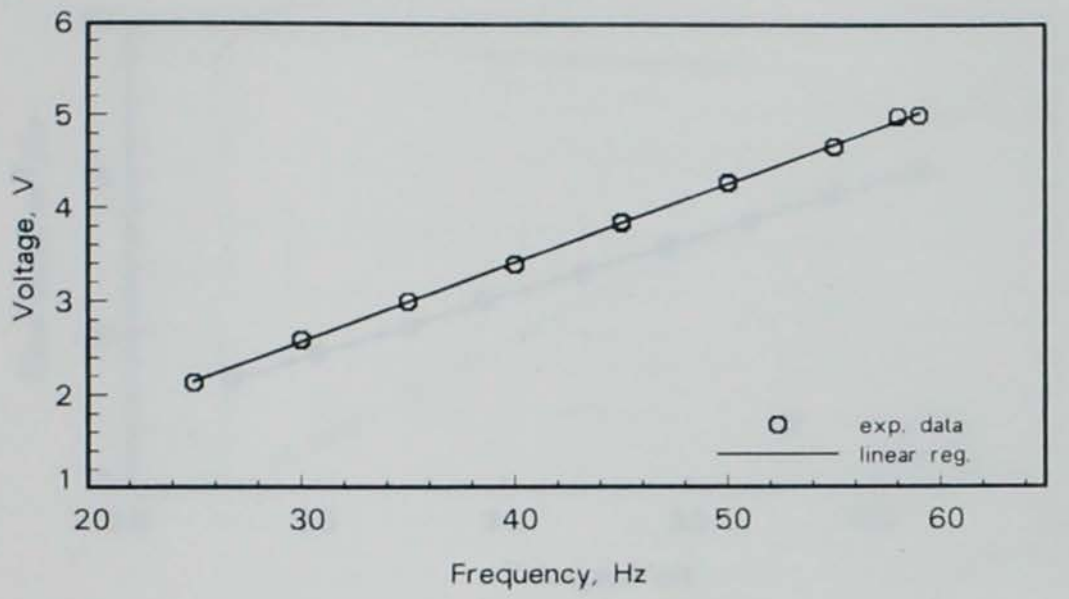

Figure D.1: Calibration line for the 60Hz frequency-to-voltage converter

where

f=the frequency input from a function generator in Hz and

V=the voltage output in volts.

The coefficient of determination for the equation is 0.9996.

The calibration data to relate the voltage produced by the frequency-to-voltage converter to the actual air flow rate were obtained by adjusting the particulate sampling ball valve, which is shown in Figure 4.2, to nine different flow rates. At each setting, the sampling volume flow rate and the voltage were recorded. The former was displayed on the KEPTROL R/T counter and the latter was read from the voltage meter which was connected to the output of the converter. The calibration line is shown in Figure D.2.

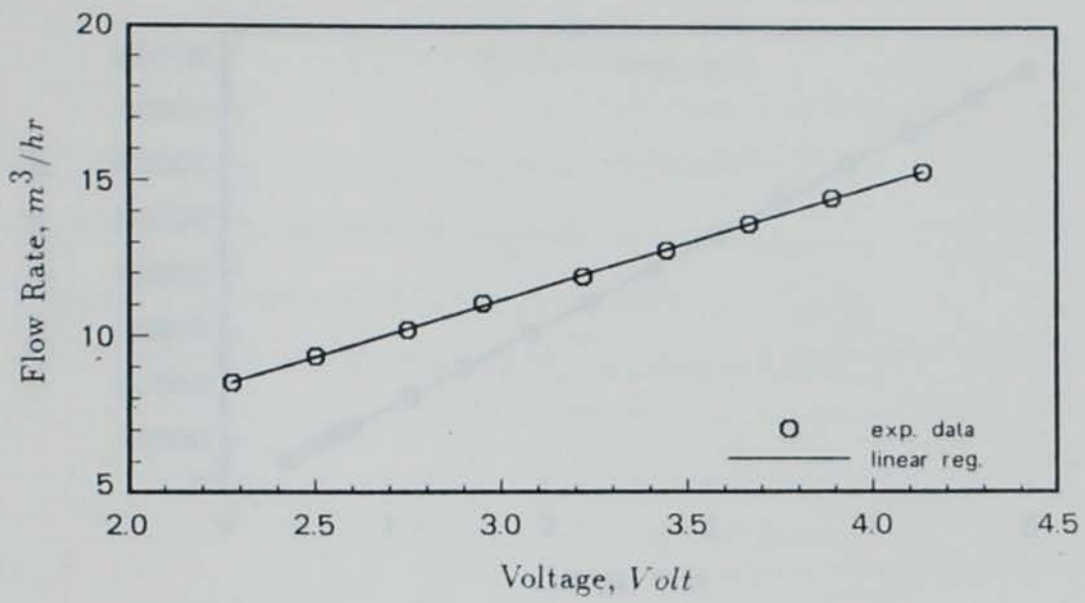

Figure D.2: Sampling volume flow rate vs. voltage

A linear regression gave the following equation to calculate the flow rate from the voltage with a coefficient of determination of 0.9997.

$$Q_{rt} = 0.1623 + 3.6610V \tag{D.2}$$

where

Q_{rt}=the volume flow rate through the ROOTS meter in m^3/h, and

V=the voltage output in volts.

It can be calculated that the frequency-to-voltage converter is able to measure the sampling flow rate up to 18.5 m^3/h which corresponds to an input of 60 Hz to the converter and an output of 5 V from the converter.

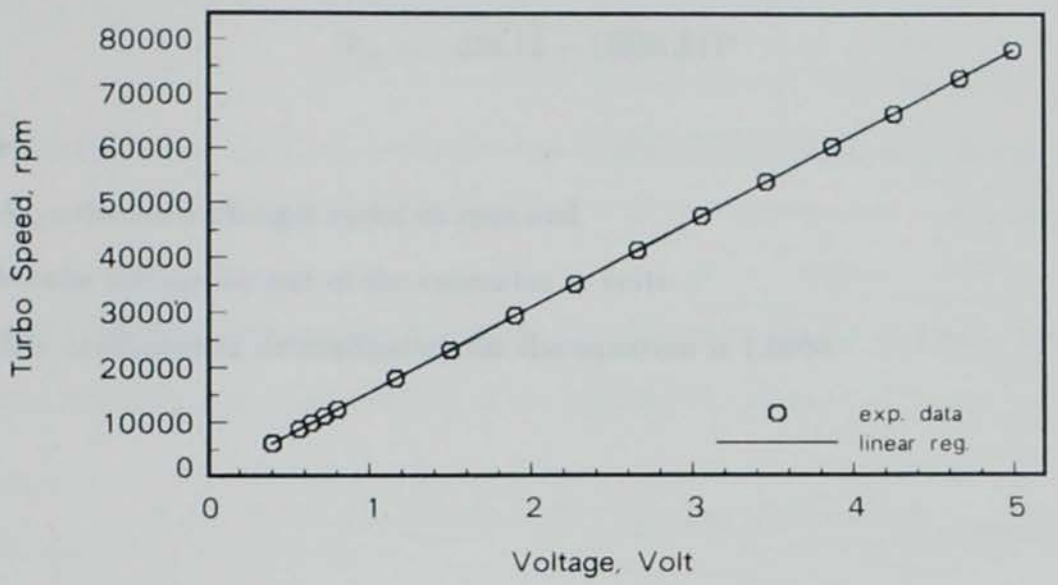

Figure D.3: Calibration line for the 1.300 Hz frequency-to-voltage converter

D.2 1300 Hz Frequency-to-Voltage Converter Calibration

A frequency-to-voltage converter was used to convert the frequency signal generated from the turbocharger speed sensor to an analog voltage signal so that the computer could record the turbocharger speed as discussed in Section 4.1. The converter could be linearly operated at a frequency up to 1300 Hz which corresponded to a 5 Vdc output. Thirteen measurements were taken with a function generator and a voltage meter. The minimum and maximum frequency input to the converter were 102 Hz and 1300 Hz which correspond to minimum and maximum turbocharger speeds of 6,120 rpm and 78,000 rpm. The calibration line was generated by fitting the measured data to a straight line expression as indicated by Figure D.3.

Eq. D.3 can be used to calculate the turbocharger speed with the measured

output voltage of the converter.

$$N_{tc} = -234.75 + 15635.51V \tag{D.3}$$

where

N_{tc}=the turbocharger speed in rpm and

V=the voltage output of the converter in volts.

The coefficient of determination for the equation is 1.0000.

APPENDIX E. CALIBRATION OF THE DILUTION AIR SYSTEMS

This appendix discusses the calibration procedures for the primary and secondary dilution air systems and the validity of the calibration curves.

E.1 Primary Dilution Air System Calibration

The primary dilution air flow rate was controlled by a 3.68 cm diameter smooth-edged orifice, whose location is shown in Figure 4.1. The calibration had been performed before the author started the project. The following equation was extracted from Bennett Murray's M.S. Thesis [39].

$$\dot{m}_{pda} = -0.195 + 0.0705\left(\frac{P_{por}}{\sqrt{T_{por}}}\right) - 8.806 \times 10^{-4}\left(\frac{P_{por}}{\sqrt{T_{por}}}\right)^2 \qquad \text{(E.1)}$$

where

$\dot{m}_{pda}$=the mass flow rate of primary dilution air in kg/s,

P_{por}=the absolute static pressure upstream of the orifice in kPa, and

T_{por}=the temperature upstream of the orifice in K.

E.2 Secondary Dilution System Calibration

The location of the smooth-edged orifice in the secondary dilution tunnel is shown in Figure 4.1. The diameter of the orifice is 2.0 mm. Ten different pressure

settings were obtained by changing the setting of the pressure regulator that was located upstream of the orifice. The pressures were large enough to achieve choked flows. There was a ROOTS meter attached to the pipe downstream of the orifice to measure the air flow rate. The calibration set-up also included a vacuum pump which was installed between the orifice and the ROOTS meter. The pump was in operation during the calibration, which simulated the actual operation of the particulate sampling system. The data recorded during the calibration were the atmospheric pressure, the pressure and temperature upstream of the orifice, and the air temperature before the ROOTS meter.

The following equation was developed for determining the mass flow rate in the secondary dilution tunnel. The coefficient of determination, r^2, for the linear regression line is 0.9998.

$$\dot{m}_{sda} = 4.2608 \times 10^{-4} + 0.64435\left(\frac{P_{sor}}{\sqrt{T_{sor}}}\right) \qquad \text{(E.2)}$$

The units of $\dot{m}_{sda}$, P_{sor}, and T_{sor} are kg/min, bar, and K, respectively. Figure E.1 shows the calibration curve for the secondary dilution air flow.

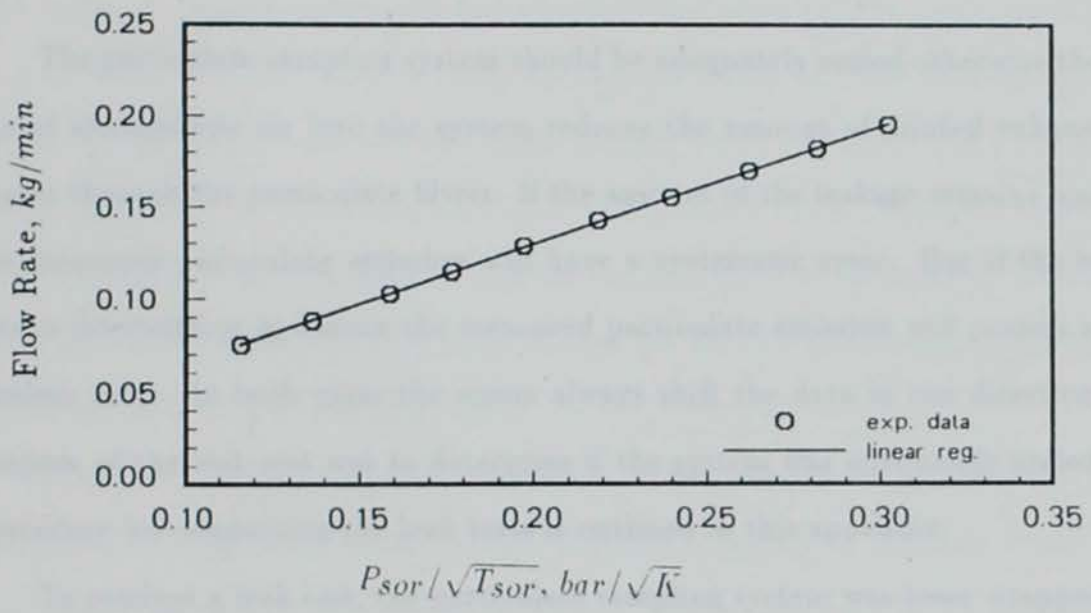

Figure E.1: Calibration curve for secondary dilution air system

APPENDIX F. SAMPLING SYSTEM LEAK TEST

The particulate sampling system should be adequately sealed otherwise the leakage of atmospheric air into the system reduces the amount of diluted exhaust that passes through the particulate filters. If the amount of the leakage remains constant, the measured particulate emission will have a systematic error. But if the leakage rate is intermittent in nature the measured particulate emission will possess a more random error. In both cases the errors always shift the data in one direction. The purpose of the leak test was to determine if the system was adequately sealed. The procedure for conducting the leak tests is outlined in this appendix.

To conduct a leak test, the particulate sampling system was loose wrapped with plastic bags. The space between the system and the plastic was filled with 99.99% pure CO_2 gas. The system was operated as usual with two filters placed on the filter holder. The volume flow rate was maintained at 12.1 m^3/h and the system kept at a vacuum of 50.8 kPa between the sample pump and the filter holder, which were the normal operating conditions for the particulate sampling system. If the system has a leak, some CO_2 should appear at the exit of the system. A Beckman Model 864 non-dispersive infrared radiation analyzer was used to make the carbon dioxide measurements. The concentration of the sample gas downstream of the ROOTS meter was measured to be only 0.16%. The concentration was so low that the leakage

of atmospheric air into the system was considered to be negligible. Most of the leakage was believed to be associated with the shaft seals on the sampling pump. Since the flow was negligible relative to the total sample flow, no action was taken to reduce this leakage flow.

A system vacuum test was also performed to characterize the system leakage. The valve in the secondary dilution air line, the valve on the particulate sample transfer tube, and the valve between the sample pump and the ROOTS meter, as shown in Figure 4.2, were all shut. The vacuum valve was opened and the vacuum pump used to draw the system down to a vacuum of 71.1 kPa. A stopwatch was used with the system's vacuum gage to monitor the leak-down of the system. The vacuum valve was closed during the leak-down so that the vacuum pump and connecting hose would not be a part of the leak test.

Figure F.1 shows a normal leak-down curve. The normal leak-down rate is acceptable as mentioned above because the rate of leakage is less than 0.16% of the mass flow rate of the particulate sample as long as the vacuum in the system is less than 50.8 kPa. During the actual particulate sampling process, the vacuum of the system was usually in the range of 27.1 to 61.0 kPa depending on the particulate loading of the filter. Throughout the experiments the system was periodically checked for leakage using the vacuum pump. It was concluded that the system was adequately sealed for the test program.

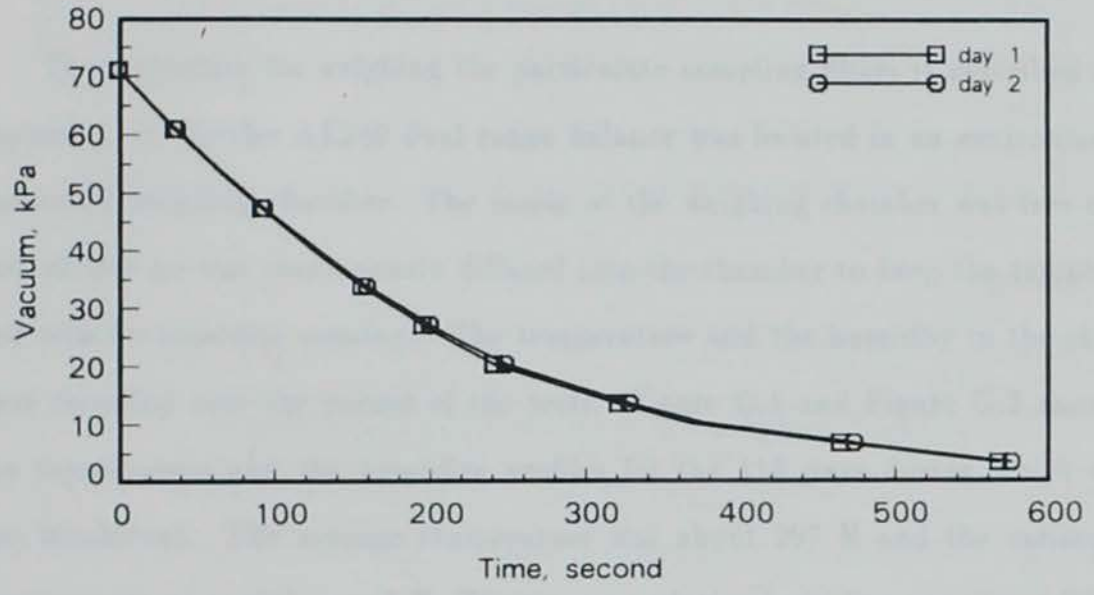

Figure F.1: Normal leak test results

APPENDIX G. FILTER WEIGHING PROCEDURE

The procedure for weighing the particulate sampling filters is described in this appendix. A Mettler AE240 dual range balance was located in an environmentally controlled weighing chamber. The inside of the weighing chamber was free of dust and oil-free air was continuously diffused into the chamber to keep the temperature and relative humidity constant. The temperature and the humidity in the chamber were recorded over the period of the tests. Figure G.1 and Figure G.2 show both the temperature and the humidity profiles for the 112 days during which testing was conducted. The average temperature was about 297 K and the variations of temperature were within $\pm$ 3 K. The average relative humidity was about 30% and the variations of the humidity were within $\pm$ 5%. The environmental conditions of the weighing chamber met the weighing chamber specifications set by the EPA [3].

The weighing range of the balance was selected to be 40 grams. The balance was calibrated after the selection of the range and after the power supply had been left on for more than 60 minutes. Both the integration time (measuring cycle) and the stability detector were selected at normal settings. The balance gave the best performance in terms of measuring accuracy and precision for these selections. The power supply for the balance was usually left on if the balance was frequently used.

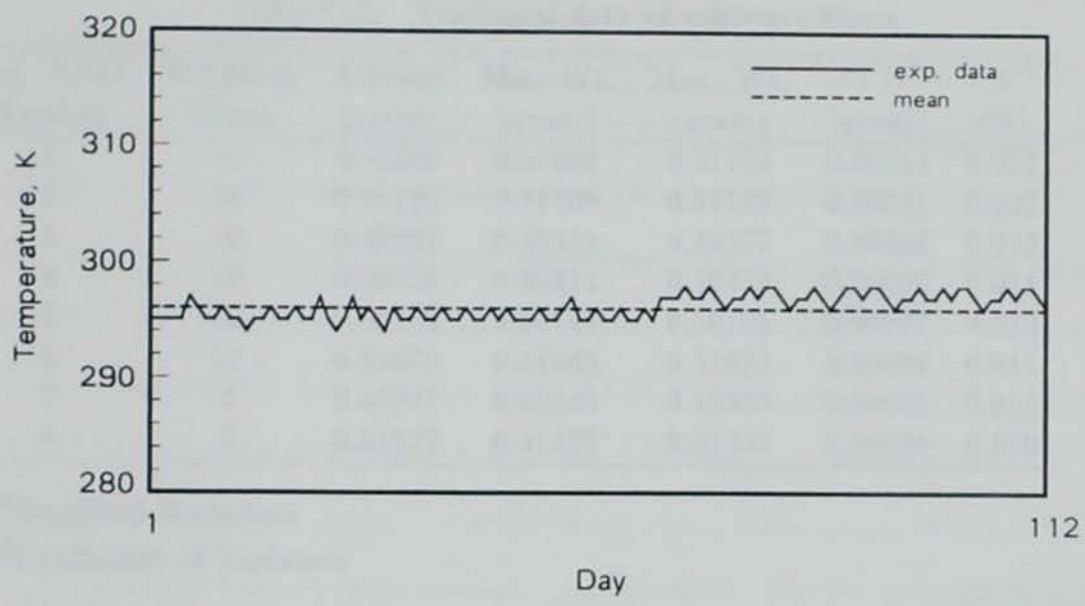

Figure G.1: Temperature in the weighing chamber

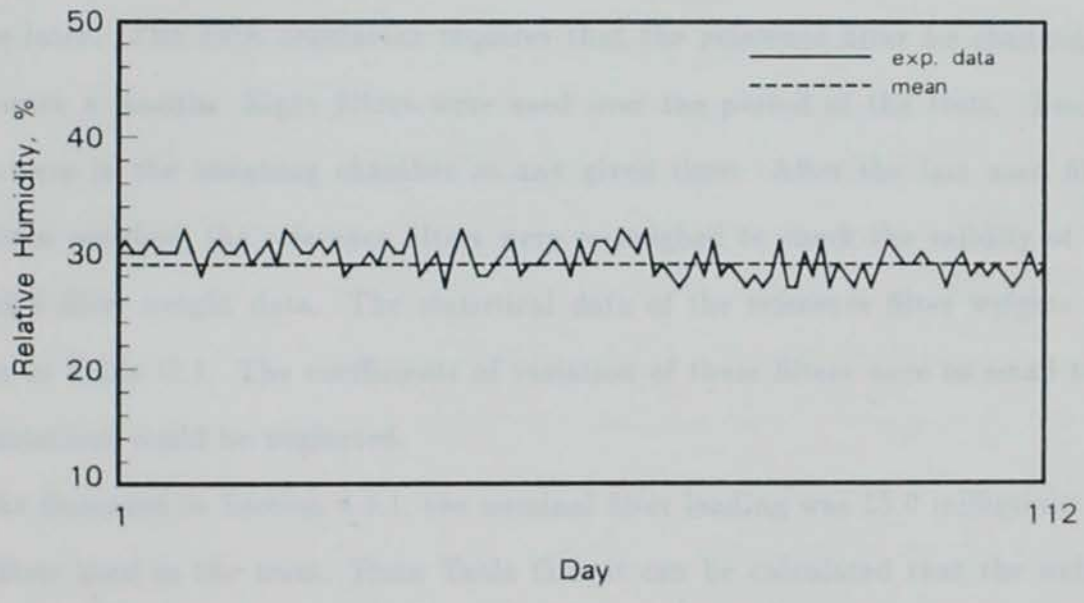

Figure G.2: Relative humidity in the weighing chamber

Table G.1: Statistical data of reference filters

Ref. Filter Number	Weighing Times	Average (gram)	Min. Wt. (gram)	Max. Wt. (gram)	STD^a (gram)	CV^b (%)
1	16	0.51680	0.51669	0.51704	0.00011	0.022
2	16	0.51121	0.51109	0.51148	0.00011	0.022
3	10	0.49527	0.49515	0.49537	0.00006	0.012
4	10	0.50424	0.50414	0.50432	0.00006	0.011
5	12	0.50755	0.50745	0.50765	0.00007	0.013
6	12	0.51674	0.51665	0.51682	0.00006	0.011
7	6	0.48947	0.48940	0.48955	0.00005	0.011
8	6	0.51327	0.51321	0.51335	0.00005	0.010

[a]Standard Deviation
[b]Coefficient of Variation

After having stabilized for at least 48 hours in the weighing chamber, the filters were ready to be weighed. Before weighing the used filters, two reference filters were weighed first to make sure the balance and weighing chamber were working properly. The weights of the reference filters were recorded so they could be used as reference values later. The EPA regulation requires that the reference filter be changed at least once a month. Eight filters were used over the period of the tests. Two of them were in the weighing chamber at any given time. After the last used filter had been weighed, the reference filters were re-weighed to check the validity of the recorded filter weight data. The statistical data of the reference filter weights are shown in Table G.1. The coefficients of variation of these filters were so small that the variations could be neglected.

As discussed in Section 4.4.1, the nominal filter loading was 15.0 milligrams for the filters used in the tests. From Table G.1, it can be calculated that the weight change for any reference filter is less than $\pm 3.0\%$ of 15.0 milligrams, which is below

the EPA tolerance of ±5%.

The weighing process is described as follows. First, the display of the balance was set to zero by pressing the control bar briefly. Then, the sliding glass door of the balance was opened slowly. The used filter was removed from a petri dish and placed on the center of the weighing pan using steel forceps. The glass door was slowly closed for the purpose of reading the weight accurately. When the green dot in the display went out, which meant that stability was achieved, the filter weight was recorded. Finally, the filter was removed from the weighing pan and replaced in the petri dish. Usually, the display returned to zero in a short period of time. If it was zero, the balance was ready to measure another filter. For the purpose of checking the reproducibility of the balance, the filter was usually weighed three times. The final weight was the average value of the three readings.

The weighed sample filters were usually kept in the weighing chamber until the entire data analysis was completed. If there were any doubts about the weight record for a particular filter, the filter could be re-weighed. Though such a situation rarely happened, it was a good way to handle the filters. After weighing was complete, the filters were either discarded or kept for soluble hydrocarbon extraction.

APPENDIX H. DIESEL FUEL FLOW RATE EQUATION AT STEADY-STATE CONDITIONS

To compare the engine equivalence ratio predicted by the computer model with the experimental value, both the instantaneous air and fuel flow rate to the engine must be known during a transient test. The air flow rate could be measured by using the laminar flow element, which was discussed in Section 4.1. Unfortunately, it was not possible to measure the instantaneous fuel flow rate during a transient cycle test by using the equipment available. Instead of measuring the actual fuel flow rate over a transient cycle, an equation was developed to predict the rate based on steady-state tests.

The quantity of diesel fuel consumed during a steady-state test was measured with a Toledo balance and a stopwatch. The diesel fuel flow rate depends only on the engine speed and the rack position of the fuel pump. The rack position was controlled by an actuator, which was discussed in Section 4.1, and was measured using the voltage output from a potentiometer mounted on the actuator. Both the engine speed and the actuator position were recorded by the computer during the steady-state test. The engine speed was varied from 1200 rpm to 2100 rpm and the actuator position was changed so that ten different engine loads were obtained. A two-variable polynomial equation, Eq. H.1, was developed to calculate the diesel fuel

flow rate from the speed and actuator position.

$$\dot{m}_f = a_0 + a_1 X_{act} \tag{H.1}$$

where

X_{act}=the actuator position in volts,

$\dot{m}_f$=the fuel flow rate in kg/min, and

a_0 and a_1=the polynomial coefficients which are the function of the engine speed.

a_0 and a_1 are expressed as follows:

$$a_0 = 7.8776 - 1.2270 \times 10^{-2} N_e + 7.2926 \times 10^{-6} {N_e}^2 - 1.4114 \times 10^{-9} {N_e}^3 \tag{H.2}$$

$$a_1 = -2.3623 + 3.5961 \times 10^{-3} N_e - 2.0249 \times 10^{-6} {N_e}^2 + 3.3478 \times 10^{-10} {N_e}^3 \tag{H.3}$$

where N_e is the engine speed in rpm.

Figure H.1 shows the experimental data and the fit curve. The coefficient of determination, r^2, is 0.9979 from a linear regression analysis. This polynomial experimental equation could be used to estimate the experimental fuel flow rate during the transient cycle using recorded values of engine speed and actuator position.

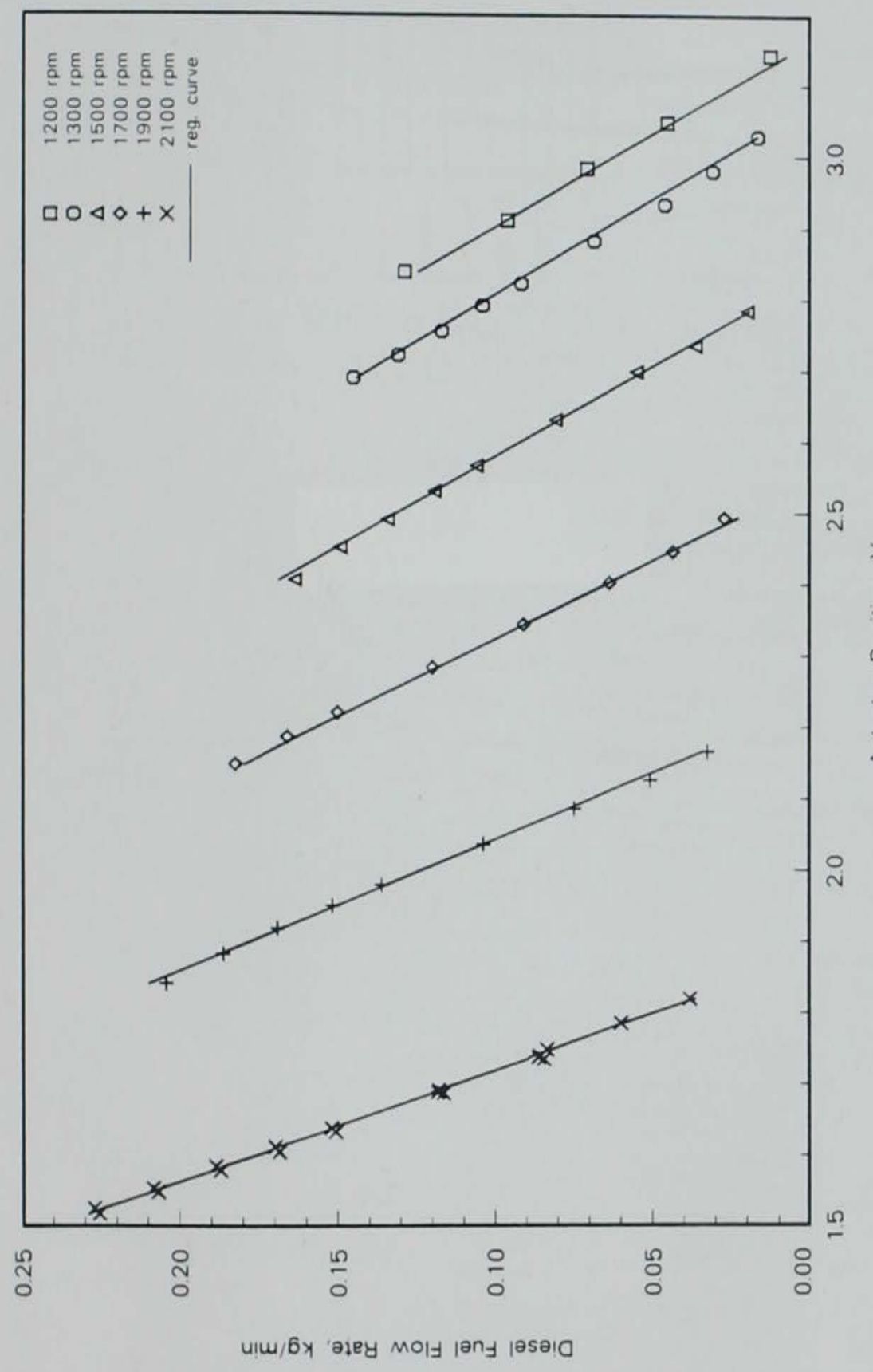

Figure H.1: Diesel fuel flow rate as the function of engine speed and rack position